



Tertiary Nitrification of Oil Refinery Wastewater in Moving Bed Biofilm Reactors:
Biofilm Development and Operational Stability

Bitá Movasati

Dissertação de Mestrado apresentada ao Programa de Pós-graduação em Engenharia Química, COPPE, da Universidade Federal do Rio de Janeiro, como parte dos requisitos necessários à obtenção do título de Mestre em Engenharia Química.

Orientadores: João Paulo Bassin

Márcia Walquíria de Carvalho

Dezotti

Rio de Janeiro

Março de 2026

Tertiary Nitrification of Oil Refinery Wastewater in Moving Bed Biofilm Reactors:
Biofilm Development and Operational Stability

Bitá Movasati

DISSERTAÇÃO SUBMETIDA AO CORPO DOCENTE DO INSTITUTO ALBERTO LUIZ COIMBRA DE PÓS-GRADUAÇÃO E PESQUISA DE ENGENHARIA (COPPE) DA UNIVERSIDADE FEDERAL DO RIO DE JANEIRO COMO PARTE DOS REQUISITOS NECESSÁRIOS PARA A OBTENÇÃO DO GRAU DE MESTRE EM CIÊNCIAS EM ENGENHARIA QUÍMICA

Orientadores: João Paulo Bassin

Márcia Walquíria de Carvalho Dezotti

Aprovada por: Prof. João Paulo Bassin

Prof. Márcia Walquíria de Carvalho Dezotti

Prof. Giorgio Bertanza

Dr. Jéssica Antunes Xavier

RIO DE JANEIRO, RJ – BRASIL

MARÇO DE 2026

Movasati, Bitá

Tertiary Nitrification of Oil Refinery Wastewater in Moving Bed Biofilm Reactors: Biofilm Development and Operational Stability / Bitá Movasati. – Rio de Janeiro: UFRJ/COPPE, 2026.

XX, 142 p.: il.; 29,7 cm.

Orientadores: João Paulo Bassin

Márcia Walquíria de Carvalho Dezotti

Dissertação (mestrado) – UFRJ/ COPPE/ Programa de Engenharia Química, 2026.

Referências Bibliográficas: p. 125-142.

1. Moving Bed Biofilm Reactor. 2. Tertiary nitrification.
3. Oil refinery wastewater. I. Bassin, João Paulo et al. II. Universidade Federal do Rio de Janeiro, COPPE, Programa de Engenharia Química. III. Título

AGRADECIMENTOS

در ابتدا، با تمام وجود از خانواده عزیزم سپاسگزارم که همواره با عشق، حمایت و باور بی‌قید و شرط خود در کنارم بودند. دوری از آنها در طول این دو سال، بیش از هر زمان دیگری ارزش حضورشان را در زندگی‌ام برایم آشکار کرد. در این مدت دلتنگی‌شان همواره همراه من بود، اما دلگرمی و ایمانشان به من نیروی بود که مرا در مسیر رسیدن به آرزوهایم استوار نگه داشت.

همچنین از عموی عزیزم تشکر می‌کنم؛ کسی که همیشه با صبوری و مهربانی راهنمای من بوده و در مهم‌ترین تصمیم‌های زندگی‌ام کنارم ایستاده است. نقش او در شکل‌گیری مسیر زندگی و موفقیت‌هایم برای همیشه در قلبم خواهد ماند و تا پایان عمر قدردان محبت‌ها، راهنمایی‌ها و حضور دلگرم‌کننده‌اش خواهم بود.

Gostaria de agradecer aos meus orientadores, Profa. Márcia Dezotti e Prof. João Paulo Bassin, pelos valiosos ensinamentos, apoio e incentivo ao longo do desenvolvimento deste trabalho. Sou profundamente grata pela oportunidade de aprender com sua experiência e sinto-me honrada por ter sido sua aluna.

Quero agradecer ao meu namorado, Pedro. Ao longo destes dois anos, ele foi minha maior fonte de força, sempre me apoiando, me incentivando e acreditando em mim. Ele esteve ao meu lado em todos os momentos, trazendo alegria, serenidade e luz à minha vida. Sou imensamente grata pelo seu amor e por tê-lo ao meu lado.

Também gostaria de agradecer a todos os meus colegas do LABPOL pelo apoio, colaboração e por proporcionarem um ambiente de pesquisa positivo e motivador. Agradeço especialmente à Jéssica e à Nicololy pela paciência, por compartilharem seus conhecimentos comigo e por estarem sempre dispostas a ajudar sempre que precisei. Estendo ainda minha sincera gratidão à Rafa e à Manuela por toda a dedicação e pela fundamental contribuição durante as análises, cuja ajuda foi essencial para a realização deste trabalho.

Aos ilustres professores do PEQ, expresso minha sincera gratidão pela atenção dedicada e pelo inestimável conhecimento compartilhado ao longo desta trajetória. Aos colegas da turma PEQ 2024/1, agradeço pela acolhida calorosa e por todos os momentos, tanto desafiadores quanto celebrativos, que vivenciamos juntos.

Ao Programa de Engenharia Química (PEQ/COPPE/UFRJ), manifesto meu sincero agradecimento pelo apoio e pela oportunidade proporcionados ao longo desta trajetória acadêmica.

À CAPES pela concessão da bolsa de mestrado e pelo apoio financeiro fundamental para a realização deste trabalho.

Resumo da dissertação apresentada à COPPE/UFRJ como parte dos requisitos necessários para a obtenção do grau de Mestre em Ciências (M.Sc.)

Nitrificação Terciária de Efluente de Refinaria de Petróleo em Reatores de Leito Móvel com Biofilme: Desenvolvimento do Biofilme e Estabilidade Operacional.

Bitá Movasati

Março/2026

Orientadores: João Paulo Bassin

Márcia Walquíria de Carvalho Dezotti

Programa: Engenharia Química

Os efluentes de refinarias de petróleo apresentam desafios significativos para o tratamento biológico devido à presença de compostos potencialmente inibitórios, como óleo e fenóis. Este estudo investigou o desempenho e a resiliência da nitrificação terciária em reatores de leito móvel com biofilme (MBBRs) tratando efluente real de refinaria. A abordagem experimental foi dividida em duas fases. A primeira avaliou o desenvolvimento do biofilme sob quatro estratégias distintas de aclimação, variando desde o uso de efluente sintético até a aplicação direta de efluente real, submetidas a reduções progressivas no tempo de retenção hidráulica (TRH) de 6 para 2 h. Os resultados indicaram que estratégias empregando transição gradual ou suplementação de fonte de carbono externa aceleraram significativamente a maturação e a estabilidade do biofilme em comparação com a aplicação direta de efluente real, a qual exibiu uma fase de adaptação prolongada. No entanto, uma vez estabelecido, o biofilme em todos os reatores permitiu obter altas eficiências de remoção de amônio (>95%), demonstrando robustez contra o estresse hidráulico. A segunda parte do estudo avaliou o efeito de concentrações de óleo de até 500 mg L⁻¹ no desempenho da nitrificação. Níveis elevados de óleo resultaram em acúmulo no material suporte, levando à aglomeração, formação de biofilme com estrutura irregular e aumento do desprendimento de biomassa. Apesar dessas alterações estruturais, as eficiências de remoção de amônio permaneceram elevadas e se recuperaram rapidamente após quedas temporárias. Esses resultados indicaram que o óleo afetou principalmente a estrutura física do biofilme, e não o desempenho global da nitrificação, demonstrando a resiliência operacional do sistema MBBR sob cargas elevadas e flutuantes de óleo.

Abstract of dissertation presented to COPPE/UFRJ as a partial fulfillment of the requirements for the degree of Master of Science (M.Sc.)

Tertiary Nitrification of Oil Refinery Wastewater in Moving Bed Biofilm Reactors:
Biofilm Development and Operational Stability

Bitá Movasati

March/2026

Advisors: João Paulo Bassin

Márcia Walquíria de Carvalho Dezotti

Program: Chemical Engineering

Petroleum refinery wastewaters present significant challenges for biological treatment due to the presence of potential inhibitory compounds, such as oil and phenols. This study investigated the performance and resilience of tertiary nitrification in moving bed biofilm reactors (MBBRs) treating real refinery wastewater. The experimental approach was divided into two parts. The first evaluated biofilm development under four distinct acclimation strategies, ranging from synthetic wastewater to direct application of real refinery wastewater, subjected to progressive reductions in the hydraulic retention time (HRT) from 6 to 2 h. Results indicated that strategies employing gradual transition or carbon supplementation significantly accelerated biofilm maturation and stability compared to the direct application of real wastewater, which exhibited a prolonged lag phase for adaptation. However, once established, the biofilms in all reactors demonstrated high ammonium removal efficiencies (>95%) and robustness against hydraulic stress. The second part of the study evaluated the effect of oil concentrations up to 500 mg L⁻¹ on nitrification performance. Elevated oil levels resulted in accumulation on the carrier media, leading to agglomeration, irregular biofilm structure, and increased biomass detachment. Despite these structural changes, ammonium removal efficiencies remained high and recovered rapidly after temporary declines. These findings indicated that oil mainly affected the physical structure of the biofilm rather than the overall nitrification performance, demonstrating the operational resilience of the MBBR system under high and fluctuating oil loads.

LIST OF CONTENTS

CHAPTER 1 INTRODUCTION.....	1
1.1 Motivation.....	1
1.2 Objectives.....	4
1.2.1 General Objectives.....	4
1.2.2 Specific Objectives.....	5
CHAPTER 2 LITERATURE REVIEW	6
2.1 Oil Refinery Wastewater.....	6
2.1.1 Characteristics of Wastewater from Oil Refineries	8
2.1.2 Treatment Stages.....	9
2.1.3 Brazilian Legislation on Industrial Wastewater Disposal	11
2.2 Tertiary Treatment of Wastewater.....	13
2.2.1 Microbial Growth in Biological Processes.....	13
2.2.2 Biological Organic Matter Removal	20
2.2.3 Biological Nitrogen Removal.....	23
2.2.3.1 Nitrogen Pollution in Wastewater Systems	23
2.2.3.2 Nitrogen cycle.....	25
2.2.3.3 Nitrification.....	26
2.3 Moving Bed Biofilm Reactor (MBBR)	30
2.3.1 Basic Characteristics of the MBBR	31
2.3.2 Factors Affecting MBBR Performance.....	34
2.4 Overview of Previous Studies on Biological Treatment of Oil Refinery Wastewater	38
CHAPTER 3 MATERIALS AND METHODS	41
3.1 Wastewater Source and Characteristics	41
3.2 Moving-Bed Biofilm Reactors.....	44

3.2.1 Experimental Setup	44
3.2.2 Start-up of MBBRs	46
3.3 Operational Phases of MBBRs.....	47
3.3.1 Part I: Development of Stable Nitrifying Biofilm under Variable COD and HRT Conditions	48
3.3.2 Part II: Effect of Oil Concentration on Nitrification.....	51
3.3.2.1 Oil Emulsification Procedure.....	51
3.5 Analytical Methods.....	53
3.5.1 Total Suspended (TSS), Fixed (FSS), and Volatile Solids (VSS)	55
3.5.2 Total Attached (TAS), Fixed (FAS), and Volatile Solids (VAS).....	56
3.5.3 Biofilm Visualization and Thickness Measurement	56
3.5.4 Determination of Oil Concentration.....	57
3.6 Assessment of Maximum Nitrifying Activity in Batch Trials.....	57
3.7 Calculations.....	58
3.7.1 Removal Efficiency.....	58
3.7.2 Nitrogen Mass Balance	58
3.7.3 Biofilm Surface-Specific Detachment Rate	59
3.7.4 Surface Loading Rate (SLR)	59
CHAPTER 4 RESULTS AND DISCUSSION	60
4.1 Part I: Development of Stable Nitrifying Biofilm under Variable COD and HRT Conditions.....	60
4.1.1 Organic Matter Removal	60
4.1.2 Nitrification Performance and Oxidized Nitrogen Species Distribution	62
4.1.3 Batch Assessment of Nitrification Activity.....	75
4.1.4 Attached and Suspended Solids Assessment.....	86
4.1.5 Visual Observation of Attached Biomass and Biofilm Thickness.....	93

4.1.6 Microscopic Visualization of Biofilm.....	97
4.1.7 Operational Parameters: pH and Temperature.....	100
4.2 Part II: Effect of Oil Concentration on Nitrification	102
4.2.1 Visual Observation.....	102
4.2.2 Biofilm Behavior and Solids Dynamics	104
4.2.3 Nitrification Performance	111
4.2.4 Batch Trials.....	116
4.2.5 Operational Parameters: pH and Temperature.....	118
CHAPTER 5 CONCLUSIONS	120
5.1 Conclusions of Part I	120
5.2 Conclusions of Part II	122
5.3 Suggestions for Future Works.....	123
CHAPTER 6 REFERENCES.....	125

LIST OF FIGURES

Figure 1 - Categories of oil droplets commonly found in oily wastewater streams. Source: OTITOJU <i>et al.</i> , 2016.	8
Figure 2 - A simplified schematic representation of the wastewater treatment processes. Source: BAHADORI, 2020.	10
Figure 3 - Basic schematic of an activated sludge system. Source: KAYSER, 2004. ...	14
Figure 4- Composition of EPS in biofilms. Source: MAURYA, RAJ, 2020.	15
Figure 5 - Formation, development, and aging of biofilm in wastewater treatment. Source: HUANG <i>et al.</i> , 2019.	17
Figure 6 - Schematic representation of the main types of biofilm formation in wastewater environments. Source: MAURYA <i>et al.</i> , 2023.	17
Figure 7 - An overview of bacterial biofilm formation, the factors influencing it, and its potential applications. Source: MAURYA <i>et al.</i> , 2023.	18
Figure 8 - Schematic diagrams of the biofilm structure and typical concentration profiles of the limiting substrates. Source: LI, LIU, 2019.	19
Figure 9 - Simplified process of aerobic degradation of organic substances by bacteria. Source: adapted from DEZOTTI (2008).	22
Figure 10- Microbial nitrogen transformations occurring above, below, and across the oxic–anoxic interface in aquatic environments are illustrated, with nitrite highlighted in red to underscore its central role as a key metabolic intermediate linking multiple nitrogen cycling pathways. Source: adapted from FRANCIS <i>et al.</i> (2007).	25
Figure 11 - Variation in the oxidation state of the nitrogen atom during the complete nitrification process. Source: adapted from VAN HAANDEL and VAN DER LUBBE (2012).	27
Figure 12 - The published literature on MBBR applications for wastewater treatment from 2000 to 2025. Source: Scopus database.	31
Figure 13 - Schematic representation of a typical MBBR, in which the biofilm carriers are maintained in suspension by (a) aeration in aerobic systems or (b) mechanical mixing in anoxic or anaerobic systems, and (c) axes of rotation of a typical biofilm carrier in a	

generic MBBR system. Source: BASSIN, DEZOTTI., 2018; DEENA <i>et al.</i> , 2022; RUSTEN <i>et al.</i> , 2006.	32
Figure 14 - Reaction mechanisms of the MBBR process under aerated conditions for the removal of organic matter and nutrients. Source: GUPTA <i>et al.</i> , 2022.....	34
Figure 15 – Diagram of the real oil refinery wastewater treatment plant.	42
Figure 16 - Visual comparison of real oil refinery effluent (left) versus synthetic wastewater (right).	43
Figure 17 – (a) Schematic view of the MBBR system and (b) the lab-scale MBBR system experimental set-up.....	44
Figure 18 - MBBR2 during the inoculation period.....	46
Figure 19 - Preparation and homogenization of oily wastewater influent using high-speed ULTRA-TURRAX mixing.....	52
Figure 20 - Schematic view of MBBR4 during the operation with oil.....	53
Figure 21 - COD concentrations in the influent and effluent of the reactors and removal efficiency throughout the operational phases. The vertical lines indicate transitions between experimental phases: a) MBBR1, b) MBBR2, c) MBBR3, and d) MBBR4....	62
Figure 22 - Evolution of ammonium removal efficiency and corresponding influent and effluent oxidized nitrogen species during the operational phases of the MBBR systems: a-b) MBBR1, c-d) MBBR2, e-f) MBBR3, and g-h) MBBR4.....	64
Figure 23 - Average Influent (I) and Effluent (E) nitrogen species profiles in MBBR systems across operational phases: a) MBBR1, b) MBBR2, c) MBBR3, and d) MBBR4.	65
Figure 24 - Average ammonium surface loading rate (SLR) and ammonium surface removal rate (SRR) for all reactors throughout the operational phases: a) MBBR1, b) MBBR2, c) MBBR3, and d) MBBR4.....	72
Figure 25 - Correlation between ammonium SLR and SRR for all reactors: a) MBBR1, b) MBBR2, c) MBBR3, and d) MBBR4.....	74
Figure 26 - Temporal profiles of nitrogen species in MBBR1 obtained during the activity batch tests corresponding to phases P2–P6.	77

Figure 27 - Temporal profiles of nitrogen species in MBBR2 obtained during the activity batch tests corresponding to phases P2–P8.	78
Figure 28 - Temporal profiles of nitrogen species in MBBR3 obtained during activity batch tests corresponding to phases P1–P7.	79
Figure 29 - Temporal profiles of nitrogen species in MBBR4 obtained during activity batch tests corresponding to phases P1–P3.	80
Figure 30 - Temporal variation of volatile attached solids (VAS) and fixed attached solids (FAS)), and the VAS/TAS ratio and average biofilm surface-specific detachment rate (k_d) determined for experimental phases applied to each reactor: a-b) MBBR1, c-d) MBBR2, e-f) MBBR3, and g-h) MBBR4. TAS represents the sum of VAS and FAS.	87
Figure 31 - Concentration of total, volatile, and fixed suspended solids in the influent (I) and effluent (E) throughout the operational phases: a) MBBR1, b) MBBR2, c) MBBR3, and d) MBBR4. (TSS = VSS + FSS).	91
Figure 32 - Temporal distribution of total attached solids (TAS), total suspended solids (TSS), and TAS/TS ratio in reactors: a) MBBR1, b) MBBR2, c) MBBR3, and d) MBBR4. TS represents the sum of TAS and TSS.	92
Figure 33 - (a) Biofilm thickness variation over time under different COD concentrations, and visual assessment of biofilm development on carriers in the MBBRs over the experimental phases: (b) MBBR1, (c) MBBR2, (d) MBBR3, and (e) MBBR4.	95
Figure 34 - Average biofilm thickness across operational phases of the reactors: (a) MBBR1, (b) MBBR2, (c) MBBR3, and (d) MBBR4.	96
Figure 35 - Optical micrographs (400× magnification) obtained during different operational phases of the reactors: (a) MBBR1, (b) MBBR2, (c) MBBR3, and (d) MBBR4.	99
Figure 36 - pH values recorded throughout the reactors operating periods, with phase transitions indicated by vertical dashed lines. Upper and lower limits defining optimal nitrification performance are shown as dotted horizontal lines: a) MBBR1, b) MBBR2, c) MBBR3, and d) MBBR4.	101
Figure 37 - Visual observation of MBBR4 before and after exposure to high oil loading (300–500 mg L ⁻¹).	103

Figure 38 - Visual appearance of MBBR4 under high oil concentrations (300–500 mg L ⁻¹), showing carrier agglomeration and accumulation of solids.....	104
Figure 39 - Biofilm behavior and solids distribution in MBBR4 during phases P3–P7: (a) Variation of suspended solids in the influent (I) and effluent (E), (b) Biofilm specific surface detachment rate, (c) Oil concentrations in influent, effluent, and biofilm carriers, as well as oil reduction percentage.	106
Figure 40 - Dynamics of attached and suspended biomass in MBBR4 during P3-P7: (a) Temporal variation of volatile attached solids (VAS), fixed attached solids (FAS), and the VAS/TAS ratio, (b) Temporal distribution of total attached solids (TAS), total suspended solids (TSS), and TAS/TS ratio in the reactor. TS represents the sum of TAS and TSS.	107
Figure 41 - (a) Visual characterization of biofilm development on Kaldnes K1 carriers in MBBR4 during P3–P7 and (b) average biofilm thickness across operational phases..	108
Figure 42 - Optical micrographs (400× and 1000× magnification) obtained during P3-P7 from MBBR4.....	111
Figure 43 - (a) Evolution of ammonium removal efficiency and (b) corresponding influent and effluent oxidized nitrogen species during the operational phases of MBBR4.....	113
Figure 44 - Average Influent (I) and Effluent (E) nitrogen species profiles in MBBR4 across operational phases.	114
Figure 45 - (a) Average ammonium surface loading rate (SLR) and ammonium removal rate (SRR), and (b) relationship between ammonium SLR and SRR in MBBR4 during P3–P7.	115
Figure 46 - Temporal profiles of nitrogen species in MBBR4 obtained during batch tests corresponding to phases P3, P5, P6, and P7.....	118
Figure 47 - pH values recorded throughout the MBBR4 operational period with oil addition. Upper and lower discharge limits defining optimal nitrification performance are shown as dotted horizontal lines.....	119

LIST OF TABLES

Table 1- Refining capacity of Brazilian refineries. Source: adapted from PETROBRAS (2026).	6
Table 2 - Wastewater sources from petroleum refinery processing units. Source: adapted from THORAT and SONWANI (2022).	7
Table 3 - Significance of contaminants in wastewater treatment. Source: adapted from BAHADORI (2020).	9
Table 4 - General wastewater discharge standards.	12
Table 5 - Advantages and limitations of activated sludge and MBBR systems. Source: adapted from KAWAN <i>et al.</i> (2016).	33
Table 6 - Key characteristics of selected Kaldnes® biofilm carriers. Source: adapted from BASSIN, DEZOTTI (2018).	35
Table 7 - Overview of Previous Studies on Biological Treatment of Oil Refinery Wastewater	39
Table 8 - Characteristics of the refinery wastewater.	43
Table 9 - Physical and structural characteristics of the K1 carrier used in the biological reactors. Source: adapted from RUSTEN <i>et al.</i> (2006).	45
Table 10 - Experimental conditions of the MBBR1, MBBR2, MBBR3, and MBBR4 during the entire operational period.	50
Table 11 - Operational phases of MBBR4 during the operation with oil.	51
Table 12 - Analytical methods applied throughout the experimental operations of MBBRs.	54
Table 13 - Ammonium removal and specific ammonium removal rate obtained in all experimental phases of MBBR1, MBBR2, MBBR3, and MBBR4.	84
Table 14 – pH and temperature evaluated at the beginning and end of the batch activity tests.	85
Table 15 - Biofilm thickness in nitrifying MBBR systems.	97

Table 16 - Ammonium removal and specific ammonium removal rate obtained during P3-P7 of MBBR4.....	117
Table 17 - Parameters evaluated at the beginning and end of the activity batch tests..	119

SYMBOLS

AOB	Ammonia-Oxidizing Bacteria
BOD	Biological Oxygen Demand
COD	Chemical Oxygen Demand
EPS	Extracellular Polymeric Substances
FAS	Fixed Attached Solids
FSS	Fixed Suspended Solids
HRT	Hydraulic Retention Time
MBBR	Moving Bed Biofilm Reactor
$\text{NH}_4^+\text{-N}$	Ammoniacal Nitrogen
NOB	Nitrite-Oxidizing Bacteria
$\text{NO}_2^-\text{-N}$	Nitrogen-Nitrite
$\text{NO}_3^-\text{-N}$	Nitrogen-Nitrate
RW	Real Wastewater
SLR	Surface Loading Rate
SW	Synthetic Wastewater
TS	Total Solids (attached and suspended)
TSS	Total Suspended Solids
VAS	Volatile Attached Solids
VS	Volatile Solids (attached and suspended)

CHAPTER 1

INTRODUCTION

1.1 Motivation

Water is essential for sustaining life, as it constitutes a fundamental requirement for all living organisms; however, rapid industrialization and population growth have intensified wastewater generation. Petroleum refineries, although vital to economic development, are among the major sources of inadequately treated industrial wastewaters (ELMOBARAK *et al.*, 2021). Wastewater produced throughout these petroleum refining processes contains numerous toxic compounds, including polyaromatic hydrocarbons, phenols, heavy metals, and ammonia. Among these contaminants, ammonium nitrogen is one of the main pollutants due to its significant environmental and public health implications. Elevated ammonium levels contribute to eutrophication, oxygen depletion in receiving waters, and toxicity to aquatic organisms (FANG *et al.*, 1993, FIGUEROLA, ERIJMAN, 2010, KUMAR *et al.*, 2022).

Biological nitrogen removal is widely applied in wastewater treatment due to its high efficiency and cost-effectiveness (ZHANG *et al.*, 2024). Nitrification is typically the rate-limiting step in the biological nitrogen removal, being carried out by two main functional groups: ammonium-oxidizing bacteria (AOB) and nitrite-oxidizing bacteria (NOB). The first group oxidizes ammonium to nitrite, a process known as nitrification, while the second group is responsible for converting nitrite to nitrate (nitrification) (METCALF & EDDY, 2003). Nitrification is generally regarded as a viable process for ammonium removal and has been effectively applied to treat domestic sewage, aquaculture wastewater, and other types of easily biodegradable wastewater. However, removing ammonium by nitrification from wastewater generated by chemical industries can be challenging due to its complex composition and the presence of potentially inhibitory compounds (BASSIN *et al.*, 2011).

In most cases, biological treatment processes remain the preferred option for a wide range of wastewater. Microorganisms can grow either in suspension or attached to surfaces, with biofilm-based processes gaining increasing attention for municipal and industrial wastewater treatment. Biofilm reactors provide higher biomass retention and

enhanced stability under variations in loading rate, temperature, and toxicity, while simplifying solids separation compared to conventional suspended-growth systems (BASSIN, DEZOTTI, 2018). Biofilms consist of complex and heterogeneous microbial communities embedded within a self-produced matrix of extracellular polymeric substances (EPS), composed of proteins, polysaccharides, nucleic acids, lipids, and various other biopolymers and humic substances. Biofilm formation on biocarrier surfaces occurs through cell attachment and subsequent growth, eventually developing into a mature, structured layer (FLEMMING *et al.*, 2016).

The Moving Bed Biofilm Reactor (MBBR) is an advanced biofilm-based technology that has gained considerable attention over the past two decades. Developed in Norway in the early 1980s, MBBR was introduced as a compact and efficient solution for the removal of organic matter and nitrogen (ØDEGAARD *et al.*, 2000). The process integrates features of conventional activated sludge and biofilter systems, employing moving plastic carriers that support biofilm formation and high biomass retention. Compared with other biofilm-based fixed bed reactors, MBBRs exhibit minimal head loss, require no periodic backwashing, and are not prone to clogging (ØDEGAARD, 2006, RUSTEN *et al.*, 2006).

Research on nitrification in MBBRs highlights several parameters that strongly influence performance. Hydraulic retention time (HRT) is a critical factor, as it directly affects nitrification efficiency (WU *et al.*, 2023). Chemical oxygen demand (COD) also plays a key role: higher organic loads tend to suppress nitrification because heterotrophic bacteria outcompete nitrifiers for oxygen and space in the biofilm (TORKAMAN *et al.*, 2015). Furthermore, operational conditions shape biofilm development and microbial community dynamics. The presence of organic carbon during startup can accelerate the formation of stable nitrifying biofilms due to the EPS produced by fast-growing heterotrophs. As COD levels decrease, heterotrophic biofilm sloughing occurs, ultimately favoring the enrichment of nitrifying populations (BASSIN *et al.*, 2012).

Most studies on MBBRs have been conducted under carbon-rich or balanced C/N conditions (CAO *et al.*, 2016, WANG *et al.*, 2023, ZHANG *et al.*, 2024). Under such conditions, Pourrostami Niavol *et al.* (2025) reported that lowering the C/N ratio from 20 to 10 and 7 reduced NH_4^+ -N removal, indicating that proper C/N control is essential for maintaining nitrification efficiency. However, conventional tertiary applications differ substantially from these conditions. In tertiary treatment, applied post-secondary

treatment to produce high-quality effluent, the limited biodegradable carbon restricts heterotrophic growth and shifts biofilm development toward nitrifying populations (SINGH, SHIKHA, 2019). MBBRs have demonstrated effective tertiary nitrification, achieving significant ammonium removal under diverse conditions (HOUDA *et al.*, 2015, SALVETTI *et al.*, 2006, YOUNG *et al.*, 2016). Specifically, Shore *et al.* (2012) demonstrated that MBBR systems can achieve >90–95% ammonia removal in high-temperature industrial wastewater (35–45 °C), consistently producing effluent below 1 mg N L⁻¹. Bassin *et al.* (2011) further validated MBBR's performance, showing tertiary nitrification effectiveness in industrial wastewaters with high salinity. Despite these promising results, studies addressing tertiary MBBRs treating real industrial wastewater remain scarce, as most existing research relies on synthetic wastewater, which does not reflect the complexity of real matrices. Under these conditions, the effects of microconstituents, organic matter, and water matrix interferences are often overlooked (ASHKANANI *et al.*, 2019), which raises concerns about the validity of the results in the real-world context.

Among industrial streams, oil refinery wastewater represents a particularly complex matrix for tertiary nitrification. In addition to ammonium, these wastewaters retain a diverse array of contaminants, such as petroleum hydrocarbons, phenols, sulfides, and various organic and inorganic compounds, even after secondary treatment. The biological treatment of such wastewater is inherently challenging, as these residual constituents can collectively alter biofilm behavior compared to idealized experimental conditions (JAFARINEJAD, 2019; SHETTIMA LAWAN *et al.*, 2023). Of particular concern within this mixture is the residual oil fraction. In certain cases, oil and grease can negatively impact receiving waters by exerting toxic effects and inhibiting nitrification. Furthermore, they may impair the oxygen transfer capacity of the water body (BAHADORI, 2020). However, the magnitude of this inhibition is determined by the intensity of the oil load increase and the resilience and adaptive capacity of the nitrifying microbial community (GALI *et al.*, 2005). In petroleum refineries, sudden increases in pollutant concentrations may occur due to accidental spills, operational changes, or fluctuations in production, leading to shock loads that can disrupt biological processes (MALLICK, CHAKRABORTY, 2021). In addition, although the inhibitory nature of oil on biological treatment is recognized, the specific effects of increasing oil loads on nitrification performance, particularly under tertiary treatment conditions, remain

insufficiently understood. This lack of knowledge highlights the need for systematic investigation into the response and stability of nitrifying systems subjected to elevated oil loading, providing the basis and motivation for the present study.

Considering these aspects, this study investigated tertiary nitrification in MBBRs treating oil refinery wastewater. Four lab-scale MBBRs were operated under distinct acclimation strategies, either gradually shifting from synthetic to real wastewater or directly treating refinery wastewater post-secondary stage, while being subjected to progressive reductions in HRT and elevated oil load. Alongside reactor performance, biofilm dynamics were monitored through thickness measurements, solids analysis, and microscopic evaluation. The novelty of this work lies in demonstrating the adaptability and resilience of nitrifying biofilms under real industrial wastewater conditions, highlighting operational strategies that support stable nitrification despite inhibitory compounds like oil, low carbon availability, and hydraulic stress, contributing to the advancement of tertiary biological polishing technologies and highlighting the potential of MBBRs as robust and sustainable systems for industrial wastewater treatment.

1.2 Objectives

1.2.1 General Objectives

The main goal of the research was to investigate the performance, stability, and resilience of tertiary nitrification in moving bed biofilm reactors treating oil refinery wastewater, evaluating the adaptability of nitrifying biofilms under real industrial conditions, and addressing the operational strategies that support stable nitrification despite the presence of inhibitory compounds (such as oil), low carbon availability, and hydraulic stress.

1.2.2 Specific Objectives

- ✓ To investigate the influence of different startup and acclimation strategies on biofilm formation, microbial adaptation, and nitrification stability in MBBR systems;
- ✓ To evaluate the impact of biodegradable organic carbon on biofilm development, heterotrophic competition, and the biomass-specific ammonium removal capacity of nitrifying biofilms;
- ✓ To assess the resilience of nitrifying communities under reduced hydraulic retention times;
- ✓ To analyze the structural behavior of the biofilm, including growth and detachment dynamics, as well as solids distribution over the carriers;
- ✓ To determine the impact of increasing influent oil concentrations on nitrification, biofilm stability, and reactor performance;
- ✓ To compare the performance of multiple MBBR configurations in terms of nitrification efficiency, operational stability, and adaptation to real oil refinery wastewater.

CHAPTER 2

LITERATURE REVIEW

2.1 Oil Refinery Wastewater

Oil and gas remain pivotal components of the global energy landscape and economic infrastructure. Given their status as premier industrial activities of the 21st century, the imperative for effective waste treatment and disposal within the petroleum, chemical, and unconventional sectors has intensified significantly (BAHADORI, 2020).

Petroleum refineries are complex factories that use many different steps to turn crude oil into finished products. Since each refinery processes a specific type of oil to create different goods, no two plants operate in the same way. These facilities also use much more water than most other industries, though the exact amount depends on the refinery's size, the oil it uses, and how complex its operations are (SINGH, SHIKHA, 2019). However, as a general guideline, petroleum refineries generate approximately 0.4 to 1.6 volumes of wastewater for every unit volume of crude oil processed (COELHO *et al.*, 2006). Table 1 presents the 11 Brazilian refineries along with their respective installed production capacities.

Table 1- Refining capacity of Brazilian refineries. Source: adapted from PETROBRAS (2026).

Refinery	Installed capacity (bbl day ⁻¹)
Abreu e Lima (Rnest)	230,000
Complexo de Energias Boaventura	21 million cubic meters of gas per day
Capuava (Recap)	53,000
Duque de Caxias (Reduc)	239,000
Alberto Pasqualini (Refap)	280
Gabriel Passos (Regap)	150,000
Presidente Getúlio Vargas (Repar)	207,563
Presidente Bernardes (RPBC)	178,000
Paulínia (Replan)	415,000
Henrique Lage (Revap)	252,000
Lubrificantes e Derivados do Nordeste Lubnor	8,000

Wastewater generated from the different unit operations and processing stages in petroleum refining can generally be classified into four main streams: (1) desalter wastewater originating from the desalter unit; (2) sour wastewater produced by processes such as atmospheric and vacuum distillation, fluidized catalytic cracking, stripping, and hydrotreating; (3) spent caustic wastewater arising from units including the Merox process, alkylation, ethylene production, and visbreaking; and (4) oily wastewater discharged from crude oil and slop storage tanks (THORAT, SONWANI, 2022). Table 2 presents a summary of the various wastewater sources associated with different units of a petroleum refinery:

Table 2 - Wastewater sources from petroleum refinery processing units. Source: adapted from THORAT and SONWANI (2022).

Unit	Description
Crude Desalting	This initial washing process removes salts and solids, generating wastewater heavily contaminated with free oil, ammonia, sulphides, suspended solids, and dissolved organics.
Atmospheric and Vacuum Distillation	These separation units use steam to isolate volatile products, producing sour water condensates rich in ammonia, hydrogen sulphide, chlorides, and phenols.
Hydrotreating	Designed to remove impurities from distillates using hydrogen, these units generate sour water containing high levels of ammonia, hydrogen sulphide, and phenols.
Catalytic Cracking (FCC)	This process breaks down heavy hydrocarbons into lighter products, releasing sour wastewater polluted with ammonia, hydrogen sulphide, oil, and spent catalyst particles.
Thermal Cracking	Operating under high pressure and temperature to crack hydrocarbons, this unit produces sour wastewater characterized by dissolved solids, phenols, ammonia, and high COD.
Alkylation	This unit uses strong acid catalysts (sulphuric or hydrofluoric acid) to produce high-octane fuel, generating acidic waste streams containing oil and sulphides.
Polymerization	Converts light olefin gases into liquid fuels using acid catalysts; the water scrubbing step generates wastewater containing sulphides, mercaptans, and ammonia.
Isomerization	Upgrades light naphtha using metal catalysts, producing both caustic wash water (containing calcium chloride) and sour water (containing ammonia and sulphides).
Amine Regeneration	Removes acid gases (H ₂ S and CO ₂) from process streams, discharging amine-rich wastewater that can be toxic to aquatic life.
Sulphur Recovery	Recovers elemental sulphur from sour gas (typically via the Claus process), producing effluents containing toxic and odorous sulphur compounds.

2.1.1 Characteristics of Wastewater from Oil Refineries

Wastewater generated by the petroleum industry contains complex mixtures of contaminants, such as petroleum hydrocarbons, phenols, ammonia, sulfides, and other organic compounds that make it particularly hazardous to the environment (ELMOBARAK *et al.*, 2021). This wastewater is also characterized by micrometer-sized oil droplets dispersed in the aqueous phase, forming a stable oil-in-water emulsion even in the absence of added stabilizing agents. In general, oil present in wastewater from refineries can be broadly categorized based on droplet size into three groups: free-floating oil ($>150\ \mu\text{m}$), dispersed oil ($20\text{--}150\ \mu\text{m}$), and emulsified oil ($<20\ \mu\text{m}$), as illustrated in Figure 1 (OTITOJU *et al.*, 2016). However, the solubility and concentration of these components in the aqueous phase are governed by factors such as oil composition, temperature, water salinity, and the water-to-oil volume ratio during contact (TANSEL *et al.*, 1995). Due to their persistence and toxicity, these oil fractions represent major pollutants in aquatic environments and pose serious risks to both environmental integrity and human health.

To assess such impacts and guide treatment strategies, wastewater is commonly characterized using a range of chemical and physical parameters, the most frequently applied of which are summarized in Table 3.

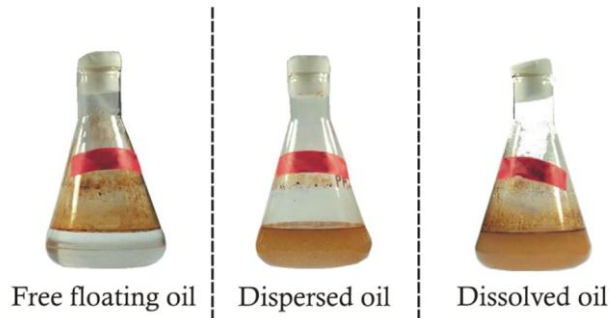


Figure 1 - Categories of oil droplets commonly found in oily wastewater streams. Source: OTITOJU *et al.*, 2016.

Table 3 - Significance of contaminants in wastewater treatment. Source: adapted from BAHADORI (2020).

Contaminant Category	Key Components & Examples	Environmental & Operational Implications
Physical Suspended Solids	Insoluble particles	<ul style="list-style-type: none"> • Creates sludge deposits. • Leads to anaerobic conditions. • Degrades the esthetic quality of water.
Biodegradable Organics	Proteins, carbohydrates, fats (Measured by biochemical oxygen demand (BOD) and COD)	<ul style="list-style-type: none"> • Decomposition consumes natural dissolved oxygen. • Can cause septic conditions in receiving waters.
Nutrients	Nitrogen, Phosphorus	<ul style="list-style-type: none"> • Aquatic: Triggers excessive growth of undesirable aquatic life (eutrophication). • Land: Excessive discharge can contaminate groundwater aquifers.
Refractory Organics	Surfactants, phenols, and agricultural pesticides	<ul style="list-style-type: none"> • These compounds resist standard biological treatment methods, making them difficult to remove.
Heavy Metals	Toxic metallic elements	<ul style="list-style-type: none"> • Toxicity can disrupt biological treatment processes.
Dissolved Inorganic Solids	Calcium, Sodium, Sulfate	<ul style="list-style-type: none"> • These are often added during domestic water use, and their presence complicates or prevents the reuse of wastewater
Biological Pathogens	Bacteria, Viruses, Protozoans	<ul style="list-style-type: none"> • Responsible for the transmission of communicable diseases.

2.1.2 Treatment Stages

A wastewater treatment plant is typically integrated into petroleum refineries to collect and treat the wastewater streams produced during crude oil processing (YOUNIS *et al.*, 2020).

Treating oily wastewater before environmental discharge is crucial, as its elevated organic and mineral content can lead to significant contamination of coastal waters, rivers, estuaries, shorelines, soils, and groundwater (UAN, 2013). Therefore, wastewater generated by petroleum refineries cannot be discharged directly into aquatic environments and must undergo sequential primary, secondary, and tertiary treatment processes to adequately remove the associated pollutant load (BAHADORI, 2020; SINGH, SHIKHA, 2019). Figure 2 illustrates the typical processes to which the wastewater is subjected.

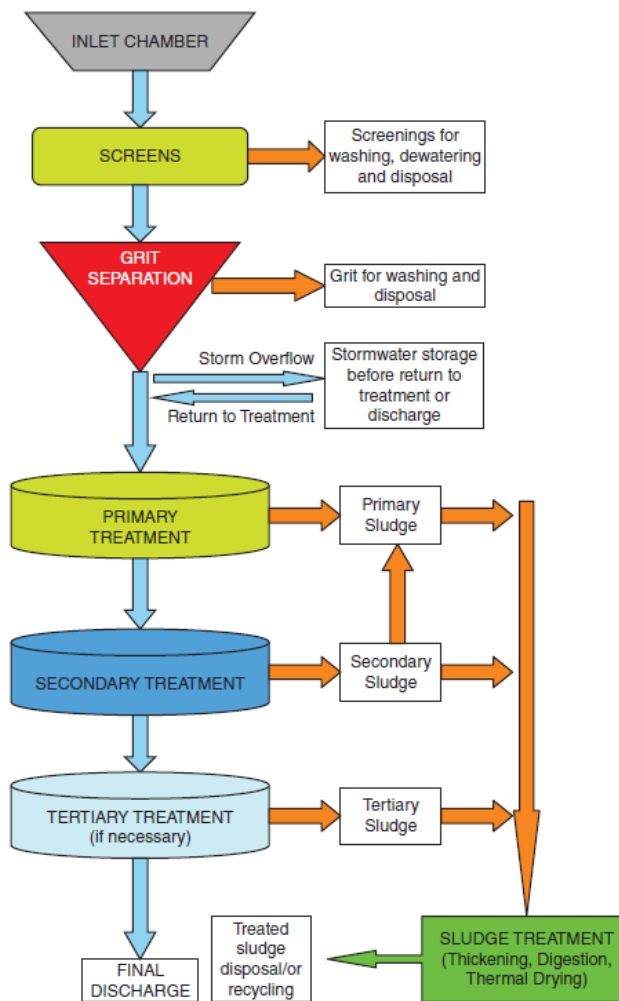


Figure 2 - A simplified schematic representation of the wastewater treatment processes. Source: BAHADORI, 2020.

Petroleum refinery wastewater requires a multistage treatment approach due to its complex composition. Primary treatment removes floating and settleable materials such as oil, grease, and suspended solids using physical processes, achieving partial reductions in COD/BOD and settleable solids (ALJUBOURY *et al.*, 2017; ENGLANDE *et al.*, 2015). The primary treatment stage mainly involves an oil–water separator, in which oil, water, and solid particles are separated. This is followed by a secondary separation step using dissolved air flotation (DAF) or induced air flotation (IAF) units to further remove residual contaminants (SINGH, SHIKHA, 2019).

Secondary treatment primarily targets dissolved oil, biodegradable organic pollutants, and nutrients (e.g., nitrogen and phosphorus) through biological processes, where microorganisms convert organic matter into stable end products such as H₂O, CH₄,

and CO₂. These systems may operate as suspended- or attached-growth processes and require adequate nutrient availability (BAHADORI, 2020; SONWANI *et al.*, 2019; U.S. EPA, 1995).

Tertiary treatment comprises further advanced water depuration processes applied to secondary treated effluents to meet specific discharge or reuse requirements. This stage provides additional polishing by removing residual contaminants that are not adequately eliminated during conventional treatment, including trace organics, dissolved solids, metals, and pathogens. Typical tertiary processes include chemical treatments and pressure-driven filtration, and this stage is therefore commonly referred to as advanced wastewater treatment (BAHADORI, 2020).

2.1.3 Brazilian Legislation on Industrial Wastewater Disposal

Wastewater discharge in Brazil is regulated at the federal level by CONAMA Resolution 430 (Brazil, 2011), which expands upon the provisions of CONAMA Resolution 357 (Brazil, 2005). In addition, state regulations are required to meet or exceed federal standards, with NT-202.R-10 (INEA, 1986) and DZ-205.R-6 (INEA, 2007) governing this framework in Rio de Janeiro State.

Table 4 provides an overview of the general wastewater discharge standards established by CONAMA.

Table 4 - General wastewater discharge standards.

Parameter	Limit / Condition
pH	Between 5.0 and 9.0
Temperature	Less than 40°C (and must not raise the receiving body's temperature by more than 3°C)
Settleable Solids	Up to 1 mL L ⁻¹ in a 1-hour test in an Imhoff cone.
Floating Materials	Virtually absent
Oils & Greases (Mineral)	Up to 20 mg L ⁻¹
Oils & Greases (Veg/Animal)	Up to 50 mg L ⁻¹
BOD (Biochemical Oxygen Demand)	Minimum removal of 60% (unless the water body has high self-depuration capacity)
Total Ammoniacal Nitrogen	Up to 20.0 mg L ⁻¹
Total Phenols	0.5 mg L ⁻¹
Sulfide	1.0 mg L ⁻¹
Benzene	1.2 mg L ⁻¹
Toluene	1.2 mg L ⁻¹
Xylene	1.6 mg L ⁻¹
Ethylbenzene	0.84 mg L ⁻¹
Arsenic (Total)	0.5 mg L ⁻¹
Mercury (Total)	0.01 mg L ⁻¹
Cadmium (Total)	0.2 mg L ⁻¹

2.2 Tertiary Treatment of Wastewater

While secondary treatment efficiently reduces bulk organic loads, it often proves insufficient for meeting stringent discharge limits regarding specific residual pollutants. Secondary effluents frequently retain inorganic nutrients, primarily nitrogen and phosphorus, along with emerging contaminants and microbial pathogens, all of which pose significant risks to receiving water bodies. To mitigate these deleterious effects and meet the rigorous quality criteria required for water reuse, advanced purification steps known as tertiary treatment are essential (BHANDARI, RANADE, 2014; HOLMES *et al.*, 2019; ZAGKLIS, BAMPOS, 2022).

A wide range of technologies is available for the tertiary treatment of refinery wastewater, with biological processes playing a particularly important role. Biological treatment is widely recognized as one of the most practical and cost-effective approaches for industrial wastewater management, as it generally requires lower capital investment and operational costs than physicochemical alternatives (NAGDA *et al.*, 2021). In addition, biological processes can be successfully applied to the treatment of oily wastewaters (AL-ATTABI, 2018). Biological wastewater treatment relies on bacteria and other microorganisms to remove pollutants by assimilating and transforming them into less harmful compounds. Consequently, treatment strategies based on bacteria, fungi, plants, and other living organisms constitute sustainable and economically viable solutions for reducing the polluting potential of secondary treated effluents and promoting environmental recovery (MEENA *et al.*, 2019; SANTO *et al.*, 2013).

2.2.1 Microbial Growth in Biological Processes

Biological treatment processes are commonly distinguished based on how microorganisms grow, with biomass developing either as suspended solids in the liquid phase or as biofilm attached to support media.

One of the most commonly applied suspended-growth systems is the activated sludge process. This process originated in the early 1900s from studies on wastewater aeration (Figure 3). Arden and Lockett demonstrated that repeated cycles of aeration and settling led to the accumulation of biomass capable of achieving complete nitrification, which they termed activated sludge. Activated sludge is defined as a suspension of microorganisms, both living and dead, in wastewater, whose activity is sustained by the

continuous supply of air; under these conditions, organic matter is metabolized into stable end products and new microbial biomass (Singh; Shikha, 2019).

The first full-scale system operated in a fill-and-draw mode, later known as the sequencing batch reactor (SBR) process, but operational challenges led to the adoption of continuous-flow configurations (KAYSER, 2004). In a conventional activated sludge system, wastewater is treated in an aeration tank where it is continuously mixed with a high concentration of microorganisms, known as mixed liquor suspended solids (MLSS) or mixed liquor volatile suspended solids (MLVSS). This biomass is mainly composed of floc-forming bacterial aggregates, typically ranging from 50 to 200 μm in size, and is maintained under aerobic conditions for sufficient contact time to promote organic matter degradation. The treated effluent then flows to a final clarifier, where the biomass is separated by settling. Part of the settled sludge is recirculated to the aeration tank to sustain biological activity, while excess sludge is removed to control biomass concentration in the system (KAYSER, 2004). Activated sludge has been demonstrated to be an effective and well-established treatment technology in the oil refinery industry (ZABERMAWI, BESTAWY, 2024).

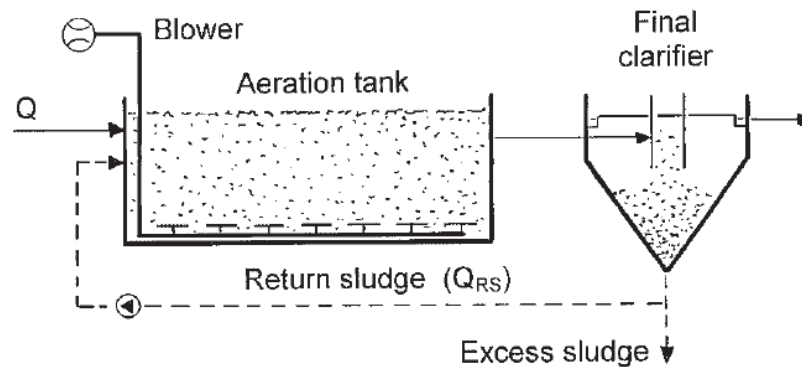


Figure 3 - Basic schematic of an activated sludge system. Source: KAYSER, 2004.

Despite its widespread application and effectiveness, the conventional activated sludge process presents several disadvantages. It typically requires large installation areas due to the need for extensive settling tanks and the low concentration of biomass in the aeration basins. In addition, the process generates significant amounts of excess sludge, shows high sensitivity to fluctuations in organic loading, and exhibits relatively low

volumetric treatment capacity. Its performance is strongly dependent on good sludge settling properties, and poor floc formation, often associated with excessive growth of filamentous microorganisms or unfavorable operational conditions, can lead to biomass washout from clarifiers and deterioration of effluent quality, particularly when treating complex industrial wastewaters (BASSIN, DEZOTTI, 2018; GÜVEN *et al.*, 2023).

In attached-growth systems, microbial communities develop as biofilms on inert carrier materials rather than remaining suspended in the liquid phase. A biofilm can be described as a structured microbial community in which microorganisms adhere to living or inert surfaces and are embedded within a self-produced matrix of extracellular polymeric substances (EPS). EPS is composed of a variety of components, including proteins, polysaccharides, nucleic acids, lipids, surfactants, and humic substances (Figure 4). This matrix promotes cell-to-cell adhesion as well as attachment to solid surfaces or interfaces, creating a stable and organized mode of growth distinct from planktonic microorganisms suspended in the liquid phase (MAURYA, RAJ, 2020; SINGH *et al.*, 2020; UNAL TURHAN *et al.*, 2019).

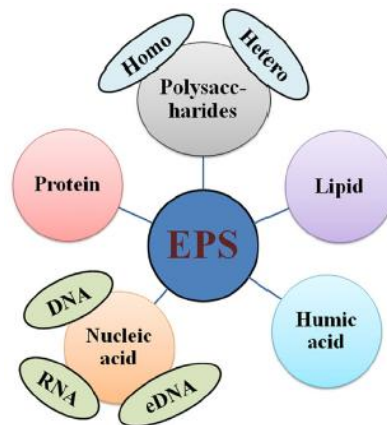


Figure 4- Composition of EPS in biofilms. Source: MAURYA, RAJ, 2020.

Among biological treatment technologies, biofilm-based processes have demonstrated strong effectiveness in removing toxic, recalcitrant, and carcinogenic contaminants from wastewater. Due to their robustness and high microbial retention, biofilms are increasingly exploited in water and wastewater treatment technologies. At the same time, their persistence can be detrimental in industrial processes and civil

infrastructure, where they may cause material degradation, corrosion, and hydraulic head losses. Growth in a biofilm provides several advantages to microorganisms, including protection against predation and toxic chemicals, as well as enhanced resistance to dehydration, enabling persistence at gas–liquid interfaces. Biofilms also act as reservoirs of nutrients, since enzymes retained within the extracellular matrix can degrade complex organic compounds into simpler, more readily metabolizable substrates. In addition, the high cell density within biofilms facilitates horizontal gene transfer. This robustness makes biofilms particularly attractive for wastewater treatment and other biotechnological applications, while at the same time posing significant challenges in settings where biofilm formation must be controlled (BUTLER, BOLTZ, 2014; LAZAROVA, MANEM, 1995).

Biofilm formation occurs through a sequence of well-defined steps (Figure 5). Initially, organic and inorganic molecules adsorb onto a surface, forming a conditioning film that modifies surface properties and provides nutrients for microbial attachment. This is followed by the attachment of microorganisms to the conditioned surface. Subsequently, attached cells produce extracellular polymeric substances, which bind the cells together and to the surface, leading to the development of a structured and mature biofilm. These stages are commonly described as adsorption, attachment, and biofilm maturation/colonization, although the terminology may vary in the literature (ALI, AZIZ, 2024). Biofilm development and maturation primarily involve microbial growth and accumulation on the surface. As biofilm systems continue to operate, the biofilm layer becomes progressively thicker, which can hinder nutrient and mass transfer. This limitation leads to reduced microbial activity and lower treatment efficiency, a condition commonly referred to as biofilm aging. The detachment of aged biofilm through erosion and sloughing plays a crucial role in restoring biofilm activity and maintaining system performance (HUANG *et al.*, 2019).

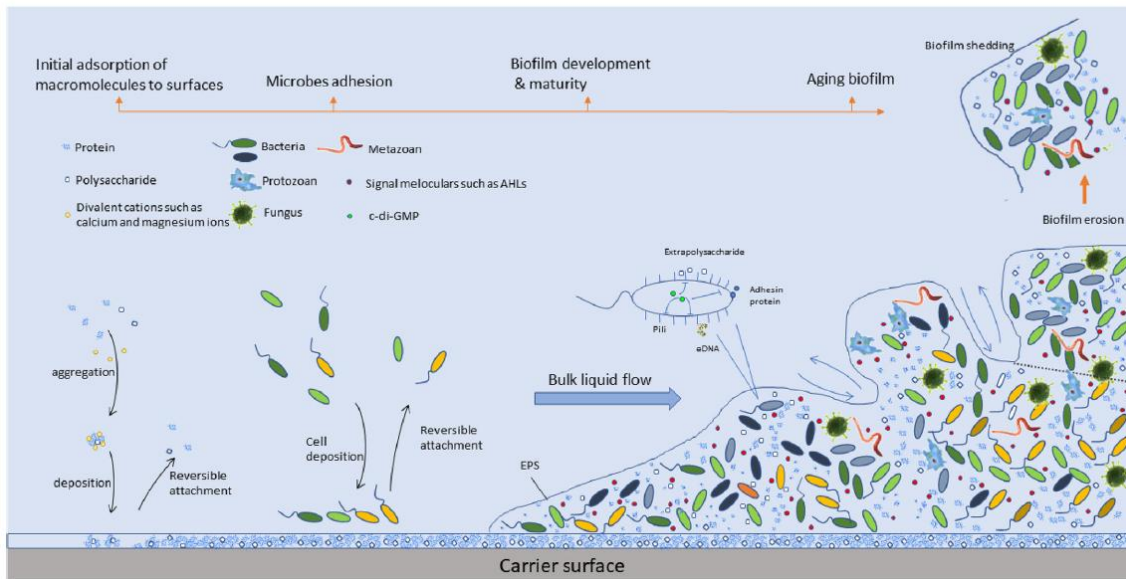


Figure 5 - Formation, development, and aging of biofilm in wastewater treatment. Source: HUANG *et al.*, 2019.

Wastewater treatment systems can host various forms of bacterial biofilms, including: (i) biomass attached to solid surfaces, known as submerged or attached biofilms; (ii) suspended, unattached microbial aggregates in the liquid phase, referred to as flocs; (iii) macroscopic, mat-like structures formed at air–liquid interfaces, known as pellicles; and (iv) dense microbial aggregates developing at liquid–liquid interfaces, commonly called granules (AQEEL *et al.*, 2019; RAJITHA *et al.*, 2020; MAURYA *et al.*, 2023) (Figure 6).

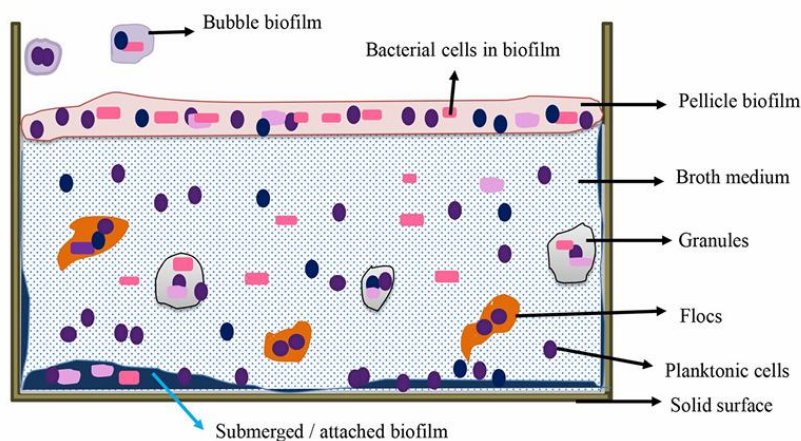


Figure 6 - Schematic representation of the main types of biofilm formation in wastewater environments. Source: MAURYA *et al.*, 2023.

The performance of biofilm-based systems is strongly governed by the efficiency of biofilm formation, which is influenced by both biotic and abiotic factors. These include the diversity of the microbial community, the physical properties of the carrier surface, such as surface energy and electrostatic interactions affecting bacterial adhesion, the surface topography and roughness, and the chemical characteristics of the carrier material, including the presence of functional groups. Environmental conditions, particularly pH and temperature, also play an important role (KERR *et al.*, 2003; MURSHID *et al.*, 2023). Figure 7 provides a schematic overview of biofilm formation, key regulating factors, EPS functions, types of biofilms, associated impacts, and their other main applications and reactor configurations.

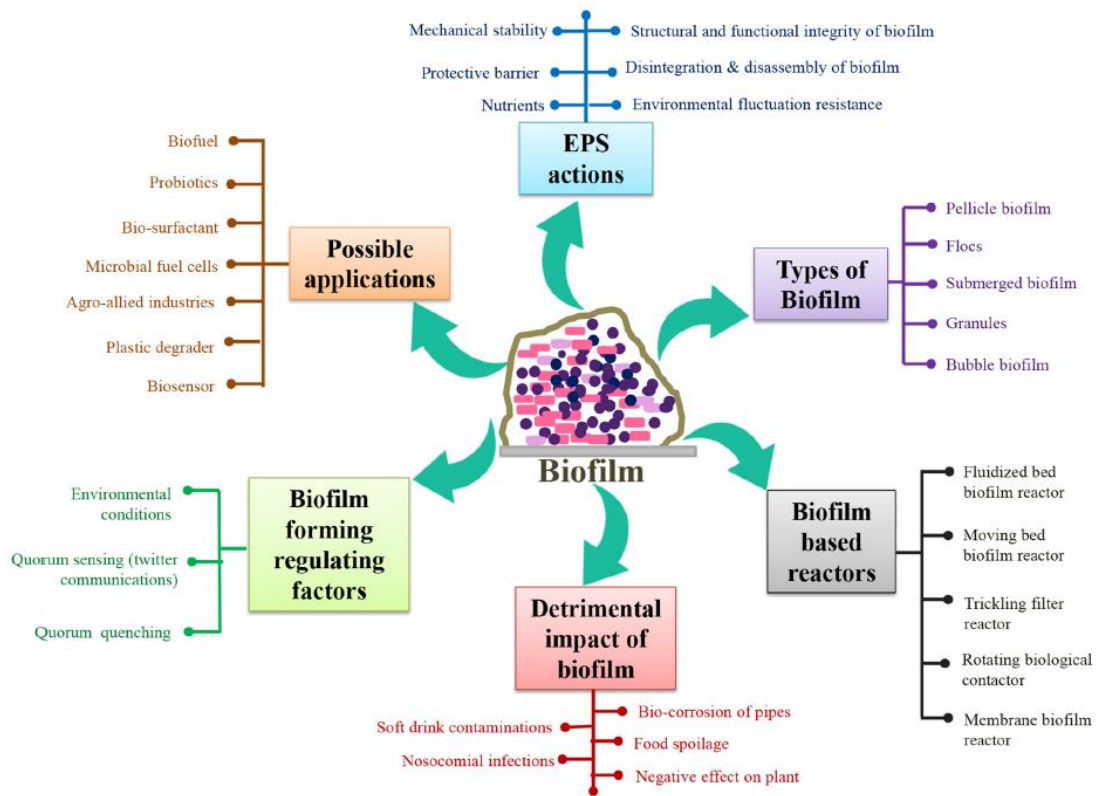


Figure 7 - An overview of bacterial biofilm formation, the factors influencing it, and its potential applications. Source: MAURYA *et al.*, 2023.

Microbial activity within a biofilm depends on the transport of essential components such as organic matter, oxygen, and nutrients (Figure 8). These substances are first adsorbed onto the biofilm surface and then transferred by diffusion through the liquid layer, across the liquid–biofilm interface, and into the biofilm, where they are metabolized (BASSIN, DEZOTTI, 2018). For example, as oxygen diffuses into the biofilm and its concentration progressively decreases with depth, the environment shifts from aerobic conditions to anoxic conditions (in the presence of nitrate) and ultimately to anaerobic conditions (METCALF & EDDY; TCHOBANOGLOUS *et al.*, 2014). The resulting biodegradation products diffuse outward toward the bulk liquid. Because biofilm systems are subject to diffusional mass transfer limitations, these constraints can reduce overall reaction rates, making the minimization of diffusion resistance essential for improving the performance of immobilized-biomass bioreactors (BASSIN, DEZOTTI, 2018).

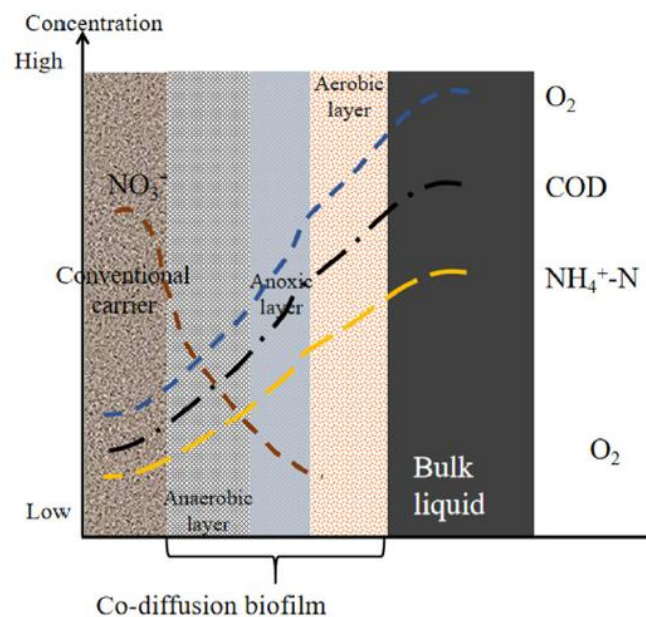


Figure 8 - Schematic diagrams of the biofilm structure and typical concentration profiles of the limiting substrates. Source: LI, LIU, 2019.

Since the transport of substrates and oxygen occurs mainly by diffusion, biofilm thickness becomes a key parameter controlling biofilm structure and activity. As biofilm thickness increases, concentration gradients intensify, leading to stratification of metabolic processes across the biofilm depth. This results in a more heterogeneous biofilm structure, where different microbial populations coexist according to substrate

and oxygen availability, potentially increasing microbial diversity but also imposing diffusional limitations that can affect overall system efficiency (NAYERI *et al.*, 2025; TORRESI *et al.*, 2016). Systems developed for nitrification generally rely on thinner biofilms than those used primarily for organic matter removal. This is mainly due to the greater sensitivity of nitrifying processes to environmental variations and the slower growth rates of autotrophic nitrifying bacteria compared with heterotrophic microorganisms (BASSIN *et al.*, 2011).

Several biofilm reactor configurations, such as fluidized-bed biofilm reactors (FBBR), trickling filters (TFR), rotating biological contactors (RBC), and moving bed biofilm reactors (MBBR), are commercially available and have been successfully applied in industrial wastewater treatment (MAURYA *et al.*, 2023).

2.2.2 Biological Organic Matter Removal

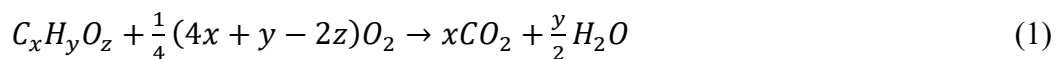
By the time oil refinery wastewater reaches the tertiary treatment stage, the majority of readily biodegradable organic matter has been oxidized and removed during secondary biological processes. Consequently, the influent entering the tertiary unit is characterized by significantly lower COD and BOD levels (OMAR *et al.*, 2024; SHI *et al.*, 2016). Despite this low overall concentration, understanding the specific composition of this residual organic matter is essential. According to VON SPERLING (2007), the carbonaceous material in wastewater can be classified based on its biodegradability as either inert or biodegradable:

- ✓ Inert (non-biodegradable) organic matter passes through the treatment system without being transformed. It can be divided into two fractions based on its physical state: soluble inert organic matter, which remains unchanged and exits the system at the same concentration as it enters, and particulate inert organic matter, which becomes associated with the biomass and is removed along with it.
- ✓ Biodegradable organic matter in wastewater can be broadly classified into two distinct fractions based on its biodegradation rate and accessibility to microorganisms. Rapidly biodegradable organic matter is primarily soluble and composed of simple, low-molecular-weight compounds that can be directly and quickly assimilated by heterotrophic bacteria. In

contrast, slowly biodegradable organic matter is mainly present in particulate or complex forms, although a minor soluble fraction may also exist. These compounds cannot be immediately utilized by microorganisms and must first undergo enzymatic hydrolysis to be converted into soluble substrates, resulting in a slower and delayed biodegradation process.

Biodegradable organic matter, mainly composed of proteins, carbohydrates, and animal fats, is generally quantified in terms of BOD and COD. When discharged into the environment without prior treatment, its biological stabilization can lead to the depletion of natural oxygen resources and the development of septic conditions (METCALF & EDDY, 2014). The biodegradation of organic compounds in wastewater treatment can occur under aerobic conditions through respiration, under anoxic conditions via denitrification, or under anaerobic conditions through processes such as methanogenesis or sulfidogenesis. During aerobic respiration, soluble organic matter is oxidized using oxygen as the terminal electron acceptor, resulting in the formation of carbon dioxide and water, along with the generation of a significant amount of excess biomass (sludge) (KAYSER, 2004).

The aerobic stabilization of carbonaceous material in sewage is primarily carried out by decomposer organisms, predominantly aerobic and facultative heterotrophic bacteria. In general terms, the aerobic transformation of carbonaceous matter can be described by Equation (1) (VON SPERLING, 2007):



The equation provided can be used to estimate the oxygen required for the complete oxidation of a generic substrate, expressed as chemical oxygen demand; however, it does not account for the assimilation of carbon and nutrients into new biomass. COD represents the total oxygen needed to oxidize all organic matter to carbon dioxide and water, without distinguishing between biodegradable and inert fractions. In contrast, BOD quantifies the oxygen consumed by microorganisms during the aerobic degradation of biologically available organic matter (METCALF & EDDY, 2004; BHAT *et al.*, 2004). The removal of biodegradable pollutants by biomass involves successive processes (Figure 9), beginning with the adsorption and absorption of soluble or colloidal

organic matter by bacterial flocs. The retained compounds are then broken down by extracellular enzymes into simpler molecules that can be assimilated by the cells. These substrates are subsequently metabolized through intracellular biochemical reactions that supply energy for biomass synthesis. Under conditions of substrate limitation, microorganisms undergo progressive self-oxidation of their cellular constituents, releasing organic by-products back into the medium (DEZOTTI, 2008). Equation (2), presented in unbalanced form, represents these processes in a more general manner than Equation (1), as it also accounts for the assimilation of carbon and nutrients required for the formation of new biomass (METCALF & EDDY, 2004):

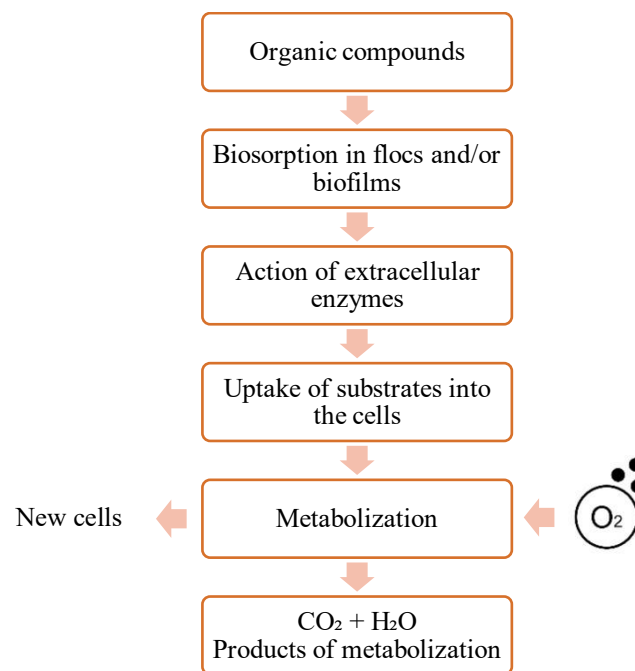
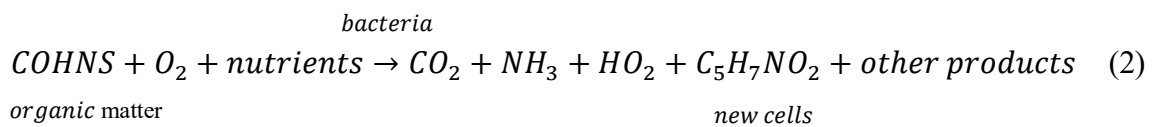


Figure 9 - Simplified process of aerobic degradation of organic substances by bacteria. Source: adapted from DEZOTTI (2008).

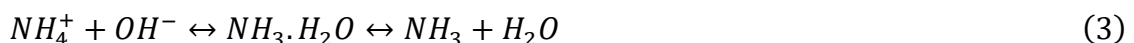
2.2.3 Biological Nitrogen Removal

2.2.3.1 Nitrogen Pollution in Wastewater Systems

Nitrogen, the fifth most abundant element in the solar system, is an essential nutrient for all living organisms and a fundamental component of nucleic acids and proteins, which underpin the structures and biochemical processes of life. The biological demand for nitrogen is therefore considerable, with approximately 2 to 20 nitrogen atoms incorporated into cellular material for every 100 carbon atoms assimilated, depending on the organism. Owing to its central role in sustaining life, nitrogen has even been suggested as a potential biosignature for the detection of life on other planets (CANFIELD *et al.*, 2010; CAPONE *et al.*, 2006; FRANCIS *et al.*, 2007). However, despite its essential role, excess nitrogen in aquatic environments can lead to severe environmental impacts. Since the 1980s, it has been recognized that wastewaters may exert significant polluting effects even in the absence of organic matter, particularly when nitrogen compounds are present. When present alongside phosphorus, nitrogen promotes excessive primary production, leading to rapid phytoplankton growth and algal blooms, a phenomenon known as eutrophication. The subsequent degradation of this biomass stimulates microbial activity and sharply increases oxygen demand, often resulting in oxygen depletion, fish mortality due to asphyxiation, higher water treatment costs, and the loss of suitability of affected waters for multiple uses (BASSIN, DEZOTTI, 2018).

According to NOAA's National Ocean Service, the excessive growth of algae and aquatic plants ultimately undergoes decomposition, releasing significant quantities of carbon dioxide that reduce seawater pH, a phenomenon known as ocean acidification. This acidification impairs the growth of fish and shellfish and can inhibit shell formation in bivalve mollusks, resulting in declines in commercial and recreational fisheries and, consequently, smaller yields and higher seafood costs.

In wastewater, the most common and significant forms of nitrogen include ammonia (NH₃), ammonium (NH₄⁺), gaseous nitrogen (N₂), nitrite ions (NO₂⁻), and nitrate ions (NO₃⁻) (CHAN-PACHECO *et al.*, 2021; URAKAWA *et al.*, 2019). In aqueous ammonia solutions, un-ionized ammonia is in equilibrium with ammonium and hydroxide ions. This equilibrium relationship can be expressed by the following equation (QUINN *et al.*, 1992):



The relative proportions of NH_4^+ and NH_3 are primarily controlled by the pH and temperature of the water. As pH and temperature increase, the fraction of NH_3 rises while the concentration of NH_4^+ decreases. Many chemical methods are unable to distinguish between ammonium and un-ionized ammonia; instead, they quantify both forms together, commonly referred to as total ammonia. This parameter, defined as the sum of NH_4^+ and NH_3 , is therefore the standard measure reported in water analyses (COLLOS, HARRISON, 2014; EMERSON *et al.*, 1975; URAKAWA *et al.*, 2019). At acidic to near-neutral pH values, the equilibrium shifts toward the formation of ammonium, resulting in ammoniacal nitrogen being predominantly present as NH_4^+ , particularly at temperatures around 25–35 °C (COLLOS, HARRISON, 2014; HUANG *et al.*, 2018; VON SPERLING, 2007).

Among the various contaminants present in refinery wastewater, ammonium nitrogen stands out as one of the major pollutants because of its pronounced environmental and public health impacts. High concentrations of ammonium promote eutrophication, increase oxygen depletion in receiving water bodies, and exert toxic effects on aquatic organisms (FANG *et al.*, 1993; FIGUEROLA; ERIJMAN, 2010; KUMAR *et al.*, 2022). In particular, ammonium-derived compounds can be highly harmful, as even low concentrations of ammonia, around 3 ppm, are toxic to certain fish species (BOOPATHY *et al.*, 2013; HAN *et al.*, 2021). Moreover, nitrate (NO_3^-) and nitrite (NO_2^-) derived from ammonium oxidation by nitrification are linked to adverse effects on both aquatic ecosystems and human health, including disorders such as methemoglobinemia. In aquatic organisms, particularly fish and crayfish, the primary toxic mechanism involves the oxidation of oxygen-transport pigments, such as hemoglobin and hemocyanin, into methemoglobin and methemocyanin, which are incapable of effectively carrying oxygen (HAN *et al.*, 2021; URAKAWA *et al.*, 2019).

A significant fraction of ammonium present in aqueous systems may also be lost through ammonia volatilization. As a relatively strong and corrosive base, gaseous ammonia can generate unpleasant odors and cause severe irritation or burns to the eyes, skin, and respiratory tract at concentrations as low as 50–100 ppm. In addition, ammonia can react with atmospheric pollutants such as SO_x and NO_x to form ammonium salts, contributing to the formation of fine particulate matter ($\text{PM}_{2.5}$) in the atmosphere (HAN *et al.*, 2021). Therefore, greater emphasis must be placed on achieving acceptable

These same biological transformations underpin nitrogen removal in wastewater treatment, which is generally accomplished in two sequential stages. Nitrification promotes the aerobic conversion of ammonium to nitrate using oxygen as the electron acceptor, while denitrification reduces nitrate to nitrogen gas under anoxic conditions, with nitrate serving as the terminal electron acceptor (BASSIN *et al.*, 2011).

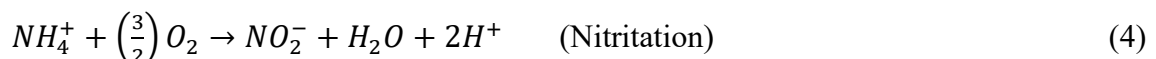
Another important biological pathway for nitrogen removal is anaerobic ammonium oxidation (anammox), which has the potential to enable more cost-effective nitrogen removal technologies, particularly for nitrogen-rich wastewaters (FRANCIS *et al.*, 2007). Since the experimental investigations in this study focused exclusively on nitrification, this process is discussed in detail below, while the remaining nitrogen cycle pathways are described elsewhere in the literature (CHEN *et al.*, 2023).

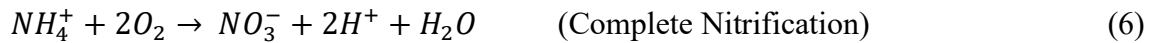
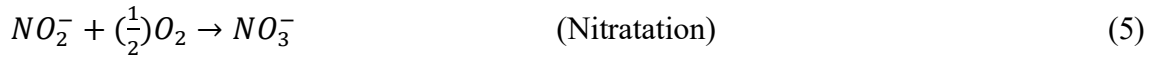
2.2.3.3 Nitrification

Nitrification is a biological process in which ammonium nitrogen ($\text{NH}_4^+\text{-N}$) is oxidized by microorganisms to nitrite ($\text{NO}_2^-\text{-N}$) and subsequently to nitrate ($\text{NO}_3^-\text{-N}$). Due to its high oxygen requirement and the toxic effects of ammonium on aquatic macroorganisms, the removal of $\text{NH}_4^+\text{-N}$ is mandatory for certain types of wastewaters (RITTMANN; MCCARTY, 2012).

Nitrifying bacteria are obligate aerobic chemolithoautotrophs that utilize carbon dioxide as their primary carbon source and derive energy from the oxidation of inorganic substrates, such as ammonia, to mineralized forms (RITTMANN; MCCARTY, 2012; VON SPERLING, 2007). Nitrifying bacteria exhibit very low growth rates, which can complicate the operation of biological treatment systems under certain conditions. Because biomass production is limited, the nitrification process is particularly vulnerable to inhibition by numerous compounds and is considered one of the most sensitive biological processes occurring in wastewater treatment bioreactors (BASSIN, DEZOTTI, 2018; METCALF & EDDY, 2004).

The nitrification process occurs through a series of steps, as represented by Equations (4–6):





The conversion of ammonia to nitrite is mediated by ammonia-oxidizing bacteria (AOB) such as *Nitrosomonas*, *Nitrospira*, *Nitrosovibrio*, and *Nitrosococcus*, whereas the subsequent oxidation of nitrite is performed by nitrite-oxidizing bacteria (NOB), including *Nitrobacter*, *Nitrospira*, and *Nitrococcus* species (WONG *et al.*, 2003; PROSSER, 1990).

As indicated by the ammonia oxidation reactions, hydrogen ions are generated during nitrification. In the absence of adequate alkalinity to neutralize these ions, a decrease in pH may occur, which can ultimately inhibit the nitrification process. In this context, alkalinity, particularly in the form of carbonate and bicarbonate, is considered essential for nitrifying bacteria, as it both supplies buffering capacity and supports stable nitrification (METCALF & EDDY, 2004).

During nitrification, the oxidation state of nitrogen in ammonium increases from -3 to +5 as eight electrons are transferred to the oxidizing agent, molecular oxygen (Figure 11). These electrons are taken up by two oxygen molecules (four oxygen atoms), reducing oxygen from an oxidation state of 0 to -2 as it transforms into water (H₂O). Consequently, the oxidation of 1 mol of ammonium nitrogen (14 g N) requires 2 mol of oxygen (64 g O₂), resulting in a stoichiometric oxygen demand of 64/14, or 4.57 mg O₂ per mg of nitrogen (VAN HAANDEL; VAN DER LUBBE, 2012).

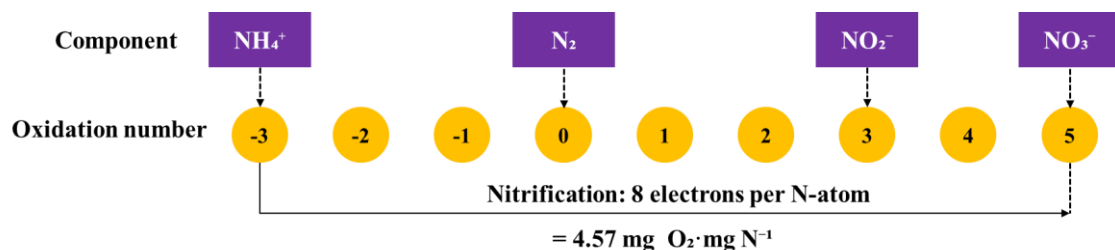


Figure 11 - Variation in the oxidation state of the nitrogen atom during the complete nitrification process.

Source: adapted from VAN HAANDEL and VAN DER LUBBE (2012).

The primary parameters that directly affect nitrification activity are pH, temperature, alkalinity, dissolved oxygen (DO) levels, the organic carbon-to-nitrogen (C/N) ratio, and competition for ammonia and oxygen by heterotrophs (BASSIN, DEZOTTI, 2018). Wong *et al.* (2003) reported that nitrification is most effective at pH values between 8 and 9, whereas pH levels below approximately 6.0 are unfavorable for this process. Nitrifying bacteria are particularly sensitive to dissolved oxygen concentrations, with growth rates decreasing at DO levels below 3–4 mg L⁻¹ and experiencing a marked reduction when concentrations fall below 2 mg L⁻¹ (U.S. EPA 1995; METCALF & EDDY, 2004). Moreover, high temperatures can significantly hinder nitrification performance. Bench-scale studies have shown that the optimal temperature range for AOB is approximately 30–35 °C, while NOB exhibits optimal activity at slightly higher temperatures, around 35–40 °C (SHORE *et al.*, 2012).

Another critical parameter affecting the nitrification process is the concentration of organic substrates in the wastewater, as it directly governs the competition between heterotrophic and autotrophic bacterial populations (BASSIN *et al.*, 2012; POURROSTAMI NIAVOL *et al.*, 2025). The chemical oxygen demand to nitrogen (COD/N) ratio plays an important role in nitrification efficiency, particularly in biofilm-based systems, where competition between heterotrophic and nitrifying bacteria for both oxygen and attachment sites is intensified (BASSIN *et al.*, 2012; ELENTER *et al.*, 2007). Elevated COD levels stimulate the growth of heterotrophic microorganisms, which have substantially higher growth rates than autotrophs and therefore outcompete them for oxygen and nutrients. As a result, autotrophic nitrifying bacteria can be overgrown and displaced, leading to reduced nitrification efficiency.

In biofilm systems, these fast-growing heterotrophs preferentially occupy the outer biofilm layers and consume most of the oxygen diffusing into the biofilm under high organic loading conditions, limiting oxygen penetration to the inner layers and constraining nitrification activity (BASSIN *et al.*, 2012; ELENTER *et al.*, 2007; OKABE *et al.*, 2004). However, under certain conditions, heterotrophic bacteria can also play a supporting role in nitrification. The biofilm matrix formed by heterotrophs may protect nitrifying bacteria by reducing biomass detachment and providing structural stability, thereby creating a more favorable microenvironment for autotrophic growth. Autotrophic nitrifiers are known to have a limited capacity for biofilm formation due to their slow growth rates and low EPS production, which constrains cell adhesion. Consequently, in

wastewater with low or absent organic carbon, sustaining an adequate nitrifying population in autotrophic biofilm reactors can be challenging. Therefore, promoting nitrifying biofilm development can be achieved through the appropriate regulation of heterotrophic growth and EPS production microorganisms (BASSIN *et al.*, 2012; TSUNEDA *et al.*, 2001)

In addition to the mentioned parameters, the presence of oil and grease, for instance, in refinery wastewater represents another critical factor influencing nitrification performance (BAHADORI, 2020). The impact of oil becomes particularly critical under shock-loading events, which frequently occur in such wastewaters. Rapid increases in oil and other contaminants may result from accidental releases, process upsets, or fluctuations in production, causing sudden alterations in influent composition. These disturbances challenge the resilience of biological treatment systems and can strongly inhibit sensitive processes such as nitrification. Although many toxic compounds can be biologically degraded by microorganisms, abrupt variations in pollutant concentrations may impair microbial metabolism and alter community structure. Such rapid loading fluctuations within bioreactors can compromise operational stability, ultimately reducing treatment efficiency and process reliability (MALLICK; CHAKRABORTY, 2021).

Oily wastewater may contain harmful compounds, including phenols, petroleum hydrocarbons, and polycyclic aromatic hydrocarbons (D'LAMARE *et al.*, 2022). These compounds can inhibit nitrification both through direct toxic effects on nitrifying microorganisms and by limiting oxygen transfer, which is essential for autotrophic ammonia oxidation (HYDROSCIENCE, INC., 1971). Oily compounds may impose physical limitations on nitrification through hydrophobic interactions within the biofilm structure. According to Boleydei *et al.* (2018), oil adsorption onto biomass occurs through interactions between hydrocarbon compounds and functional groups on biological surfaces, together with the porous and hydrophobic nature of the biomass that favors rapid attachment and accumulation. Since biofilms are surface-attached microbial communities embedded in a matrix composed of exopolysaccharides, proteins, and extracellular DNA (SZCZEPANSKI; LIPSKI, 2013), they provide multiple adsorption sites and hydrophobic regions that promote oil adherence. Together, these mechanisms suggest that nitrifying biofilms may adsorb and retain oil on their surface, potentially forming a diffusion barrier that limits oxygen and substrate transfer.

In addition to physical mass transfer limitations, refinery oil may exert direct toxic effects on nitrifying communities. It has been reported in the literature (MISITI *et al.*, 2013; URAKAWA *et al.*, 2012) that ammonia-oxidizing microorganisms are particularly susceptible to petroleum contamination because, as chemolithoautotrophic organisms, they are unable to utilize crude oil as a carbon or energy source. As a result, petroleum hydrocarbons function primarily as toxic stressors rather than growth substrates, increasing the vulnerability of nitrifying communities to inhibition. However, the severity of this inhibition depends on the magnitude of the oil load increase as well as the resilience and adaptive capacity of the nitrifying microbial community (GALI *et al.*, 2005). Consequently, a comprehensive understanding of how oil influences nitrifying communities is crucial for sustaining process stability, preserving the activity of sensitive microorganisms, and achieving reliable nitrification performance.

2.3 Moving Bed Biofilm Reactor (MBBR)

Although biofilm systems offer advantages, they also present limitations: trickling filters require large reactor volumes, rotating biological contactors are prone to mechanical failures, fixed submerged media biofilters suffer from uneven flow distribution, and granular biofilters necessitate backwashing, which prevents continuous operation. To address these operational limitations, the compact and innovative moving bed biofilm reactor (MBBR) (Eur. pat. no.0575314, US pat. no. 5,458,779) was developed (RUSTEN *et al.*, 2006; RUSTEN *et al.*, 1997). The MBBR technology was patented following its development by the Norwegian company Kaldnes Miljøteknologi (Tønsberg, Norway), in collaboration with the Foundation for Scientific and Industrial Research at the Norwegian University of Science and Technology (SINTEF), Trondheim, Norway, in the late 1980s and early 1990s (ØDEGAARD, 2000; RUSTEN *et al.*, 1998).

MBBR is a widely used wastewater treatment technology that has received considerable research attention since 2000 due to its numerous advantages (Figure 12). This growing scientific interest has been accompanied by strong industrial acceptance. The MBBR technology is now well established in the wastewater treatment market, with numerous large-scale plants and many smaller treatment facilities operating worldwide (BASSIN, DEZOTTI, 2018; RUSTEN *et al.*, 2006). To date, more than 400 MBBR installations have been implemented globally across both industrial and municipal sectors (GZAR *et al.*, 2021).

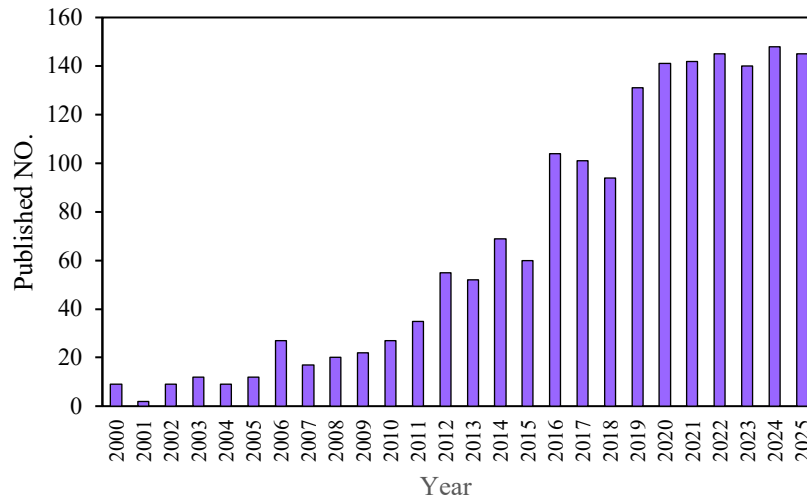


Figure 12 - The published literature on MBBR applications for wastewater treatment from 2000 to 2025. Source: Scopus database.

2.3.1 Basic Characteristics of the MBBR

The moving bed biofilm reactor combines the advantages of biofilters and activated sludge systems while avoiding their main limitations. It is designed as a continuously operated, non-cloggable biofilm reactor with low head loss and a high specific surface area for biomass attachment. In this system, microorganisms grow on small carrier elements that move freely within the reactor volume, ensuring effective mass transfer and stable operation. Carrier movement is promoted by aeration in aerobic reactors (Figure 13.a) and by mechanical mixing in anoxic or anaerobic configurations (Figure 13.b) (ØDEGAARD, 2000; RUSTEN *et al.*, 1998). A device, commonly known as a sieve, is installed at the reactor outlet to prevent the media from leaving the tank (BASSIN, DEZOTTI, 2018).

In contrast to activated sludge processes, where biological activity occurs in suspended biomass, the MBBR relies on attached biofilm growth on mobile carriers. This biofilm configuration allows the decoupling of sludge retention time (SRT) from hydraulic retention time (HRT), enabling operation at shorter HRTs and longer SRTs than conventional activated sludge systems. As a result, MBBR systems achieve higher biomass retention, enhanced pollutant removal efficiency, and a reduced reactor footprint. Furthermore, continuous sludge recirculation is generally not required (GUPTA *et al.*,

2022; NAYERI et al., 2025). A comparative analysis between activated sludge and MBBR systems is presented in Table 5.

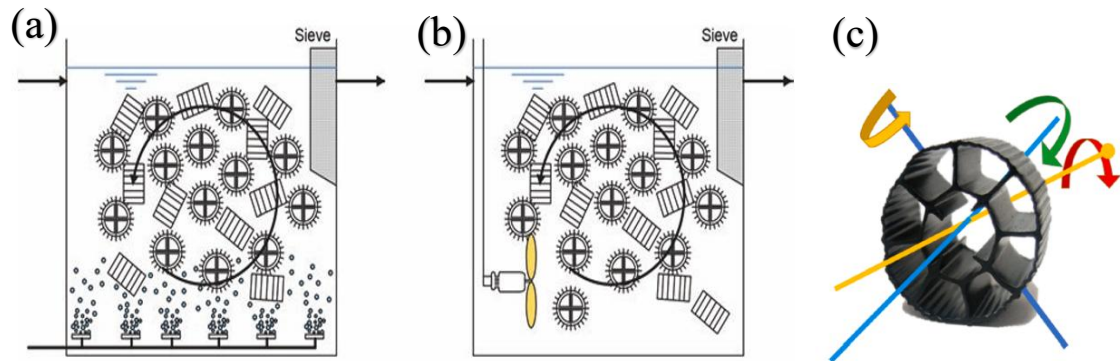


Figure 13 - Schematic representation of a typical MBBR, in which the biofilm carriers are maintained in suspension by (a) aeration in aerobic systems or (b) mechanical mixing in anoxic or anaerobic systems, and (c) axes of rotation of a typical biofilm carrier in a generic MBBR system. Source: BASSIN, DEZOTTI., 2018; DEENA *et al.*, 2022; RUSTEN et al., 2006.

Table 5 - Advantages and limitations of activated sludge and MBBR systems.
Source: adapted from KAWAN *et al.* (2016).

System	Advantages	Disadvantages
Activated Sludge	<ul style="list-style-type: none"> ✓ A well-established and widely applied process ✓ Large surfaces 	<ul style="list-style-type: none"> ✓ Typically exhibits poor sludge settleability ✓ Prone to foaming and sludge bulking issues ✓ Generates large amounts of excess biomass ✓ Sensitive to shock loads and elevated concentrations of toxic compounds in the influent
MBBR	<ul style="list-style-type: none"> ✓ Eliminates the need for a clarifier or biomass recirculation ✓ Produces low amounts of excess sludge ✓ Provides a high specific surface area with elevated biomass density ✓ Ensures strong biomass retention and long sludge age ✓ small footprint ✓ Allows easy upgrading of existing treatment systems ✓ Supports the coexistence of aerobic and anoxic microorganisms within the biofilm ✓ Offers a robust process with a resilient microbial community ✓ Capable of handling high organic loads and temporary operational disturbances ✓ Simple design with straightforward operation ✓ Low maintenance requirements ✓ Not susceptible to clogging issues 	<ul style="list-style-type: none"> ✓ May require a longer start-up period ✓ High energy demand associated with aeration, which is required both to supply oxygen to the microorganisms and to ensure the movement of carriers within the reactor ✓ Removing the carriers for reactor maintenance can be logistically challenging

In MBBR systems, which operate under aerobic conditions, the main processes involved are the biodegradation of organic matter as well as nitrification and denitrification (GUPTA *et al.*, 2022). In biofilm reactors performing simultaneous organic matter removal and nitrification, heterotrophic and nitrifying bacteria compete for both oxygen and space, leading to biofilm stratification. Faster-growing heterotrophs typically dominate the outer biofilm layers, where substrate availability and biomass detachment are higher, while nitrifiers develop in the inner layers (Figure 14). Under low dissolved oxygen conditions, the outer heterotrophic layer limits oxygen diffusion, impairing nitrification and potentially inhibiting nitrifier establishment. However, when DO levels are sufficient, this heterotrophic layer may protect nitrifiers from sloughing and support stable nitrification (BASSIN, DEZOTTI, 2018). Denitrification can occur in

aerated reactors, particularly within anoxic zones of the biofilm where oxygen penetration is limited.

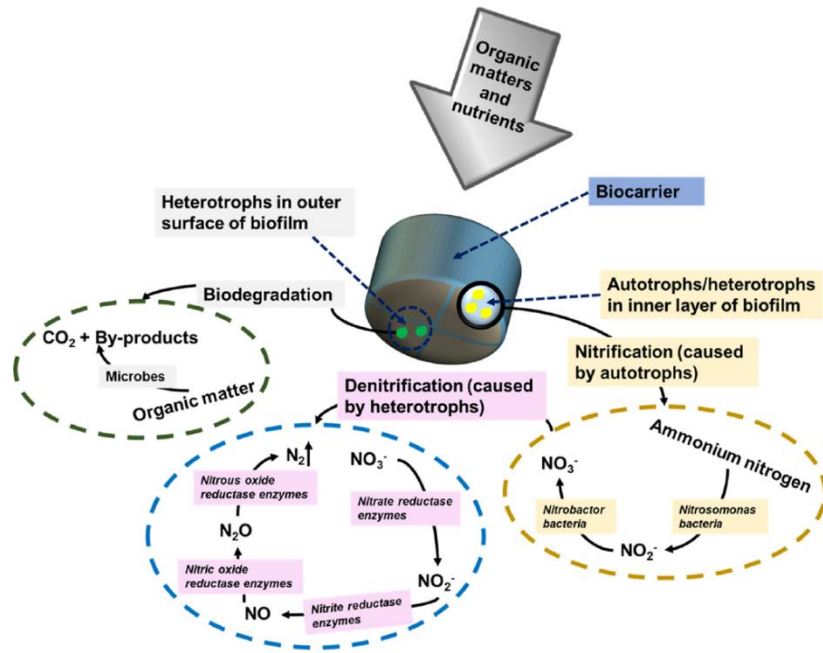


Figure 14 - Reaction mechanisms of the MBBR process under aerated conditions for the removal of organic matter and nutrients. Source: GUPTA *et al.*, 2022.

2.3.2 Factors Affecting MBBR Performance








The biological performance of the MBBR system is influenced by a range of operational and design parameters, including hydraulic retention time, surface loading rate (SLR), dissolved oxygen, carrier size and geometry, carrier filling fraction, air diffuser configuration, mixing intensity, and aeration rate (KAWAN *et al.*, 2016; MAHTO; DAS, 2021). The effects and significance of selected parameters are examined in detail as follows.

The biofilm carrier is a key element of an MBBR system, as its properties strongly affect microbial growth and the formation of an efficient biofilm. The selection of an appropriate carrier depends on several characteristics, including specific surface area, material type, shape, geometry, and surface roughness. Because the carriers are continuously suspended and exposed to wastewater, biofilm develops progressively on their surfaces. Anaerobic or facultative microorganisms typically establish in the inner biofilm layers, while aerobic bacteria dominate the outer layers. Consequently, each carrier acts as a microreactor where multiple biological processes occur simultaneously (KUMAR *et al.*, 2026). Hydrodynamic shear generated by the movement of biocarriers

within the reactor significantly influences oxygen transfer efficiency. The presence of biocarriers promotes the breakup of air bubbles into smaller sizes, increasing the gas–liquid interfacial area and thereby enhancing oxygen transfer rates (NAYERI *et al.*, 2025).

The original biofilm carriers applied in MBBR technology were developed by the patent holder AnoxKaldnes®. These carriers are manufactured from polyethylene (PE) with a density of approximately 0.95 g cm⁻³ and are available in various sizes, differing in diameter and height. Their design typically includes an internal cross structure that partitions the carrier into circular compartments, along with longitudinal ridges, or fins, on the outer surface to enhance biofilm attachment (BASSIN, DEZOTTI, 2018; RUSTEN *et al.*, 2006). Some of the most widely used AnoxKaldnes® carrier models are summarized in Table 6, together with their principal characteristics.

Table 6 - Key characteristics of selected Kaldnes® biofilm carriers. Source: adapted from BASSIN, DEZOTTI (2018).

Type of carrier	Nominal diameter (mm)	Nominal height (mm)	Protected surface area (m ² m ⁻³)	Shape
K1	9.1	7.2	500	
K2	15	15	350	
K3	25	10	500	
K5	25	3.5	800	
Natrix F3	46	37	200	
Biofilm Chip M	48	2.2	1200	
Biofilm Chip P	45	3	900	

The K-series biocarriers differ in their dimensions (diameter and height), the surface area available for biofilm growth, and the number and configuration of internal sections or openings formed by surrounding rims. The effective surface area refers to the protected portion of the carrier that does not come into contact with other carriers during mixing. The choice of biocarrier type depends on the treatment objective and operating conditions, and may vary between aerobic and anoxic or anaerobic processes (DI BIASE *et al.*, 2019).

The filling fraction (V_S/V_R) is defined as the ratio between the volume of biocarriers (V_S) and the total reactor volume (V_R). A key advantage of MBBR technology is the flexibility to design reactor size based on a selected filling fraction, allowing additional carriers to be added to enhance performance or increase volumetric capacity. However, excessive filling fractions may impair mixing and reactor hydrodynamics, leading to stagnant zones. For aerobic systems, it is recommended that the filling fraction does not exceed 70% to ensure adequate carrier movement. Therefore, an optimal filling fraction must be selected to balance effective mixing, mass transfer, and treatment efficiency. Once the carrier type and filling fraction are defined, the reactor volume can be appropriately sized, while also considering future capacity upgrades (DI BIASE *et al.*, 2019; ØDEGAARD, 2006; SALVETTI *et al.*, 2006).

HRT is another key operational parameter influencing MBBR performance, as it directly determines the contact time between microorganisms and pollutants and, consequently, the extent of biological reactions (WU *et al.*, 2023). In general, lower HRTs favor the rapid availability of substrates to heterotrophic microorganisms, enhancing organic matter removal. However, higher HRTs are more favourable to nitrification, as autotrophic nitrifying bacteria require longer contact times to grow and remain active (NAYERI *et al.*, 2025). Increasing HRT also promotes biofilm development by providing microorganisms with extended exposure to nutrients, resulting in thicker biofilms on the carrier surface (GUPTA *et al.*, 2022). Thicker biofilms can create anoxic zones in their inner layers, which are advantageous for denitrification. In contrast, reducing the HRT limits the time available for microbial growth and biofilm accumulation, as substrates and nutrients pass through the reactor more rapidly. This typically leads to thinner biofilms with lower biomass concentrations, negatively affecting process efficiency due to insufficient conditions for nitrification. Consequently, HRT must be carefully optimized in MBBR systems according to the specific treatment objectives of the wastewater

process (NAYERI *et al.*, 2025). Studies have shown that HRTs applied in MBBR systems for nitrification typically range between 4 and 24 hours (BASSIN *et al.*, 2012; KAWAN *et al.*, 2022; WU *et al.*, 2023).

Additionally, the performance of biological treatment processes is strongly influenced by the influent volumetric loading rate. In biofilm-based systems such as MBBRs, this influence is more effectively described by the surface loading rate, defined as the ratio of the volumetric load to the total surface area provided by the carrier media (RUSTEN *et al.*, 1998). For a given reactor volume, the applied surface loading can therefore be controlled by adjusting the amount of carrier media, directly impacting biomass retention and treatment efficiency (BASSIN, DEZOTTI, 2018; MCQUARRIE; BOLTZ, 2011). Optimal removal performance is generally achieved at a threshold surface loading rate, where the retained biomass concentration is sufficient to support efficient pollutant degradation without imposing mass transfer limitations (KAWAN *et al.*, 2016).

Dissolved oxygen is another key limiting parameter in biological treatment processes in MBBR, influencing both organic matter removal and nitrification. Although a concentration of around 2 mg L⁻¹ is generally sufficient for aerobic degradation of organic matter, biofilm-based systems often require higher DO levels due to diffusion limitations within the biofilm (BASSIN, DEZOTTI, 2018; METCALF & EDDY, 2014). In particular, nitrification is highly sensitive to oxygen availability, with concentrations above 2–3 mgO₂ L⁻¹ needed to initiate the process. Nitrification rates increase nearly linearly with DO concentration and may continue to rise at levels exceeding 10 mg O₂ L⁻¹. At ammonium concentrations above 3–4 mg NH₄⁺-N L⁻¹, nitrification performance is primarily governed by oxygen availability and organic loading (ØDEGAARD, 2006).

2.4 Overview of Previous Studies on Biological Treatment of Oil Refinery Wastewater

A comprehensive overview of recent studies investigating the biological treatment of oil refinery wastewater is summarized in Table 7. Recent literature highlights the flexibility and resilience of biofilm-based biological treatments, particularly MBBRs, in managing the complex and toxic profile of oil refinery wastewater. Hybrid and sequential configurations, such as anoxic-aerobic systems, have proven highly effective for the simultaneous removal of organic compounds and nitrogenous wastes in both synthetic and real effluents (LU *et al.*, 2013; MALLICK; CHAKRABORTY, 2017). A key advantage of these systems is their robustness against toxic shock loads. For instance, while high concentrations of crude oil can cause temporary inhibition and nitrite accumulation, biomass demonstrates significant resilience, often recovering near-complete nitrification and ammonium removal once the shock is withdrawn (MALLICK; CHAKRABORTY, 2021). Furthermore, hybrid fed-batch MBBR setups maintain high removal efficiencies even under variable phenol loadings (SATAPATHY; JAYAPAL, 2023), confirming the stability of biofilm systems under harsh conditions.

The success of nitrification in these systems is heavily dependent on precise operational control, most notably the HRT. Autotrophic nitrifying bacteria require adequate contact time to establish and perform effectively. Studies consistently show that reducing the HRT or increasing the hydraulic loading rate severely hinders ammonia removal. For example, an HRT of 6 hours was found to be optimal for effective ammonium removal in an aerobic MBBR, whereas an HRT of 3 hours was entirely insufficient for nitrification (SCHNEIDER *et al.*, 2011). This sensitivity is echoed in other biofilm systems, where shorter retention times create an influx of ammonia that hinders the biological process (DELASHOUB; BORGHEI, 2020; GHALEHKHONDABI *et al.*, 2021). Additionally, environmental stressors such as high salinity and increased organic loading further diminish nitrification performance, necessitating carefully optimized HRTs to counteract these inhibitory effects (DELASHOUB; BORGHEI, 2020).

Table 7 - Overview of Previous Studies on Biological Treatment of Oil Refinery Wastewater

Ref.	Wastewater type	Treatment method	Operational condition	Key findings
(MALLICK; CHAKRABORTY, 2021)	Synthetic petroleum refinery wastewater containing crude oil, phenol, and ammonia	Anoxic-aerobic sequential moving bed reactors operated in sequencing batch mode.	Crude oil: 300 mg/L (normal), 600 mg/L (shock 1), 900 mg/L (shock 2); HRT: 60 h (anoxic) + 20 h (aerobic); pH \approx 9.5	<ul style="list-style-type: none"> • Crude oil shock loads caused temporary inhibition of biological processes, including nitrification, due to toxicity and biomass loss. Ammonium removal decreased to \sim89% (shock 1) and \sim80% (shock 2), with nitrite accumulation observed. • Full nitrification and ammonium removal (\sim99%) recovered after shock withdrawal, demonstrating system resilience.
(SATAPATHY; JAYAPAL, 2023)	Synthetic Refinery wastewater containing phenol and ammonia	Hybrid fed-batch MBBR (Anaerobic-Anoxic-Aerobic)	Three units in series; 24-day total HRT; recycle ratio of 1.0; phenol range 250–1,000 mg/L and ammonia 50 mg/L	<ul style="list-style-type: none"> • Achieved 99% phenol and 95% ammonia removal. • Variations in the influent phenol concentration did not significantly affect NH₄-N removal efficiency. • Indigenous mixed culture was resilient to high phenol loading.
(LU <i>et al.</i> , 2013)	Real petroleum refinery wastewater (PRW) primarily composed of hydrocarbons	Sequential anaerobic-aerobic (A/O) MBBR	Continuous flow; total HRT varied from 72 h to 18 h; 50% (v/v) carrier filling ratio	<ul style="list-style-type: none"> • An effective and practical strategy for the simultaneous removal of COD and ammonium from PRW was demonstrated. • The results indicated that total COD and ammonia removal efficiencies exceeded 85% at hydraulic retention times of 72 and 36 h, respectively.
(SCHNEIDER <i>et al.</i> , 2011)	Real oil refinery wastewater	MBBR followed by post-ozonation and biological activated carbon (BAC)	Aerobic MBBR operated at an HRT of 3–12 h, with a bed-to-reactor volume ratio of 0.6, followed by post-treatment using O ₃ and biological activated carbon (BAC).	<ul style="list-style-type: none"> • Stable COD removal was achieved in the MBBR at HRTs of 12–3 h, with efficiencies of 69–89% and effluent COD of 40–75 mg L⁻¹ (below discharge limits). • An HRT of 6 h was optimal, providing effective ammonium removal. • An HRT of 3 h was insufficient for nitrification.

(MAHMOUDKHANI <i>et al.</i> , 2012)	Real petroleum-contaminated water from Tehran oil refinery wells	Oil separation followed by aerobic MBBR, filtration, and activated carbon treatment.		Lab-scale MBBR (550 L); polyurethane carriers (85% filling, 3% reactor volume); HRT = 240 min; DO = 4–5 mg/L; pH = 6.7–7.5; temperature = 15–25 °C;	<ul style="list-style-type: none"> • Overall removal efficiencies reached 99% for COD, 94% for total nitrogen, and 58% for phosphorus. • Ammonium removal efficiency was ~97%, indicating near-complete nitrification. • The combined MBBR–filtration–activated carbon system was identified as an effective method for treating petroleum-contaminated water, with most effluent parameters meeting environmental discharge standards.
(GHALEHKHONDABI <i>et al.</i> , 2021)	Real petroleum refinery wastewater	Four-stage Biological (RBC)	Rotating Contactor	Temperature: 25–35 °C; Influent NH ₃ -N: 20–60 mg/L; Flow rate: 5.5–16.5 mL/min; Disc rotational speed: 2–10 rpm; Hydraulic loading rate: 0.005–0.016 m ³ /m ² ·d; pH: 7.0–7.5; DO: 2–4 mg/L	<ul style="list-style-type: none"> • Optimum conditions were obtained at 32.19 °C, influent NH₃-N of 20.54 mg/L, flow rate of 5.57 mL/min, and disc rotational speed of 4.58 rpm, resulting in 99.07% ammonia removal and 85.76% COD removal. • Lower hydraulic loading rates (HLR) enhanced nitrification efficiency in the RBC system, as increasing HLR, resulting from reduced HRT, negatively affected ammonia removal.
(MALLICK; CHAKRABORTY, 2017)	Synthetic petroleum refinery wastewater	Anoxic–aerobic sequential moving bed reactors		Feed pH ≈ 9.5; Sulphide: 750 mg/L; Phenol: 750 mg/L; Diesel: 300 mg/L; Ammonia-N: 350 mg/L	<ul style="list-style-type: none"> • The optimum operating conditions included an anoxic reactor with an HRT of 2 days and a disc rotational speed of 20 rpm, followed by an aerobic MBBR with an HRT of 16 h, giving a total HRT of 64 h. Under these conditions, complete removal of phenol, ammonia-N, COD, and total hydrocarbons was achieved, confirming effective nitrification and successful treatment of complex refinery wastewater.
(DELASHOOB; BORGHEI, 2020)	Synthetic saline petroleum refinery wastewater	MBBR and Anaerobic/Anoxic/Aerobic (AOA) system		HRT: 12–24 h; COD: 800–1200 mg/L; NH ₄ ⁺ -N: 200–400 mg/L; Salinity: 10–20 g/L NaCl	<ul style="list-style-type: none"> • MBBR is identified as a top system for nutrient removal in saline conditions. • Increased salinity and organic loading negatively affected nitrification performance. • Shorter retention times increase the feed flow rate. This influx of ammonia actually slows down the nitrification speed.

CHAPTER 3

MATERIALS AND METHODS

This section describes the materials and methods applied throughout the experimental investigations. It includes a detailed description of the wastewater sources, reactor configuration, and operational conditions, startup and acclimation procedures, experimental phases, and the analytical techniques used to monitor physicochemical and biological parameters during MBBR operation. All experimental procedures were conducted at the Water Pollution Control Laboratory (LabPol), affiliated with the Chemical Engineering Program (PEQ) of COPPE/UFRJ.

3.1 Wastewater Source and Characteristics

Real wastewater (RW) used in this study was collected from a full-scale refinery wastewater treatment plant located in Minas Gerais, Brazil (Figure 15). The facility receives wastewater from oil refining activities. The plant employs a multi-stage treatment system that includes preliminary treatment (screening, grit removal, and oil separation), primary treatment (equalization, flotation, and removal of suspended solids and emulsified oil), and secondary treatment consisting of aerated lagoons. The aeration system includes two configurations: a completely mixed lagoon (South) and a facultative lagoon (North). For this study, wastewater samples were collected after the secondary treatment stage to simulate a tertiary treatment step. The samples were periodically sent to the laboratory and stored at 4°C until use, in accordance with the requirements of each operational phase, as detailed in Section 3.3. The real wastewater was supplemented with phosphorus (5–10 mgP L⁻¹) to enable microorganism growth, and alkalinity was adjusted to ensure stoichiometric requirements for nitrification. During the experimental period, various wastewater samples were collected, showing variability in several parameters. Table 8 summarizes the key characteristics of the wastewater throughout the operational period.

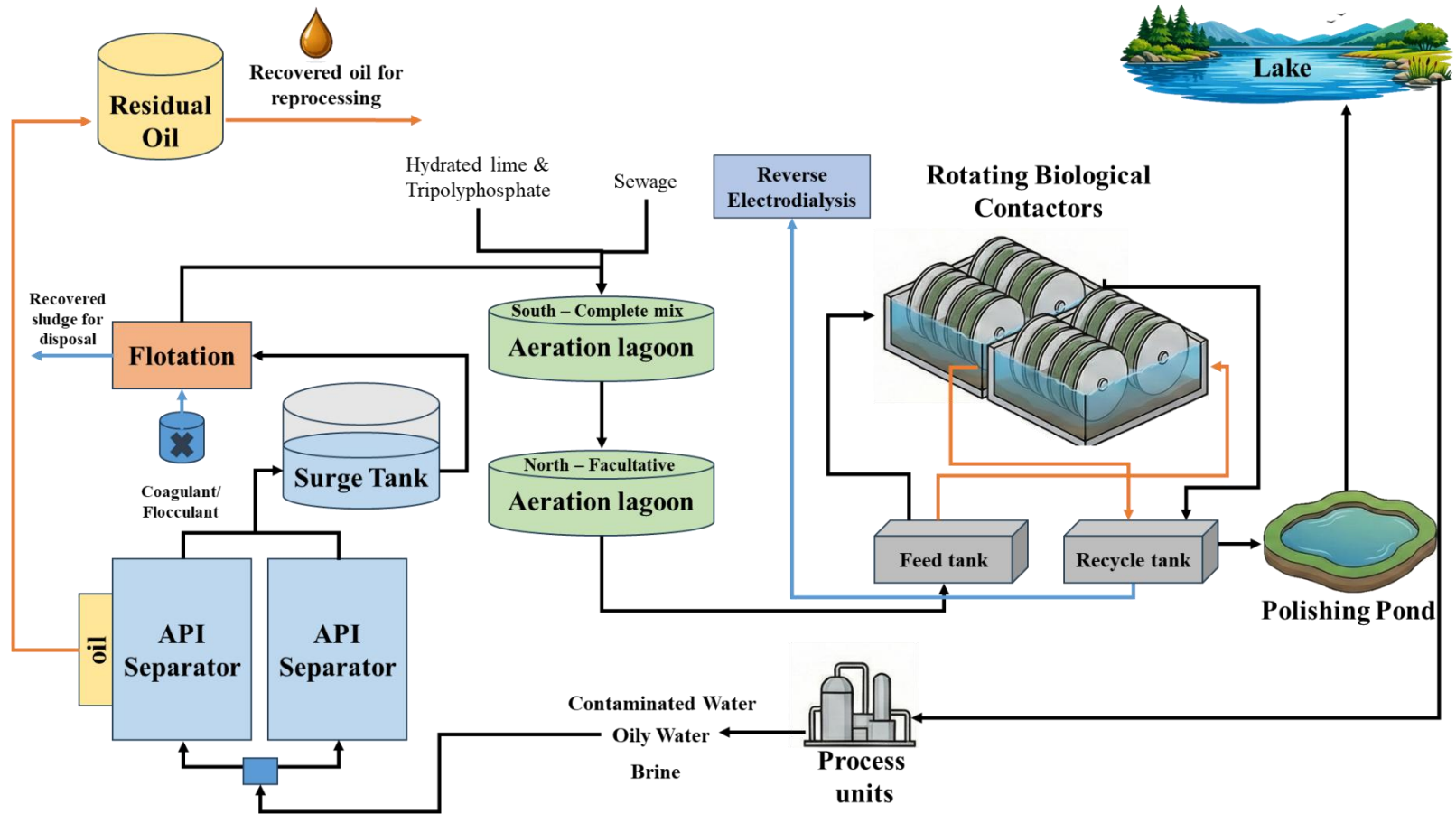


Figure 15 – Diagram of the real oil refinery wastewater treatment plant.

Table 8 - Characteristics of the refinery wastewater.

Parameter	Range
pH	7.5 – 8
Total suspended solids (mg L ⁻¹)	30 – 80
Volatile suspended solids (mg L ⁻¹)	20 – 60
COD (mgO ₂ L ⁻¹)	80 – 200
Ammonium Nitrogen (mgNH ₄ ⁺ -N L ⁻¹)	10 – 30
Nitrate (mg NO ₃ ⁻ -N L ⁻¹)	0 – 41
Nitrite (mg NO ₂ ⁻ -N L ⁻¹)	0 – 32
Alkalinity (mg CaCO ₃ L ⁻¹)	280 – 330
Total Oil and Grease (mg L ⁻¹)	10 – 34
Phosphate (mg L ⁻¹)	0.5 – 2
Chloride (gCl ⁻ L ⁻¹)	0.3 – 0.5

The composition of the synthetic wastewater (SW) used in this study was adjusted for each operational phase to meet specific ammonium, alkalinity, and external carbon requirements, using NH₄Cl, NaHCO₃, and glucose, respectively. The medium also contained 0.025 g K₂HPO₄L⁻¹, 0.02 g KH₂PO₄ L⁻¹, and 0.5 mL L⁻¹ of a trace metal solution (composition detailed in (Vishniac & Santer, 1957)). Aside from the COD, the synthetic wastewater was prepared to simulate the specific constituent concentrations typically entering the tertiary nitrification stage of a real oil refinery wastewater treatment plant. Figure 16 shows a visual comparison of real oil refinery effluent versus the synthetic wastewater formulation.

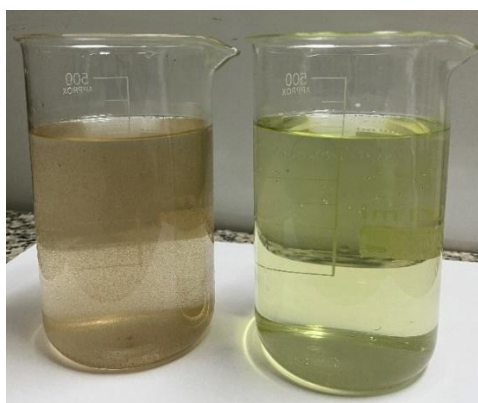


Figure 16 - Visual comparison of real oil refinery effluent (left) versus synthetic wastewater (right).

3.2 Moving-Bed Biofilm Reactors

3.2.1 Experimental Setup

The study employed four cylindrical bench-scale reactors, labeled MBBR1, MBBR2, MBBR3, and MBBR4, as shown in Figure 17.

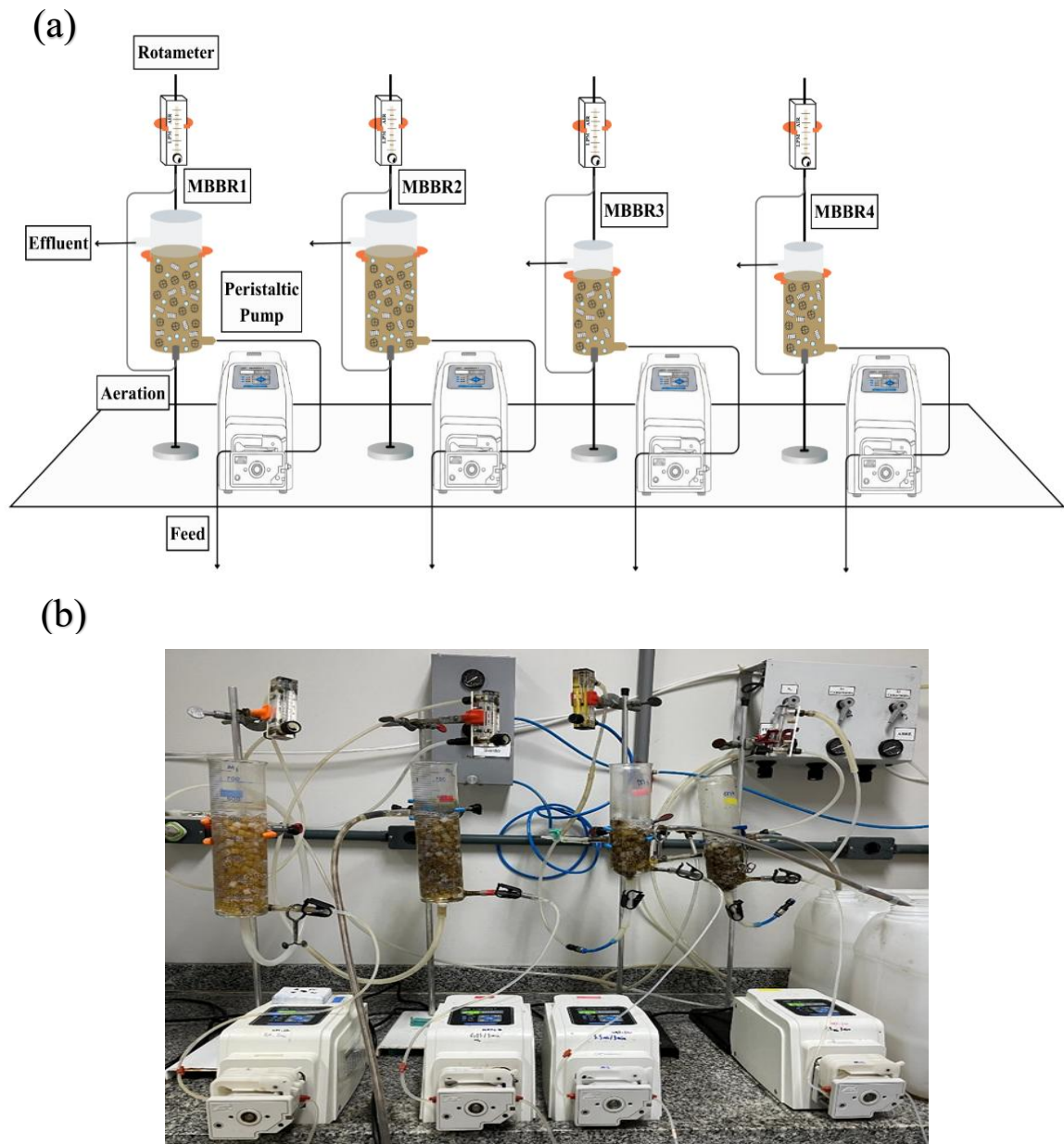



Figure 17 – (a) Schematic view of the MBBR system and (b) the lab-scale MBBR system experimental set-up.

MBBR1 and MBBR2 were constructed from glass with a cylindrical shape, each having a diameter of 7.0 cm and a usable height of 17.5 cm, providing a working volume of 0.5 L. Meanwhile, MBBR3 and MBBR4 were also made from glass, with a cylindrical design, a diameter of 5.5 cm, and a usable height of 9.5 cm, yielding a working volume of 0.22 L. MBBR1 and MBBR2 were filled with 252 units of Kaldnes K1 carriers, while MBBR3 and MBBR4 were filled with 113 units of same carrier, each having a specific surface area of 500 m² m⁻³. Table 9 summarizes the main characteristics of the K1 carrier. This configuration was designed to achieve a filling fraction of 50% ($V_{\text{carriers}}/V_{\text{reactor}}$). The experimental setup includes 20 L plastic drums used for storing feed streams, which were kept at 4°C to minimize biological activity in the wastewater before its use, especially when biodegradable COD was present.

Table 9 - Physical and structural characteristics of the K1 carrier used in the biological reactors. Source: adapted from RUSTEN *et al.* (2006).

K1 Support	Characteristics	Value
	Nominal diameter (mm)	9.1
	Nominal length (mm)	7.2
	Apparent density (kg m ⁻³)	150
	Protected specific surface area (m ² m ⁻³)	500

The dissolved oxygen (DO) concentration in the continuously operated systems was maintained between 6.5 and 7.0 mg L⁻¹. The temperature was controlled at 24 ± 3°C using air conditioning, and the pH levels in all reactors were maintained within the range of 7.0 to 8.5. The reactors were fed from the bottom in upflow mode using peristaltic pumps, and continuous aeration was maintained through a compressed air line connected to a porous diffuser at the base of each reactor. The reactors operated continuously, with the treated effluent being discharged gravitationally from the upper part of the systems.

3.2.2 Start-up of MBBRs

During the startup phase, the reactors were inoculated to promote biofilm formation on the carriers. MBBR1 and MBBR2 were inoculated with activated sludge from two sources: an industrial wastewater treatment plant of an oil refinery located in São Paulo, Brazil, and from a municipal wastewater treatment plant (Rio de Janeiro, Brazil), with 50 mL from each source. The purpose of mixing the sludge was to promote greater microbial diversity, providing a more robust and functional biological community in reactors. After insertion of the sludge, the reactors were filled to the total working volume (500 mL) using synthetic wastewater. In the first 15 days of operation, the reactors were operated in batch mode. During this period, 300 mL of the liquid fraction from each reactor was replaced daily with fresh synthetic wastewater. In the first five days, the synthetic wastewater contained 1000 mg L⁻¹ of COD, which was reduced to 500 mg L⁻¹ from the sixth day onward. This strategy was implemented to accelerate biofilm formation by initially promoting heterotrophic growth, followed by a reduction in organic loading to enrich the biofilm with nitrifying microorganisms. Figure 18 presents MBBR2 during the inoculation period. After 15 days of batch operation, the reactors switched to continuous operation mode.



Figure 18 - MBBR2 during the inoculation period.

MBBR3 and MBBR4 were inoculated with 200 mL of activated sludge obtained from a municipal wastewater treatment plant in Rio de Janeiro, Brazil. Following sludge addition, the reactors were filled to their total working volume (220 mL) using real wastewater from the petroleum refinery. For MBBR3, RW was supplemented with COD, while MBBR4 received no COD supplementation. Both reactors were initiated under continuous flow conditions. However, during the first week of operation, the settled sludge accumulating in the reactor outlet was manually recirculated back into the reactor to promote biomass retention and support initial biofilm development.

3.3 Operational Phases of MBBRs

This study was conducted in two complementary parts to evaluate tertiary nitrification performance and biofilm stability in MBBR systems treating refinery wastewater under progressively challenging conditions. In the first part of this study, four MBBRs were operated under different strategies to investigate biofilm development, acclimation pathways, and tertiary nitrification performance when treating oil refinery wastewater. Each reactor followed a distinct approach: a fully synthetic control system to establish baseline nitrification behavior; a gradual acclimation strategy transitioning from synthetic to real refinery wastewater; a strategy using external carbon supplementation to support biofilm establishment under real wastewater conditions; and a direct exposure approach in which the reactor received real refinery wastewater without any external support. This comparative design allowed evaluation of different startup and adaptation strategies and their influence on nitrifying biofilm stability and resilience under progressively more realistic and challenging conditions.

In the second part of the study, the focus shifted specifically to the influence of oil and grease on nitrification performance. Using the reactor working with only real refinery wastewater, the impact of increasing oil concentrations was systematically assessed to determine the response, tolerance, and adaptive capacity of the nitrifying biofilm. This phase aimed to isolate the effect of oil as an inhibitory factor and to better understand its role in limiting tertiary nitrification efficiency in refinery wastewater treatment.

3.3.1 Part I: Development of Stable Nitrifying Biofilm under Variable COD and HRT Conditions

In the first part of this study, the experimental system was composed of four MBBR units, each operated under distinct phases to evaluate different aspects of biofilm development and nitrification performance under varying substrate compositions and operational stresses.

MBBR1 functioned as a control system and was operated exclusively with synthetic wastewater and glucose as the carbon source. It served to establish a performance baseline under controlled conditions to assess biofilm stability and nitrification potential in the absence of real wastewater coming from the secondary treatment stage of the petroleum refinery. The reactor was initially subjected to an HRT of 6 h and a high organic load of 500 mg L⁻¹ COD to stimulate initial biomass attachment and heterotrophic growth (P1). In subsequent phases (P2 to P4), the external COD was progressively reduced to 200, 100, and finally 0 mg L⁻¹. This stepwise elimination of carbon aimed to shift the competitive advantage from fast-growing heterotrophic bacteria to slow-growing autotrophic nitrifying bacteria. Later, in the absence of external carbon, hydraulic stress was introduced by reducing the HRT from 6 to 4 h (P5) and then to 2 h (P6).

The operational methodology of MBBR2 was designed to evaluate a gradual, stepwise acclimation strategy. The goal was to build a robust microbial biofilm under optimal synthetic conditions first, and then progressively introduce the real wastewater coming from the secondary treatment stage of the petroleum refinery. The operation began with synthetic wastewater supplemented with glucose (500 and 200 mg L⁻¹ COD at an HRT of 6 hours in P1 and P2, respectively) to promote rapid biofilm formation. In P3, real wastewater was gradually introduced into the feed while the COD was lowered to 100 mg L⁻¹. The proportion of real wastewater was subsequently increased to 50% (P5) and finally to 100% (P6), effectively eliminating both the synthetic wastewater and the external carbon source. After successfully transitioning to 100% real wastewater, the system's resilience was tested by decreasing the HRT to 4 h (P7) and 2 h (P8), allowing evaluation of biofilm performance, system resilience, and nitrification efficiency under realistic industrial conditions.

The purpose of MBBR3 was to evaluate whether supplementing real wastewater coming from the secondary treatment stage of the petroleum refinery with an easily biodegradable external carbon source (ethanol) could accelerate initial biofilm formation and counteract the toxicity of the real wastewater. The reactor was continuously fed with 100% real wastewater. During the initial phases, ethanol was added to provide 300, 150, and 75 mg L⁻¹ COD (P1, P2, and P3, respectively) at a constant HRT of 6 h. After establishing a mature biofilm, the ethanol supplementation was completely withdrawn (P4), transitioning the system entirely towards autotrophic nitrification. System stress was further increased by reducing the HRT to 4 h (P5) and 2 h (P6). Finally, in P7, while maintaining the 2 h HRT, the influent ammonium concentration was reduced. The objective of this final phase was to examine the system's tertiary nitrification capacity and the biofilm's stability under conditions of low ammonium availability.

MBBR4, on the other hand, was operated under the most challenging conditions, receiving secondary refinery wastewater without any additional carbon source. This reactor was specifically used to investigate the biofilm's capacity to maintain nitrification and overall treatment performance in the presence of inhibitory compounds, under reduced HRTs. The reactor started at an HRT of 6 h (P1) to allow for the slow growth of autotrophic bacteria. Once initial stabilization was observed, the retention time was reduced to 4 h (P2) and then to 2 h (P3), aiming to assess the biofilm's robustness under severe operating conditions. Table 10 shows all the experimental phases applied in MBBR systems to evaluate the optimal conditions for tertiary nitrification of oil refinery wastewater.

Table 10 - Experimental conditions of the MBBR1, MBBR2, MBBR3, and MBBR4 during the entire operational period.

Reactor	Phase	Operating days	Influent COD (mg L ⁻¹)	Influent type	HRT (h)	Average surface ammonium load (gNH ₄ ⁺ -N m ⁻² d ⁻¹)
MBBR1	P1	0-64	500 (glucose)	100% SW	6	0.7±0.1
	P2	65-91	200 (glucose)	100% SW	6	0.9±0.1
	P3	92-112	100 (glucose)	100% SW	6	0.8±0.1
	P4	113-121	0	100% SW	6	0.6±0.1
	P5	122-133	0	100% SW	4	0.8±0.1
	P6	134-197	0	100% SW	2	1.5±0.2
MBBR2	P1	0-64	500 (glucose)	100% SW	6	0.7±0.1
	P2	65-91	200 (glucose)	100% SW	6	0.9±0.1
	P3	92-112	100 (glucose)	75% SW + 25% RW	6	0.8±0.1
	P4	113-121	0	75% SW + 25% RW	6	0.6±0.1
	P5	122-133	0	50% SW + 50% RW	6	0.5±0.1
	P6	134-147	0	100% RW	6	0.6±0.1
	P7	148-182	0	100% RW	4	0.9±0.1
	P8	183-197	0	100% RW	2	1.3±0.3
MBBR3	P1	0-70	300 (ethanol)	100% RW	6	0.5±0.2
	P2	71-85	150 (ethanol)	100% RW	6	0.5±0.1
	P3	86-97	75 (ethanol)	100% RW	6	0.5±0.1
	P4	98-120	0	100% RW	6	0.6±0.1
	P5	121-140	0	100% RW	4	0.9±0.1
	P6	141-153	0	100% RW	2	1.5±0.4
	P7	154-174	0	100% RW	2	0.9±0.2
MBBR4	P1	0-83	0	100% RW	6	0.5±0.1
	P2	84-97	0	100% RW	4	0.7±0.1
	P3	98-175	0	100% RW	2	1.6±0.3

3.3.2 Part II: Effect of Oil Concentration on Nitrification

As discussed in Chapter 2, the presence of oil and grease is a critical factor influencing nitrification performance in refinery wastewater. Oil can affect nitrifying microorganisms through potential inhibitory effects and/or by limiting oxygen transfer, thereby compromising ammonia oxidation efficiency. Therefore, the second part of this study was specifically designed to evaluate the impact of oil concentration on the nitrification performance of MBBR4 under controlled and stable operating conditions.

To isolate the effect of oil loading, the reactor was operated with a constant influent $\text{NH}_4^+\text{-N}$ concentration of 30–40 mg L^{-1} and a HRT of 2 h. Oil concentration in the influent was gradually adjusted across different operational phases to assess the response, stability, and potential adaptation of the nitrifying biomass to increasing oil loads. The sequence of operational phases applied to MBBR4 during this period is summarized in Table 11, providing an overview of the tested oil concentrations and corresponding experimental conditions.

Table 11 - Operational phases of MBBR4 during the operation with oil.

Phase	Operating days	HRT (h)	Average surface ammonium load ($\text{gNH}_4^+\text{-N m}^{-2}\text{ d}^{-1}$)	Oil concentration (mg L^{-1})
P3	98-175		1.7 ± 0.3	10-30 ^a
P4	176-188		1.4 ± 0.1	30-50
P5	189-215	2	1.2 ± 0.1	50-100
P6	216-251		1.5 ± 0.2	200-300
P7	252-281		1.5 ± 0.2	300-500

^a This value corresponds to the oil concentration measured in the real wastewater.

3.3.2.1 Oil Emulsification Procedure

To ensure a stable and homogeneous distribution of oil in the influent, refinery oil was emulsified in the wastewater using a high-speed homogenizer (IKA T25 digital ULTRA-TURRAX, IKA®-Werke GmbH & Co. KG, Germany). Given the insoluble nature of the oil, the use of an emulsifying agent was proposed to improve hydrocarbon dispersion in the liquid phase. Accordingly, sodium dodecyl sulfate (SDS) was added as

a surfactant at a concentration of 0.4 mL per liter of wastewater to improve emulsion stability. The mixture was homogenized at 20,000 rpm for 10 min before feeding the reactor (Figure 19). The influent was prepared daily to minimize changes in oil distribution and chemical composition, and its oil concentration was gradually increased over the experimental period to evaluate the system's response. To ensure a homogeneous feed, from P5 onward, at higher oil concentrations, the feed bottle was placed on a magnetic stirrer (Figure 20).



Figure 19 - Preparation and homogenization of oily wastewater influent using high-speed ULTRA-TURRAX mixing.

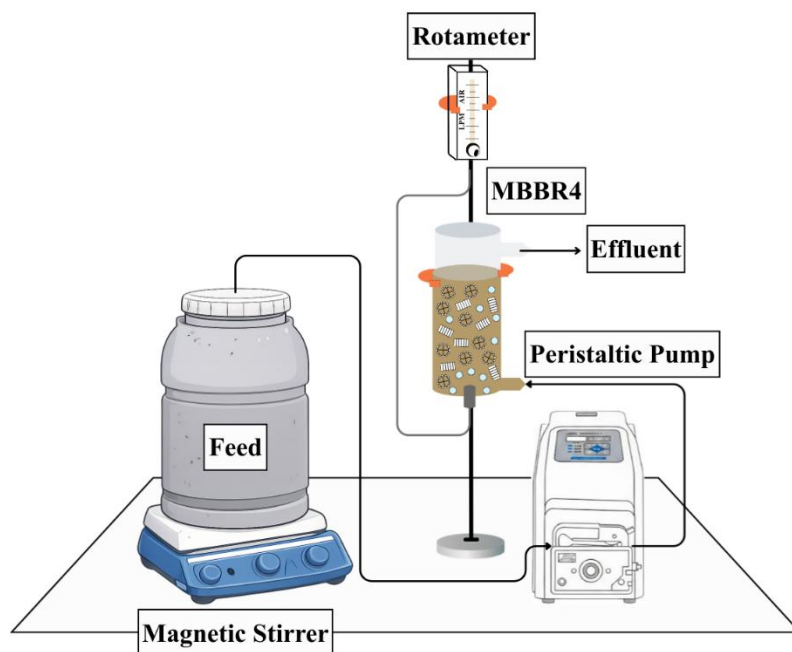


Figure 20 - Schematic view of MBBR4 during the operation with oil.

3.5 Analytical Methods

The performance of the MBBRs during the treatment of oil refinery wastewater was assessed through the monitoring of several parameters in the influent and effluent streams. Physicochemical analyses were carried out at the Water Pollution Control Laboratory (LabPol). Before analysis, all samples were filtered through 0.45 μm cellulose nitrate membrane filters to remove fine suspended solids. The physicochemical parameters analyzed and their respective analytical methods are presented in Table 12. It is important to note that, in most cases, sample analyses were conducted on the day following the preparation of the wastewater and reactor cleaning, due to the potential degradation of the compounds present and the need to ensure the representativeness of the results obtained.

Table 12 - Analytical methods applied throughout the experimental operations of MBBRs.

Parameter	Frequency	Method and Equipment
Chemical Oxygen Demand (COD)	Weekly	Cienlab digestion blocks, model CE-350; Hach® spectrophotometer, model DR3900; colorimetric method 5220 D (APHA, 2005).
Ammoniacal Nitrogen (NH ₄ ⁺ -N)	Weekly	Nessler reagent colorimetric method, according to procedure 4500-NH ₃ (APHA, 1992).
Nitrate (NO ₃ ⁻ -N)	Weekly	Brucine colorimetric method, according to procedure 352.1 (APHA, 1976)
Nitrite (NO ₂ ⁻ -N)	Weekly	NED reagent colorimetric method, according to procedure 4500-NO ₂ ⁻ B (APHA, 1992)
Dissolved Oxygen (DO)	Weekly	HANNA® Instruments dissolved oxygen ion-selective electrode, model HI98193
pH	Weekly	pH electrode, HANNA® Instruments; electrometric method 4500-H ⁺ B (APHA, 2005)
Temperature (°C)	Weekly	Temperature probes within the pH meter
Total Suspended Solids (TSS), Volatile Suspended Solids (VSS), and Fixed Suspended Solids (FSS)	2 times per month	ICAMO drying oven and muffle furnace, model 4; standardized methods 2540 D and 2540 E (APHA, 2005).
Total Attached Solids (TAS), Volatile Attached Solids (VAS), and Fixed Attached Solids (FAS)	2 times per month	ICAMO drying oven and muffle furnace, model 4; standardized methods 2540 B and 2540 E (APHA, 2005).
Visual changes in the biofilm	2 times per month	Stereomicroscope, model Stemi 508 (Carl Zeiss)
Optical Microscopy	1 time per phase	ZEISS optical microscope

3.5.1 Total Suspended (TSS), Fixed (FSS), and Volatile Solids (VSS)

The determination of total, volatile, and fixed suspended solids (TSS, VSS, and FSS) was carried out following an adaptation of Standard Methods 2540 D and 2540 E (APHA; AWWA et al., 2017). The procedure began with washing a glass fiber filter (pore size $\leq 2 \mu\text{m}$) with reagent-grade water, followed by drying at $550 \text{ }^\circ\text{C}$ in a muffle furnace for 1 h and subsequent weighing using an analytical balance (P1). A known volume of sample 20–100 mL (V) was then filtered through the same glass fiber filter, and the filter containing the retained solids was dried at $103\text{--}105 \text{ }^\circ\text{C}$ for 24 h, or until constant mass was achieved (P2). Subsequently, the filter was ignited at $550 \text{ }^\circ\text{C}$ for 1 h in a muffle furnace. After cooling, it was weighed to obtain mass P3.

Equations (7) to (9) were used to calculate suspended solids concentrations. The difference between P2 and P1 was used to determine the concentration of total suspended solids (TSS), whereas the difference between P2 and P3 was used to calculate the concentration of volatile suspended solids (VSS). The concentration of fixed suspended solids (FSS) was obtained from the difference between P3 and P1.

$$TSS \left(\frac{mg}{L} \right) = \frac{(P2 - P1) \times 10^6}{V} \quad (7)$$

$$VSS \left(\frac{mg}{L} \right) = \frac{(P2 - P3) \times 10^6}{V} \quad (8)$$

$$FSS \left(\frac{mg}{L} \right) = \frac{(P3 - P1) \times 10^6}{V} \quad (9)$$

3.5.2 Total Attached (TAS), Fixed (FAS), and Volatile Solids (VAS)

Total, volatile, and fixed attached solids (TAS, VAS, and FAS) on the K1 carriers used in the MBBR were quantified using adaptations of Standard Methods 2540 B and 2540 E (APHA; AWWA et al., 2017). Porcelain crucibles were previously washed with distilled water, ignited at 550 °C for 1 h in a muffle furnace, cooled to room temperature in a desiccator, and weighed to obtain the initial mass (P1). For each analysis, a known amount of K1 carriers was withdrawn from the reactor. The biofilm attached to the carrier surfaces was completely scraped using interdental brushes and distilled water to ensure maximum removal of solids. The detached biofilm was collected directly into the pre-weighed crucible. The crucible containing the extracted biofilm was then dried in an oven at 103–105 °C for 24 h or until constant mass, cooled in a desiccator, and weighed to obtain mass P2. Subsequently, the crucible was ignited in a muffle furnace at 550 °C for 1 h, cooled in a desiccator, and weighed again to obtain mass P3. The mass of total attached solids was calculated from the difference between P2 and P1, while the mass of volatile attached solids was determined from the mass loss between P2 and P3. Fixed attached solids were calculated as the difference between TAS and VAS. The masses of TAS, VAS, and FAS were normalized by the number of carriers used in each analysis and expressed as mg carrier⁻¹. These values were subsequently converted to concentrations per unit reactor volume (mg L⁻¹) or per unit biofilm growth area (mg m⁻²) by multiplying by the total number of carriers in the reactor and dividing by the reactor working volume or the total protected specific surface area, respectively. It is important to note that the carriers selected for analysis were marked to prevent their reuse in subsequent attached solids determinations.

3.5.3 Biofilm Visualization and Thickness Measurement

To assess biofilm formation throughout the experimental period, carriers were periodically sampled from all reactors and analyzed using a ZEISS Stemi 508 stereomicroscope. High-resolution images were acquired under stereoscopic zoom to qualitatively evaluate biofilm morphology, coverage, and distribution. During image acquisition, a calibrated 2000 µm scale bar was applied to each image, enabling subsequent thickness measurements. Quantitative analysis of biofilm thickness was

conducted using Digimizer® software, based on the pre-set image scale. For each operational phase, two carriers were randomly selected from the reactors, and multiple thickness points were measured on each carrier image. The final thickness value was obtained by averaging the results from the two carriers. This non-destructive method allowed for consistent comparison of biofilm development across different phases.

3.5.4 Determination of Oil Concentration

Oil concentrations in the influent and effluent were determined using an InfraCal 2 ATR-SP Oil-in-Water Analyzer (Spectro Scientific, USA). Samples were collected directly from the reactor influent and effluent without filtration. Concentrated H₂SO₄ was added to each sample to facilitate the extraction of soluble and emulsified oil fractions. For analysis, 50 mL of the sample was transferred into a clean glass bottle and mixed with 10 mL of n-hexane. The mixture was vigorously agitated for 2 minutes to ensure complete extraction of oil into the solvent phase. After phase separation, an aliquot of 60 µL of the hexane extract was placed onto the ATR crystal of the analyzer.

To quantify the oil attached to the carriers and biofilm at the end of each operational phase, a known number of carriers was selected and subjected to the same extraction procedure applied to influent and effluent samples. The extracted oil concentration and the corresponding extraction volume were used to calculate the total mass of oil recovered from these carriers. The oil mass was then normalized to the TAS measured for the same set of carriers used in the extraction. Results were expressed as mg oil mgTAS⁻¹. All analyses were conducted in triplicate, and mean values were reported.

3.6 Assessment of Maximum Nitrifying Activity in Batch Trials

To determine the maximum ammonium removal rate, batch assays were conducted at the end of each operational phase. These tests are essential to assess the intrinsic nitrification potential and to identify substrate limitations under different operational conditions (LIMA *et al.*, 2016). In contrast to the continuous reactors, the batch-operated reactor did not experience ammonium-limiting conditions, as high

substrate concentrations were present at the start of each operating cycle. As a result, the system was able to reach its maximum nitrification potential (BASSIN *et al.*, 2015).

Before each assay, the reactors were drained and refilled with fresh feed corresponding to the specific operating condition: 400 mL for MBBR1 and MBBR2 and 150 mL for MBBR3 and MBBR4, ensuring that only attached biomass remained within the reactors. Each batch test lasted for a period equivalent to the HRT of the corresponding phase. Samples (10 mL) were collected at regular intervals (5–7 time points), immediately filtered through 0.45 μm cellulose nitrate membranes to prevent microbial activity. Throughout the assays, pH, temperature, and DO were continuously monitored. The specific maximum ammonium removal rate was determined from the linear regression of ammonium concentration over time, using the corresponding volatile attached solids (VAS) concentration in the calculation, and was expressed as $\text{mgNH}_4^+\text{-N gVAS}^{-1} \text{d}^{-1}$.

The real specific ammonium removal rate was calculated from continuous-operation data collected on the same day as the batch test by subtracting influent and effluent ammonium concentrations and dividing the resulting value by the combined concentration of volatile attached and volatile suspended solids and the HRT.

3.7 Calculations

3.7.1 Removal Efficiency

According to Equation (10), the removal efficiency (η) of a given component was determined based on its influent (C_I) and effluent (C_E) concentrations, indicating the proportion of the component removed during the treatment process.

$$\eta = \left(\frac{C_I - C_E}{C_I} \right) \cdot 100\% \quad (10)$$

3.7.2 Nitrogen Mass Balance

The nitrogen balance of the system was calculated using Equation (11), considering the concentrations of the analyzed nitrogen species ($\text{NH}_4^+ - \text{N}, \text{NO}_2^- -$

N and $NO_3^- - N$) in the influent (I) and effluent (E), as well as the nitrogen assimilated in to cellular biomass (N_{ass}) and the nitrogen lost (N_{loss}):

$$\begin{aligned} & (NH_4^+ - N + NO_2^- - N + NO_3^- - N)_I - (NH_4^+ - N + NO_2^- - N + NO_3^- - N)_E \\ & - (N_{ass} + N_{loss}) = 0 \end{aligned} \quad (11)$$

3.7.3 Biofilm Surface-Specific Detachment Rate

Biofilm surface-specific detachment rate (K_d), Equation (12), expressed as $[\frac{g\ TSS}{m^2 \cdot d}]$, was calculated at the end of each experimental phase according to (BASSIN *et al.*, 2016):

$$K_d = \frac{Q_E \cdot X_i}{A_{biofilm} \cdot V \cdot (\frac{V_s}{V_r})} \quad (12)$$

Where Q_E [$L\ d^{-1}$] is the effluent flow rate of each reactor, X_i [$gTSS\ L^{-1}$] is the concentration of total suspended solids in the effluent of the corresponding reactor, $A_{biofilm}$ is the specific surface area of each carrier ($500\ m^2\ m^{-3}$ for K1 support), V [m^3] is the volume of reactor; and $(\frac{V_s}{V_r})$ is the media filling fraction of the reactor (50%).

3.7.4 Surface Loading Rate (SLR)

In attached-growth bioreactors, the surface loading rate (SLR) is a key design parameter because it accounts for the total surface area available for biofilm development (A), determined by the carrier's specific protected surface area (a), the reactor volume (V), and the carrier filling ratio (f). Accordingly, SLR was calculated as shown in Equation (13) and expressed as $gNH_4^+-N\ m^{-2}\ d^{-1}$ (MATHEUS, 2020).

$$SLR = \frac{Q \cdot C_i}{V \cdot a \cdot f} = \frac{C_i}{HRT \cdot a \cdot f} = \frac{Q \cdot C_i}{A} \quad (13)$$

CHAPTER 4

RESULTS AND DISCUSSION

4.1 Part I: Development of Stable Nitrifying Biofilm under Variable COD and HRT Conditions

This section introduces the first part of the study, focused on the development, adaptation, and operational stability of nitrifying biofilms across four distinct acclimation strategies. The methodology involved operating four MBBRs under different initial configurations, including the use of synthetic wastewater, gradual transition to real refinery wastewater, and direct exposure to real refinery wastewater. Throughout the experimental period, the reactors were exposed to increasing operational stress, primarily driven by progressive reductions in external COD and stepwise decreases in HRT. The analysis focuses on reactor performance and biofilm dynamics through the assessment of organic matter removal, continuous nitrification performance, batch activity tests, solids distribution (attached and suspended), biofilm thickness, and microscopic characterization, together with the monitoring of key operational parameters.

4.1.1 Organic Matter Removal

Figure 21 presents the temporal evolution of influent and effluent COD for the four MBBR systems. Reactors initially supplied with external carbon (MBBR1–3) showed high COD removal during the start-up phases, while MBBR4, operated without carbon addition, consistently exhibited low removal.

Following reactor inoculation with activated sludge, a stabilization period of approximately 20 to 30 days was required to establish a consistent concentration of attached biomass and to achieve effective biofilm formation in MBBR1, MBBR2, and MBBR3. In contrast, MBBR4 exhibited a longer start-up period, attributed to the absence of external organic carbon supplementation. This start-up phase corresponded to the colonization of the plastic carriers by microbial communities under the initially applied organic loading rates of $5.5 \text{ gCOD m}^{-2} \text{ d}^{-1}$ for MBBR1 and MBBR2, and $4.8 \text{ gCOD m}^{-2} \text{ d}^{-1}$ for MBBR3.

In MBBR1, COD removal exceeded 90% during the initial phase (P1), when synthetic wastewater contained a high biodegradable fraction. As the external carbon was reduced and later removed (P2–P4), influent COD decreased, and removal efficiency declined to approximately 30%, while effluent concentrations stabilized near 100 mg L⁻¹. Similar behavior was observed in MBBR2, with high removal (80–90%) during the synthetic wastewater phases (P1–P2), followed by a gradual decrease to 20% as real refinery wastewater was introduced (P3–P8). MBBR3 showed moderate to high removal (60–80%) during ethanol addition, with a sharp decline once carbon supplementation was reduced and ultimately eliminated (P4–P7). MBBR4, which received only real wastewater and no external carbon throughout operation, maintained low removal efficiencies (< 20%).

Overall, MBBR1 was capable of sustaining operation once external carbon was removed, whereas the remaining reactors ultimately converged to comparable effluent COD concentrations (~100 mg L⁻¹). These values correspond to the non-biodegradable fraction of organic matter present in the real wastewater originating from the secondary treatment stage of the petroleum refinery. Similar to these results, Wang et al. (2023) demonstrated that a MBBR system exhibited robust operational stability despite fluctuations in the influent organic load. The study reported that even as the C/N ratio was progressively reduced from 6 to 3, the system consistently sustained high COD removal efficiency.

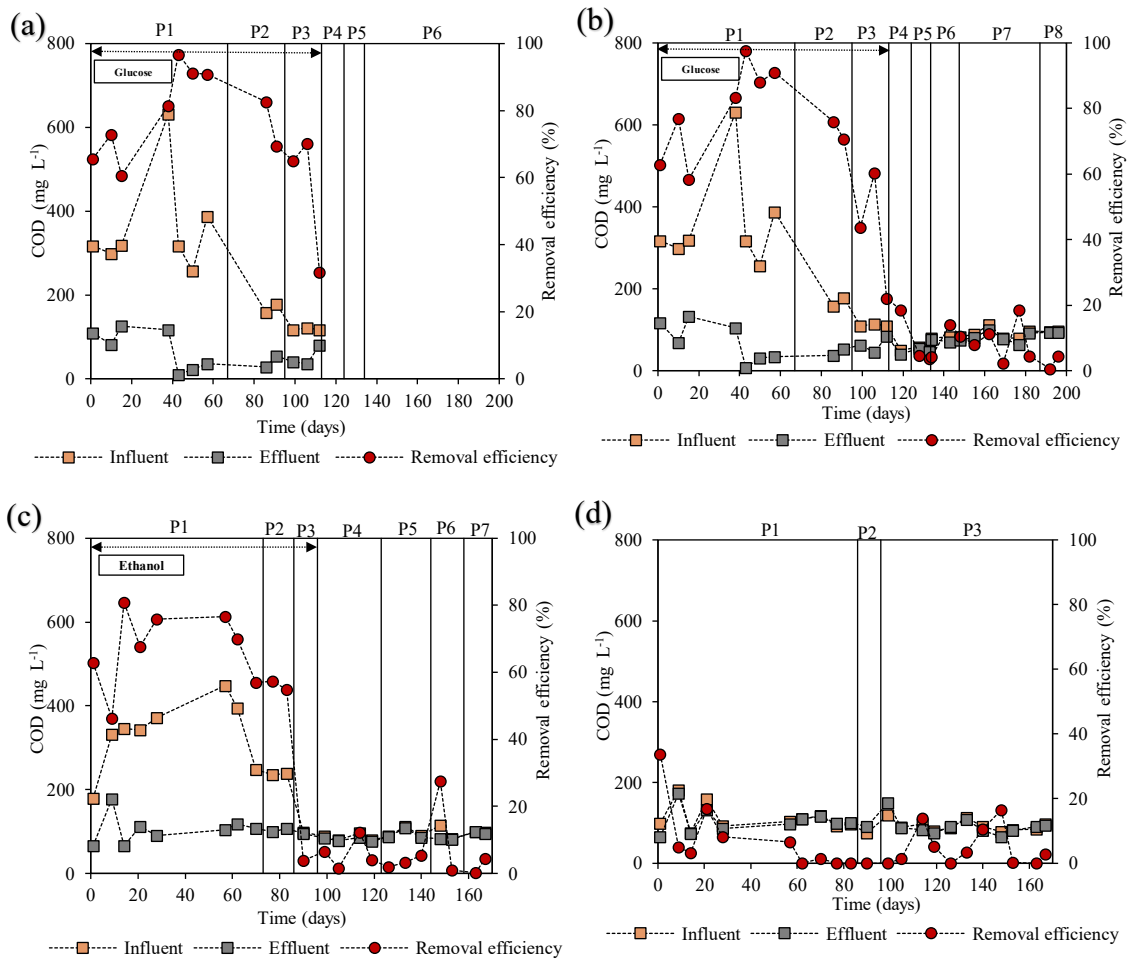


Figure 21 - COD concentrations in the influent and effluent of the reactors and removal efficiency throughout the operational phases. The vertical lines indicate transitions between experimental phases: a) MBBR1, b) MBBR2, c) MBBR3, and d) MBBR4.

4.1.2 Nitrification Performance and Oxidized Nitrogen Species Distribution

Figure 22 presents the time series of ammonium nitrogen concentrations in both the influent and effluent throughout the different operational phases of the reactors, along with the oxidized nitrogen species present during these phases. Figure 23 shows the average concentrations of these oxidized nitrogen species for each operational phase. The error bars in Figure 23 indicate the variability of each species observed within the respective phases. The elevated concentrations of nitrite and nitrate observed in certain phases in the influent of the reactors fed with real wastewater from the secondary treatment stage of the petroleum refinery were attributed to the inherent characteristics of

this type of wastewater. Overall, the four MBBR systems showed stable nitrification, maintaining high ammonium removal under carbon limitation and reduced HRT. Despite temporary declines under increased hydraulic stress, all systems ultimately achieved stable and effective nitrification, confirming the resilience of the biofilm.

MBBR1, serving as the control and receiving only SW, demonstrated the optimal potential of MBBR technology for ammonium removal under well-defined, non-toxic influent conditions. During P1, biofilm formation and nitrifying enrichment led to moderate ammonium removal that progressively increased, reaching 90% and a concentration of treated effluent of $5 \text{ mgNH}_4^+-\text{N L}^{-1}$ after 38 days (Figure 22a). In P2, under lower organic carbon availability, the system sustained approximately $76 \pm 1 \%$ removal and produced treated effluent with $13 \pm 1 \text{ mgNH}_4^+-\text{N L}^{-1}$. Partial nitrification was evident in these initial stages, with nitrite accumulation of $7 \pm 8 \text{ mgNO}_2^--\text{N L}^{-1}$ in P1 and $4 \pm 6 \text{ mgNO}_2^--\text{N L}^{-1}$ in P2 (Figure 22b). Ammonium removal improved in P3, and during P4–P5, the reactor reached near-complete nitrification, achieving an average removal efficiency of $96 \pm 2\%$. Effluent ammonium remained below $4 \pm 5 \text{ mgNH}_4^+-\text{N L}^{-1}$, and nitrate dominated the oxidized nitrogen profile, reaching $41 \pm 6 \text{ mgNO}_3^--\text{N L}^{-1}$ in P5. When hydraulic stress was introduced in P6 by shortening the HRT from 4 to 2 h, ammonium removal initially declined to approximately 50%, accompanied by an increase in effluent ammonium to $15 \text{ mg NH}_4^+-\text{N L}^{-1}$ and accumulation of nitrite to an average of $16 \pm 7 \text{ mg NO}_2^--\text{N L}^{-1}$. Despite this disruption, MBBR1 recovered by the end of the phase, reaching $92 \pm 5\%$ removal and $2 \pm 2 \text{ mgNH}_4^+-\text{N L}^{-1}$ in the effluent, while nitrite accumulation was also reduced to $2 \pm 1 \text{ mg NO}_2^--\text{N L}^{-1}$, demonstrating strong adaptation to the reduced HRT and increased nitrogen load.

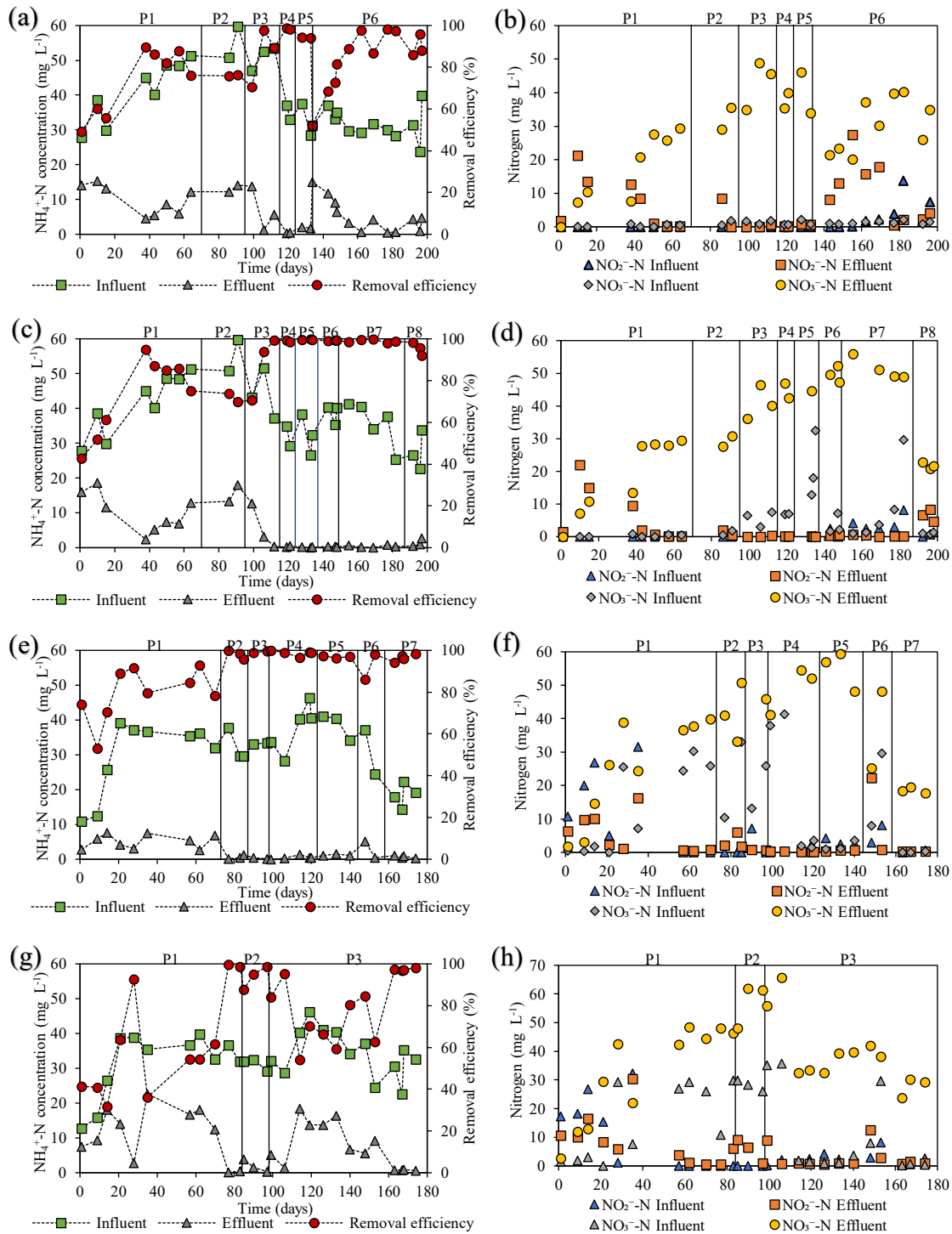


Figure 22 - Evolution of ammonium removal efficiency and corresponding influent and effluent oxidized nitrogen species during the operational phases of the MBBR systems: a-b) MBBR1, c-d) MBBR2, e-f) MBBR3, and g-h) MBBR4.

MBBR2 maintained stable and resilient nitrification among all phases. As biofilm maturation progressed during P1, ammonium removal gradually increased and reached $72 \pm 3\%$. A treated effluent ammonium concentration of $16 \pm 3 \text{ mgNH}_4^+-\text{N L}^{-1}$ was obtained at the end of P2 (Figure 22c), with nitrate content increasing to $29 \pm 2 \text{ mgNO}_3^--\text{N L}^{-1}$ under this condition (Figure 22d). After the reduction of organic carbon and complete substitution of synthetic wastewater by real wastewater, the reactor consistently maintained near-complete ammonium oxidation during P3-P6, with effluent concentrations below $1 \text{ mgNH}_4^+-\text{N L}^{-1}$. Almost all ammonium was converted to nitrate, whose concentration increased to $58 \pm 12 \text{ mgNO}_3^--\text{N L}^{-1}$ during P6, showing a well-adapted nitrifying community. Even after the reduction in HRT to 4 h in P7, MBBR2 maintained removal close to 100%, with nitrate remaining dominant ($48 \pm 1 \text{ mgNO}_3^--\text{N L}^{-1}$). A slight performance decline was detected only at 2 h HRT in P8 ($95 \pm 3\%$), and nitrite accumulation increased to $6 \pm 2 \text{ mgNO}_2^--\text{N L}^{-1}$, indicating mild inhibition of nitrite oxidation.

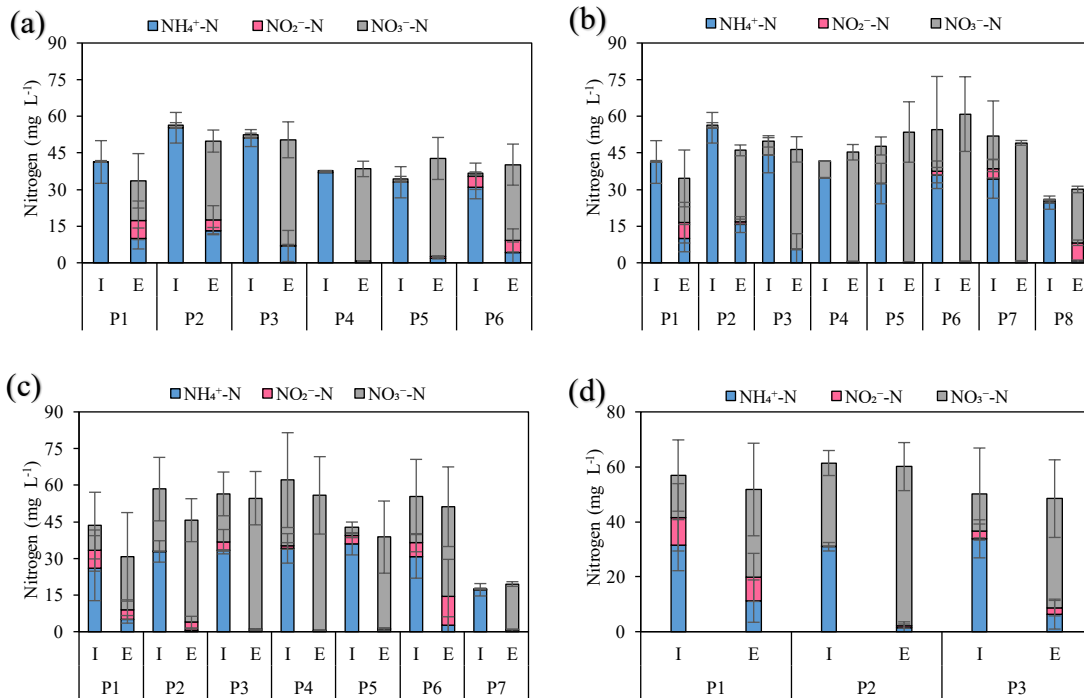


Figure 23 - Average Influent (I) and Effluent (E) nitrogen species profiles in MBBR systems across operational phases: a) MBBR1, b) MBBR2, c) MBBR3, and d) MBBR4.

MBBR3 operated solely with real wastewater but initially supplemented with ethanol. This reactor maintained the most stable and resilient nitrification among all systems. During P1–P2, ammonium removal increased to $98 \pm 2\%$, the concentration of ammonium in the treated effluent was below 2 mg L^{-1} , and nitrite accumulated to $3 \pm 2 \text{ mgNO}_2^- \text{--N L}^{-1}$, as shown in Figures 22e and 22f, respectively. As ethanol addition was reduced and later eliminated from the feeding, nitrification performance remained high and very close to 100%, maintaining $\text{NH}_4^+ \text{--N}$ below 2 mg L^{-1} in the effluent and producing nitrate concentrations of approximately $55 \pm 13 \text{ mgNO}_3^- \text{--N L}^{-1}$ during P4. Effluent nitrite remained below $1 \text{ mgNO}_2^- \text{--N L}^{-1}$, confirming effective acclimation to carbon-limited conditions up to P5 at 4 h HRT. When HRT was shortened to 2 h in P6, ammonium removal remained high ($92 \pm 6\%$), yet nitrite accumulation increased to a maximum amount of $22 \text{ mgNO}_2^- \text{--N L}^{-1}$, suggesting partial nitrification; however, by the end of the phase, nitrite was reduced to less than $1 \text{ mg NO}_2^- \text{--N L}^{-1}$. In P7, influent ammonium decreased to around $17 \pm 3 \text{ mg NH}_4^+ \text{--N L}^{-1}$ to evaluate nitrification performance under low ammonium availability. Despite this reduction, the system maintained a high ammonium removal efficiency of $97 \pm 2\%$, producing an effluent with $\text{NH}_4^+ \text{--N}$ concentrations below 1 mg L^{-1} and complete oxidation to nitrate, reaching approximately $19 \pm 1 \text{ mg NO}_3^- \text{--N L}^{-1}$.

MBBR4, operated exclusively with real wastewater without carbon supplementation, showed the most challenging acclimation period (Figure 22e). During P1, ammonium removal fluctuated between 40 and 90%, with average effluent ammonium concentrations near $11 \pm 8 \text{ mgNH}_4^+ \text{--N L}^{-1}$, accompanied by nitrite content of $9 \pm 9 \text{ mgNO}_2^- \text{--N L}^{-1}$, indicating prolonged adaptation to inhibitory compounds present in the real refinery wastewater. In P2, performance improved to $94 \pm 6\%$, nitrate increased to $58 \pm 9 \text{ mgNO}_3^- \text{--N L}^{-1}$, and residual nitrite decreased to less than 1 mg L^{-1} . After HRT was reduced to 2 h in P3, the reactor experienced a temporary performance decline, with removal efficiency dropping to 54%, effluent ammonium rising to $19 \text{ mg NH}_4^+ \text{--N L}^{-1}$, and nitrite increasing to $8.9 \text{ mg NO}_2^- \text{--N L}^{-1}$. However, it progressively recovered and ultimately reached complete ammonium removal, producing an effluent with less than $1 \text{ mgNH}_4^+ \text{--N L}^{-1}$ and nitrate near $40 \pm 14 \text{ mgNO}_3^- \text{--N L}^{-1}$. Although nitrification performance in MBBR4 was less stable than in the other reactors, the system was still capable of achieving complete ammonium oxidation under potentially inhibitory

conditions and without a carbon-supplemented startup phase, indicating a high level of biofilm resilience and operational adaptability.

The comparison of these four reactors concludes that while MBBR biofilms possess inherent adaptability and strong self-recovery capabilities regardless of the startup method, the specific acclimation strategy significantly dictates the system's initial stability and resilience. MBBR2 and MBBR3 demonstrated the most consistent nitrification and resistance to shock, whereas the direct application of real wastewater in MBBR4 caused initial instability before eventually achieving complete removal.

Based on the comparative analysis of the four reactors, it can be concluded that MBBR4, which was subjected to direct real wastewater application without labile organic carbon supplementation, exhibited a prolonged and unstable acclimation phase lasting nearly 80 days. This indicates that the presence of inhibitory compounds and complex organic matter in real wastewater roughly increases the time required for the biofilm to overcome environmental stress and develop a stable nitrification capacity. However, the experimental results demonstrate that this lag in adaptation can be effectively mitigated through strategic operational adjustments. Although treating the same complex influent as MBBR4, MBBR3 demonstrated that the supplementation of an easily biodegradable carbon (ethanol) in the initial stages enabled the reactor to rapidly attain high removal efficiencies (>80%) within a reduced operational period. Furthermore, the rapid colonization of heterotrophic organisms established a robust biofilm foundation for the nitrifiers to attach, making MBBR3 significantly more resilient to subsequent operational changes. Furthermore, the strategy of gradual acclimation employed in MBBR2 proved highly effective in ensuring operational stability during the transition to real wastewater. By allowing the biofilm to mature on synthetic wastewater first (mimicking the timeline of the control reactor (MBBR1)), the system established a resilient nitrification capacity before introducing real wastewater. Consequently, when the synthetic matrix was fully replaced with real wastewater in P6, the reactor experienced no performance deterioration, effectively eliminating the adaptation lag observed in MBBR4.

In general, the accelerated biofilm formation in reactors fed with organic material (MBBR1, MBBR2, and MBBR3) is primarily driven by the proliferation of fast-growing heterotrophic bacteria. Unlike autotrophic nitrifying bacteria, which grow slowly and lack the ability to produce significant extracellular polymeric substances for adhesion,

heterotrophs grow rapidly in the presence of organic carbon and enhance the production of EPS. These EPS components, especially polysaccharides, act as a fixation matrix that effectively glues biomass to the carrier materials (BASSIN *et al.*, 2012). This matrix facilitates the initial attachment of bacteria to the plastic surface and supports the rapid development of microcolonies, significantly reducing the startup time compared to systems that rely solely on the slow colonization by autotrophic microorganisms, such as MBBR4, whose influent consisted primarily of non-biodegradable COD originating from the secondary treatment stage at the oil refinery.

Similarly, Fang *et al.* (1993) found that the addition of glucose to refinery wastewater acts as a crucial biostimulant, accelerating the enrichment of nitrifying bacteria and facilitating the rapid oxidation of ammonia to nitrite. Their study demonstrated that supplementing the influent with glucose enabled the removal of over 90% of ammonia-nitrogen within 7 to 14 days, whereas unsupplemented systems struggled to establish nitrification. However, they noted that while glucose efficiently established the ammonia-oxidizing population, the subsequent conversion of nitrite to nitrate remained limited until yeast powder was added to stimulate *Nitrobacter* growth.

Bassin *et al.* (2012) observed that the development of stable nitrifying biofilms in MBBR systems was highly affected by the presence of organic carbon during startup. In their study, an autotrophic reactor with no COD addition needed approximately 60–70 days to form a thin biofilm and reach complete ammonium oxidation, whereas reactors that underwent an initial phase intended for heterotrophic growth achieved mature biofilms much more quickly, within 20–30 days. Using a similar methodology, Piculell *et al.* (2016) added acetate to the MBBR influent during startup to promote initial biofilm growth on the carriers. Acetate was supplied at 500 mg L⁻¹ for the first 30 days and gradually reduced, then fully removed once stable nitrification was established.

Based on the operational results, it can also be concluded that reducing the HRT to 2 h serves as a critical stressor that exposes the kinetic limitations of the biofilm, particularly impacting the stability of NOB. While the biofilm communities in all reactors demonstrated a strong capacity for recovery and adaptation, the immediate response to hydraulic shock differed significantly based on the acclimation strategy; Initially, MBBR1 and MBBR4 suffered a significant drop in ammonium removal efficiency (to ~50%), whereas MBBR2 and MBBR3 exhibited superior resilience by maintaining high

removal rates. Despite these varying impacts on initial ammonium oxidation, all four reactors experienced a specific bottleneck in the second step of nitrification at the beginning of the phase, evidenced by nitrite accumulation. Ultimately, as the systems adapted and ammonium removal efficiencies recovered, this bottleneck was resolved, and the process successfully transitioned to complete nitrification. This suggests that while robust startup strategies can effectively protect AOB from hydraulic stress, NOB populations remain the most vulnerable component in the system, being more prone to inhibition when the hydraulic load is aggressively increased. This behavior can be attributed to kinetic differences among nitrifying microorganisms. As reported by Fang *et al.* (2009), the rate of ammonium oxidation exceeded the rate of nitrate production. Moreover, due to their higher specific growth rates, AOB tend to dominate the outer biofilm layers where oxygen is more available, whereas NOB are more likely to proliferate in the inner layers, where oxygen concentrations are lower (KINDICHI *et al.*, 2006).

These findings are in agreement with previous studies showing that lower HRTs lead to reduced ammonium removal, nitrite accumulation, and a shift toward partial nitrification. Iannacone *et al.* (2019) reported that reducing HRT from 48 to 24 h significantly affected nitrification by disrupting the balance between ammonium and nitrite oxidation. The HRT reduction caused a severe but transient inhibition of nitrification, evidenced by a rapid accumulation of ammonium (N-NH_4^+) in the effluent. Although ammonium oxidation later recovered, the system shifted toward partial nitrification, with increased nitrite (NO_2^-) and decreased nitrate (NO_3^-) concentrations. Bassin *et al.* (2016) observed that reducing the HRT from 12 to 6 h caused an immediate decline in ammonium removal efficiency, with the reactor containing thinner biofilm requiring a significantly longer recovery period (60 days) compared to the system with thicker biofilm, which recovered in 20 days. This vulnerability to hydraulic changes was attributed to the critical role of suspended biomass; at higher retention times, the suspended solids resulting from biofilm detachment were estimated to contribute up to 85% of the total ammonium oxidation. Consequently, the reduction in HRT triggered the washout of this highly active suspended fraction, leading to a performance deterioration that the attached biofilm, despite increasing its specific nitrifying activity, could not fully compensate for at the lower HRTs.

Another study by Aktan *et al.* (2025) identified HRT as a key factor controlling nitrification completeness in an MBBR system. At an HRT of 12 h, complete nitrification was achieved with low effluent ammonium and no nitrite accumulation. However, when the HRT was reduced below the critical threshold (6 h in this study), excessive hydraulic stress and limited contact time between the biofilm and wastewater were imposed. This reduction destabilized the biofilm, leading to significant biomass detachment and a pronounced decrease in nitrification efficiency, accompanied by nitrite accumulation.

A comparative analysis of the reactors reveals that while synthetic wastewater is sufficient for establishing baseline nitrification activity, exposure to the complex matrix of real wastewater is critical for developing operational robustness. MBBR1, operating exclusively with synthetic wastewater, achieved effective ammonium removal under stable conditions but proved highly sensitive to hydraulic stress, experiencing a sharp performance decline to 50% removal when the HRT was reduced. In contrast, the introduction of real wastewater in MBBR2 significantly enhanced its stability; after the complete substitution of synthetic with real wastewater, the reactor became notably more resilient against operational changes, maintaining near-complete ammonium removal even under the aggressive hydraulic conditions that destabilized the control system. Similarly, MBBR3, which operated with real wastewater from the beginning, developed a highly stable and robust biofilm that consistently maintained high ammonium removal efficiencies (>97%). This demonstrates that while real wastewater presents initial toxicity challenges, the resulting biofilm community possesses superior adaptability and resistance to shock loading compared to biomass grown solely on synthetic medium. Similarly, Ashkanani *et al.* (2019) observed that reactors treating real wastewater demonstrated higher ammonia removal rates and significantly shorter adaptation times compared to those treating synthetic wastewater, attributing this superior performance to the presence of essential micronutrients, organic matter, and the natural buffering capacity found in real matrices. Additionally, the study by Zhang *et al.* (2024) showed that the MBBR treating real wastewater (R-MBBR) significantly outperformed the system treating simulated wastewater (S-MBBR) in both nitrification efficiency and startup kinetics. The authors reported that biofilm formation in the R-MBBR was achieved in only 45 days, which was 30 days faster than the 75 days required for the S-MBBR. The authors attributed this observation to differences in microbial community

structure. The real wastewater likely promoted a higher relative abundance of dominant functional bacterial genera, which enhanced biofilm formation, increased biofilm thickness, and accelerated microbial enrichment, resulting in a shorter startup period and better performance compared to the S-MBBR.

The nitrification performance observed in each reactor is strongly supported by the trends in average applied ammonium surface loading rates (SLR) and surface removal rates (SRR). In general, all reactors exhibited an increase in ammonium removal efficiency in parallel with the progressive rise in applied $\text{NH}_4^+\text{-N}$ SLR, indicating the successful development and adaptation of nitrifying biofilms over time (Figure 24).

In MBBR1, the ammonium SLR and SRR remained closely aligned in all phases, even after external organic carbon was eliminated in P4, as observed in Figure 24a. During P5, at HRT of 4 h, the ammonium SLR and SRR were $0.8 \pm 0.15 \text{ gNH}_4^+\text{-N m}^{-2} \text{ d}^{-1}$ and $0.7 \pm 0.15 \text{ gNH}_4^+\text{-N m}^{-2} \text{ d}^{-1}$, respectively. In P6, when HRT was further reduced to 2 h, the system was subjected to SLR of $1.5 \pm 0.2 \text{ gNH}_4^+\text{-N m}^{-2} \text{ d}^{-1}$ and sustained stable performance, removing $1.3 \pm 0.2 \text{ gNH}_4^+\text{-N m}^{-2} \text{ d}^{-1}$. This response indicates a mature and resilient autotrophic biofilm capable of withstanding increased nitrogen surface loading.

MBBR2 exhibited behavior similar to MBBR1 in the initial stages. When the system was subjected only to real wastewater and the HRT was reduced to 4 h in P7, the ammonium SRR approached the SLR, both converging around $0.9 \pm 0.1 \text{ gNH}_4^+\text{-N m}^{-2} \text{ d}^{-1}$ (Figure 24b). By P8, the reactor tolerated ammonium SLR near $1.3 \pm 0.3 \text{ gNH}_4^+\text{-N m}^{-2} \text{ d}^{-1}$, demonstrating the effectiveness of the acclimation strategy and the biofilm's adaptation to oil refinery wastewater composition.

MBBR3 (Figure 24c), initially supplied with ethanol as an external carbon source, achieved high ammonium removal from the beginning of operation. The ammonium SRR closely tracked the SLR, confirming that ethanol promoted rapid establishment of a functional nitrifying biofilm, even when ethanol was removed from the influent in P4 ($0.6 \pm 0.1 \text{ gNH}_4^+\text{-N m}^{-2} \text{ d}^{-1}$), and the HRT was reduced to 4 h in P5 ($0.9 \pm 0.1 \text{ gNH}_4^+\text{-N m}^{-2} \text{ d}^{-1}$). In P6, the ammonium SRR reached $1.4 \pm 0.3 \text{ gNH}_4^+\text{-N m}^{-2} \text{ d}^{-1}$, while the ammonium SLR was $1.5 \pm 0.4 \text{ gNH}_4^+\text{-N m}^{-2} \text{ d}^{-1}$. In the final phase (P7), the SLR decreased to $0.9 \pm 0.2 \text{ gNH}_4^+\text{-N m}^{-2} \text{ d}^{-1}$ due to a lower concentration of ammonium nitrogen in the wastewater, and the reactor removed $0.8 \pm 0.1 \text{ gNH}_4^+\text{-N m}^{-2} \text{ d}^{-1}$, further demonstrating its operational robustness.

Unlike the other reactors, MBBR4 was fed real wastewater from the start and operated without external carbon supplementation. Initially, the ammonium SLR was low ($0.3 \pm 0.2 \text{ gNH}_4^+\text{-N m}^{-2} \text{ d}^{-1}$), reflecting a longer acclimation period (Figure 24d). However, the performance gradually improved in P2 ($0.7 \pm 0.3 \text{ gNH}_4^+\text{-N m}^{-2} \text{ d}^{-1}$). In P3, when operating at 2 h HRT, the reactor reached an ammonium SRR of $1.3 \pm 0.2 \text{ gNH}_4^+\text{-N m}^{-2} \text{ d}^{-1}$, while the ammonium SLR was $1.6 \pm 0.3 \text{ gNH}_4^+\text{-N m}^{-2} \text{ d}^{-1}$. These results confirm that even under more severe and variable real wastewater conditions, the MBBR system could stabilize and sustain high nitrification performance.

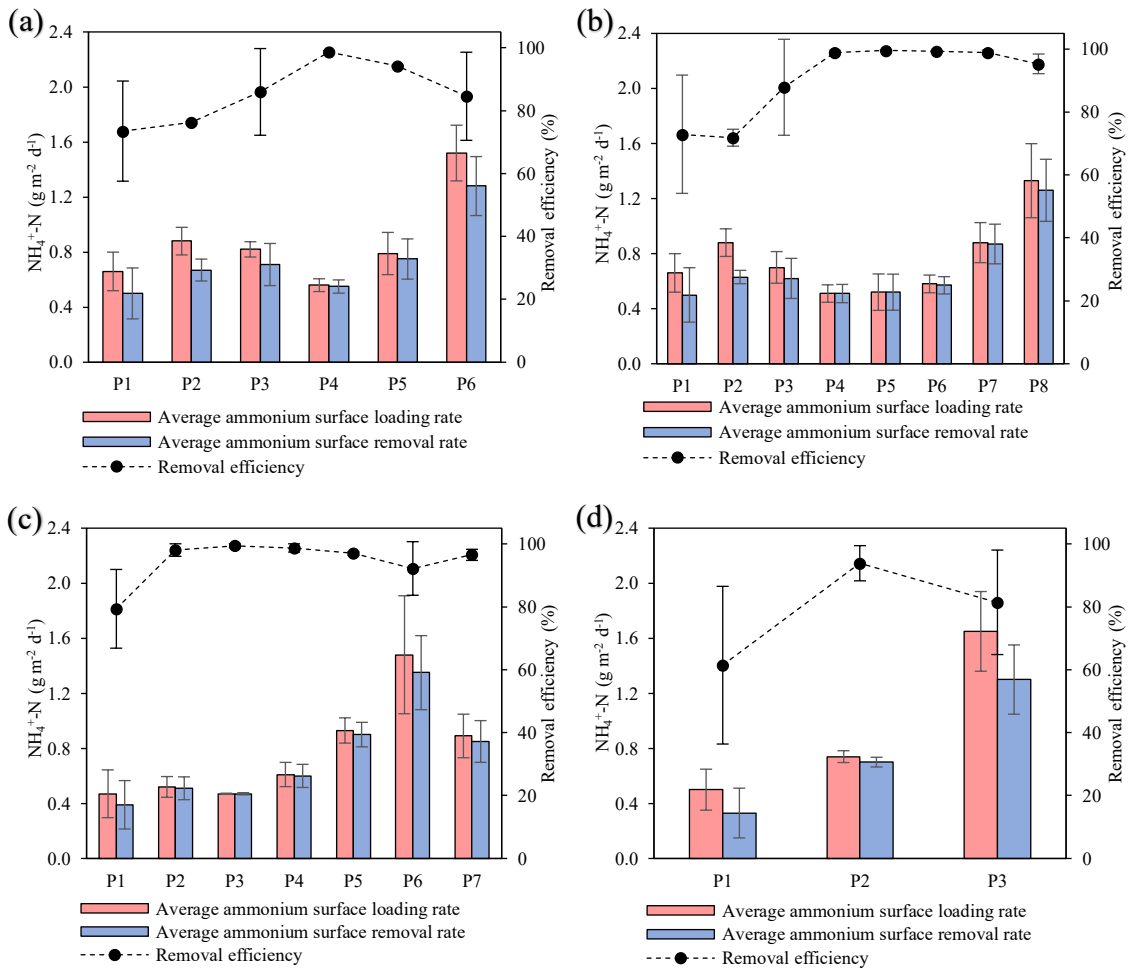


Figure 24 - Average ammonium surface loading rate (SLR) and ammonium surface removal rate (SRR) for all reactors throughout the operational phases: a) MBBR1, b) MBBR2, c) MBBR3, and d) MBBR4.

The results of ammonium SRR observed in this study are consistent with those reported in the literature. Ashkanani *et al.* (2019) showed significant variation of SRR depending on the type of carrier used. The highest ammonium SRR was obtained with

the Kaldnes K3 media, reaching $1.103 \pm 0.06 \text{ gN m}^{-2} \text{ d}^{-1}$. In comparison, the K5 carrier allowed to achieve a slightly lower SRR of $0.920 \pm 0.06 \text{ gN m}^{-2} \text{ d}^{-1}$. Despite its higher specific surface area, the M biochip carrier exhibited the lowest performance, with a SRR of only $0.295 \pm 0.05 \text{ gN m}^{-2} \text{ d}^{-1}$. As reported by Bassin *et al.* (2012), the ammonium SRR is strongly influenced by both the operational mode and reactor configuration. In a continuous autotrophic reactor, the ammonium SRR closely followed the SLR as it was progressively increased from 0.2 to $1.0 \text{ gN m}^{-2} \text{ d}^{-1}$, while maintaining ammonium removal efficiencies near 100%. In addition, Lima *et al.* (2016) reported that a MBBR system maintained robust nitrification stability during the early stages of operation, achieving over 90% ammonium removal at an average ammonium SRR of $0.5 \text{ gN m}^{-2} \text{ d}^{-1}$.

Figure 25 provides a comparative assessment of reactor performance by relating the ammonium SLR and SRR (x- and y-axes). The solid black line represents the identity line ($x = y$), indicating equal loading and removal rates, while the red regression line depicts the actual reactor response. The slope of each regression corresponds to the average global ammonium removal efficiency over the entire operational period, while the coefficient of determination (R^2) indicates the stability of this response under variable loading.

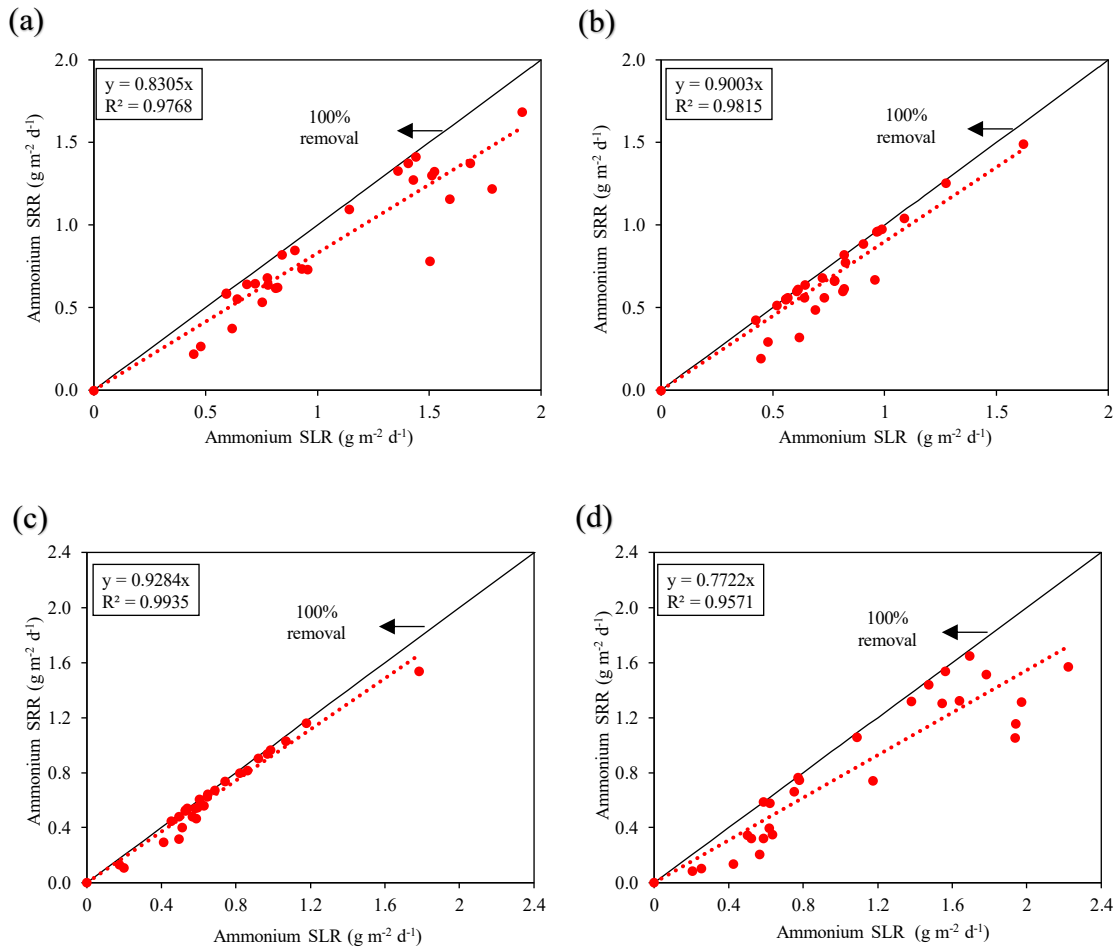


Figure 25 - Correlation between ammonium SLR and SRR for all reactors: a) MBBR1, b) MBBR2, c) MBBR3, and d) MBBR4.

These results reinforce the nitrification trends observed experimentally. MBBR3 presented the highest slope, corresponding to a global removal efficiency of 93%. This reactor exhibited the most stable response ($R^2 = 0.99$), confirming that ethanol-assisted acclimation accelerated biofilm development and sustained high removal under increased ammonium loading rates. MBBR2 followed closely with 90% efficiency and R^2 of 0.98, demonstrating that a gradual transition to real wastewater with almost no biodegradable COD supported the formation of a resilient nitrifying community. MBBR1 showed 83% overall removal efficiency and R^2 of 0.97, validating the expected baseline behavior and robustness of autotrophic nitrifiers in non-toxic synthetic wastewater. Although MBBR4 exhibited the lowest slope (77% total efficiency and R^2 of 0.95) and greater variability, its ability to approach the 100% ammonium removal line without any external carbon

supplementation highlights the adaptability of this biofilm-based system to sustain nitrification in a secondary treated stream with potential recalcitrant compounds not removed in the biological secondary treatment stage and under fluctuating influent characteristics.

4.1.3 Batch Assessment of Nitrification Activity

Figures 26–29 present the temporal profiles of nitrogen species concentrations obtained from the batch trials conducted at the end of each operational phase for each reactor. During the operational phases of the reactors, the batch activity assays provided clear evidence of the occurrence of nitrification. As shown in the Figures, simultaneous nitrate production occurred alongside the continuous decrease in ammonium concentration. Furthermore, during the tests conducted in each phase, ammonium was gradually converted into oxidized inorganic nitrogen forms, first nitrite and subsequently nitrate. However, in some phases, this conversion occurred more rapidly, such that nitrite peaks were considerably less pronounced. These results indicate that, in the reactors treating real refinery wastewater, its presence did not exert a toxic or inhibitory effect on nitrification performance, a process that is highly sensitive to inhibitory compounds and often characterized by nitrite accumulation under unfavorable conditions (CAO *et al.*, 2015).

Maximum ammoniacal nitrogen removal was achieved at different times for the tests conducted during distinct operational phases of the MBBRs. In MBBR1, maximum removal occurred after approximately 360 min during P2–P3, 180 min in P4 and P5, and 120 min in P6. In MBBR2, maximum removal was reached after about 360 min during P2–P3, 180 min during P4–P6, and 120 min during P8. For MBBR3, maximum removal was observed after 360 min in P1, 180 min in P2 and P4, 120 min in P3, P5, and P7, and 60 min in P6. In MBBR4, maximum removal was achieved after approximately 300 min in P1, 120 min in P2, and 90 min in P3.

Overall, the use of refinery wastewater previously subjected to secondary treatment did not affect the time required to reach maximum NH_4^+ -N removal. Furthermore, maximum ammonium removal consistently occurred at times equal to or

shorter than the applied hydraulic retention time, indicating that increasing the HRT does not necessarily enhance nitrification efficiency.

Linear regression analyses of the experimental data confirmed that ammonium removal followed zero-order kinetics, with coefficients of determination (R^2) exceeding 0.9 for all datasets. Data from biofilm quantification and the corresponding batch trials were used to calculate the maximum biomass-specific ammonium removal rates, which are summarized in Table 13. The attached biomass was also reported in volumetric units (g L^{-1}) to allow for consistent comparison with the suspended solids. Across all four MBBRs, the maximum specific ammonium removal rate generally increased when influent COD was eliminated, and HRT was moderately reduced to 4 h, while further decreases in HRT to 2 h or increases in VAS often led to stabilization or slight declines in specific removal rate.

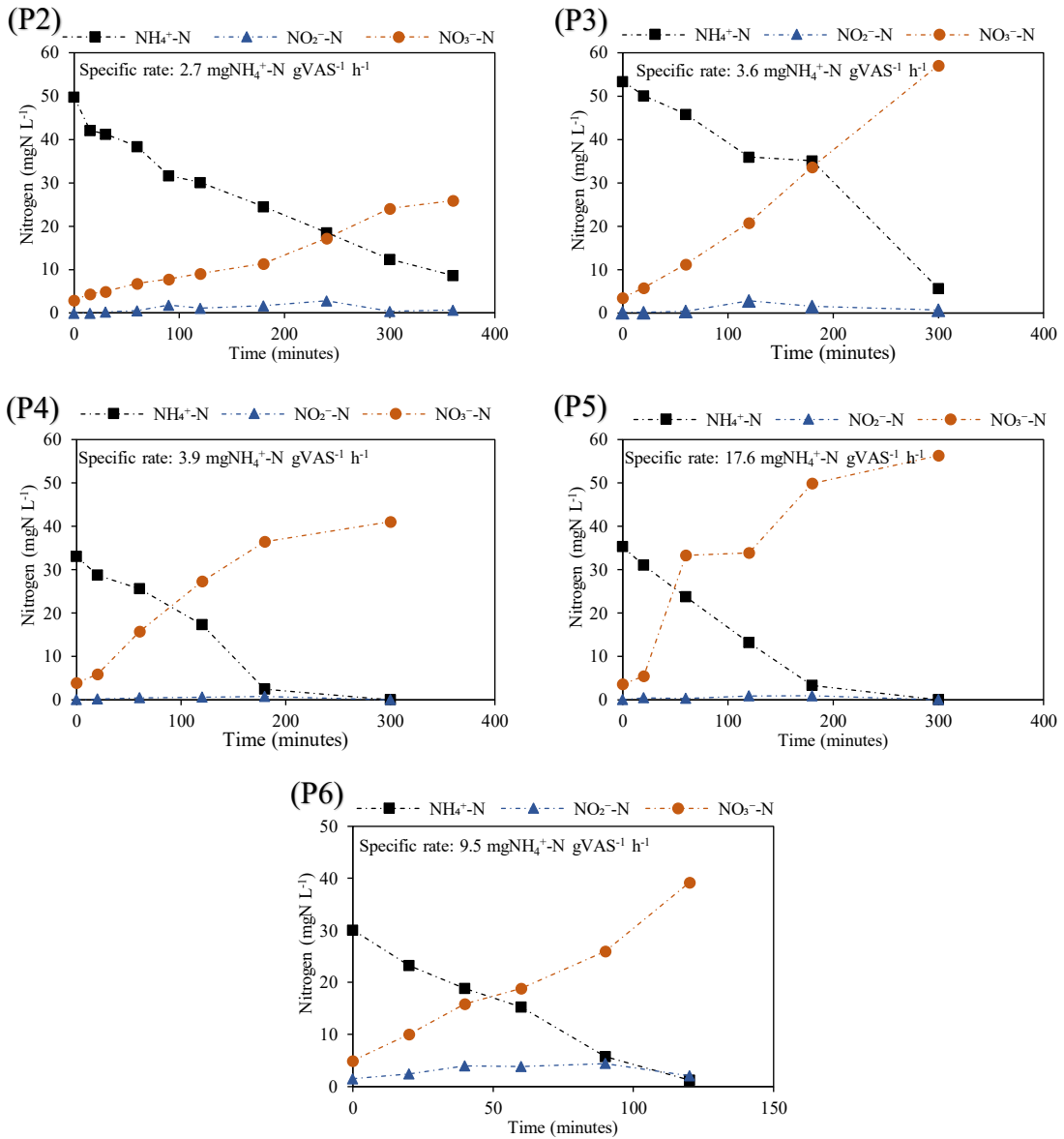


Figure 26 - Temporal profiles of nitrogen species in MBBR1 obtained during the activity batch tests corresponding to phases P2–P6.

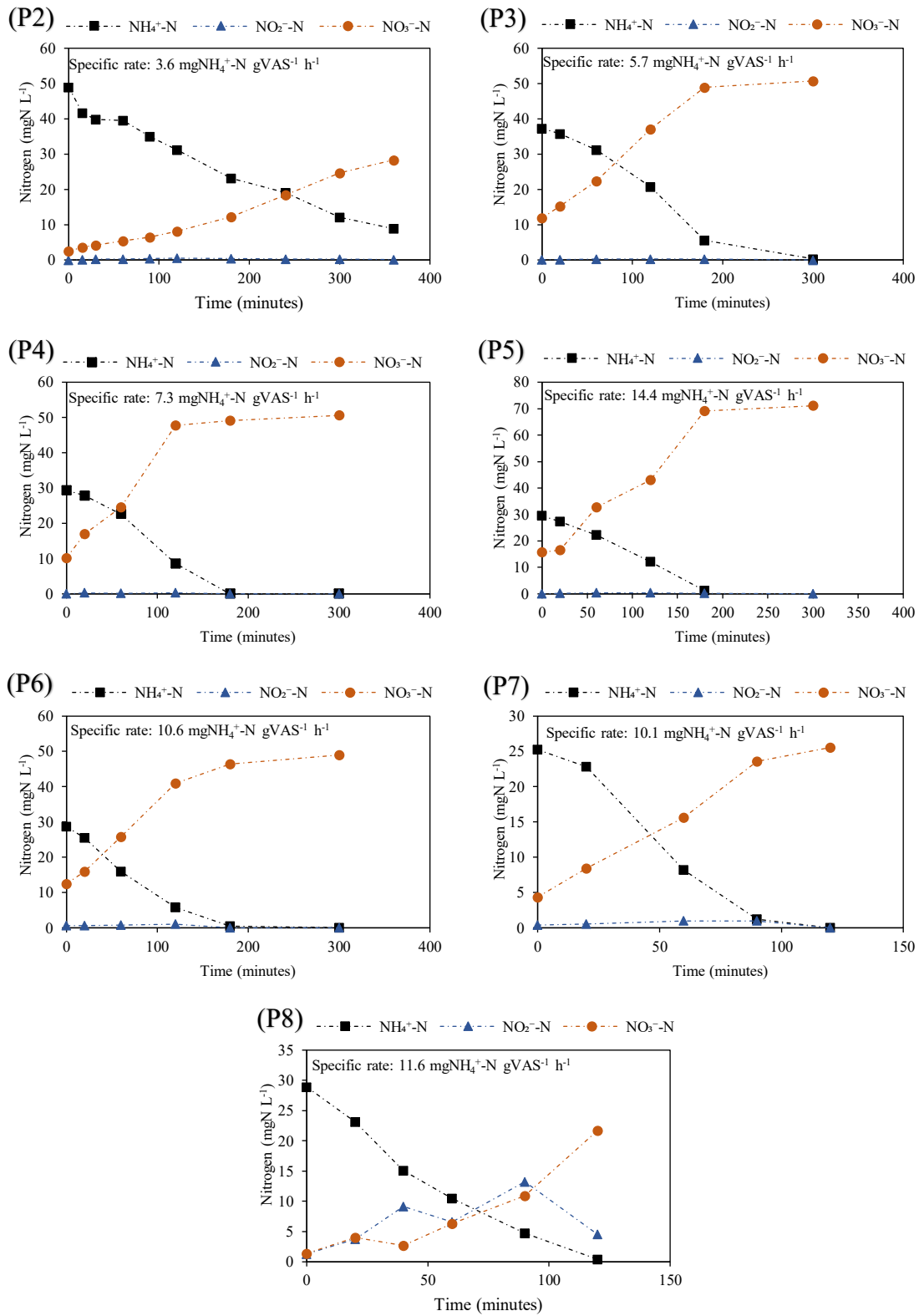


Figure 27 - Temporal profiles of nitrogen species in MBBR2 obtained during the activity batch tests corresponding to phases P2–P8.

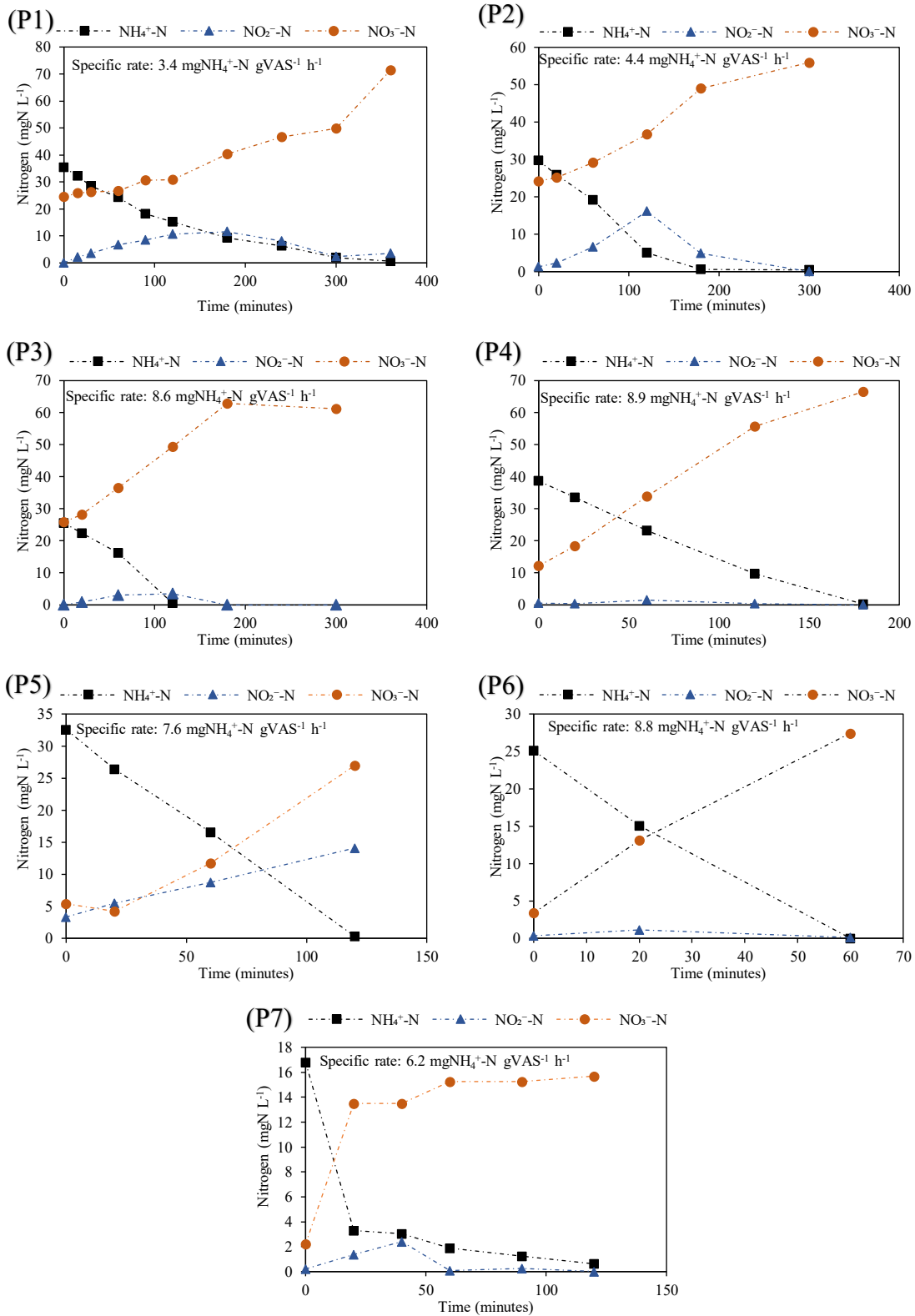


Figure 28 - Temporal profiles of nitrogen species in MBBR3 obtained during activity batch tests corresponding to phases P1–P7.

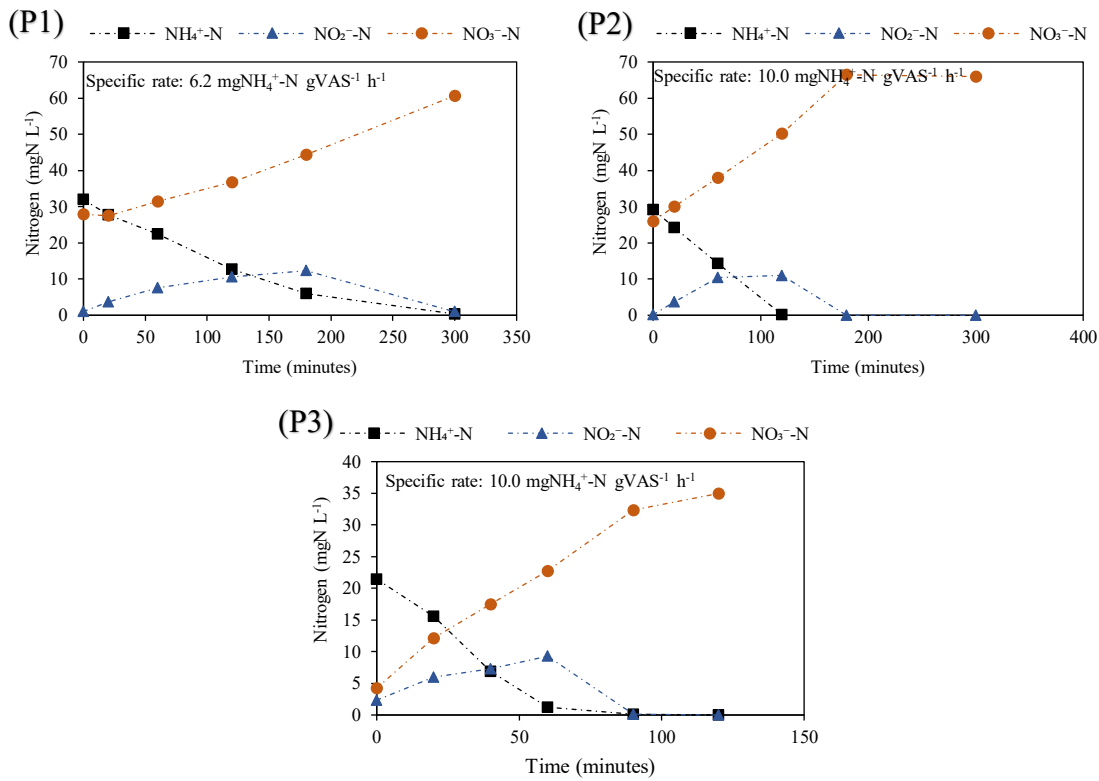


Figure 29 - Temporal profiles of nitrogen species in MBBR4 obtained during activity batch tests corresponding to phases P1–P3.

MBBR1 showed a gradual increase in the maximum ammonium removal rate from P1 to P4, attaining the highest value under organic carbon-free conditions in P4 ($97 \text{ mgNH}_4^+\text{-N gVAS}^{-1} \text{ d}^{-1}$). When the HRT was subsequently reduced to 4 h in P5, the maximum ammonium removal rate increased sharply to $422 \text{ mgNH}_4^+\text{-N gVAS}^{-1} \text{ d}^{-1}$. However, a further reduction of HRT to 2 h (P6) led to a decline in the maximum rate to $228 \text{ mgNH}_4^+\text{-N gVAS}^{-1} \text{ d}^{-1}$, likely associated with the concurrent rise in VAS concentration from 0.6 g L^{-1} in P5 to 1.5 g L^{-1} in P6. At an HRT of 2 h, a steady increase in average bacterial adhesion to the plastic carriers was observed. The lower HRT led to higher loading rates, which promoted greater biomass attachment to the carriers. As a consequence of the higher VAS concentrations, the maximum biomass-specific ammonium removal rates (expressed as $\text{mg NH}_4^+\text{-N gVAS}^{-1} \text{ d}^{-1}$) exhibited a decreasing trend.

MBBR2 exhibited a steady increase in the maximum ammonium removal rate from P2 to P5, reaching a peak of approximately $345 \text{ mgNH}_4^+\text{-N gVAS}^{-1} \text{ d}^{-1}$ in P5. Following this peak, the maximum rate exhibited a slight plateau across P6, likely due to the rise in VAS concentration from 0.6 g L^{-1} in P5 to 0.9 g L^{-1} in P6, when the reactor operated with 100% RW and in the absence of COD. As the HRT was further reduced from 6 h to 2 h across P6–P8, the maximum removal rate remained relatively stable, ranging between 240 and $280 \text{ mgNH}_4^+\text{-N gVAS}^{-1} \text{ d}^{-1}$. This stability indicates that the reactor maintained consistent nitrification capacity and sustained a resilient nitrifying biofilm despite the operational changes.

In MBBR3, the maximum ammonium removal rate was initially low in P1 ($82 \text{ mgNH}_4^+\text{-N gVAS}^{-1} \text{ d}^{-1}$) but increased progressively as influent COD was reduced to zero, reaching $214 \text{ mgNH}_4^+\text{-N gVAS}^{-1} \text{ d}^{-1}$ by P4. Comparable to the trend observed in MBBR2, the subsequent reduction in HRT to 4 h in P5 and then to 2 h in P6 did not induce major fluctuations and the maximum rate remains relatively stable, ranging between 180 and $215 \text{ mgNH}_4^+\text{-N gVAS}^{-1} \text{ d}^{-1}$. A decline was observed in P7, when the maximum rate decreased to $149 \text{ mgNH}_4^+\text{-N gVAS}^{-1} \text{ d}^{-1}$, likely reflecting the reduction in ammonium load during this phase.

MBBR4 exhibited relatively stable maximum removal rates throughout the evaluated phases. Starting at approximately $149 \text{ mgNH}_4^+\text{-N gVAS}^{-1} \text{ d}^{-1}$ in P1, the rate increased and reached a peak of about $240 \text{ mgNH}_4^+\text{-N gVAS}^{-1} \text{ d}^{-1}$ in P2 when the HRT was reduced to 4 h. This was followed by a moderate decline in P3, when the maximum rate decreased to $192 \text{ mgNH}_4^+\text{-N gVAS}^{-1} \text{ d}^{-1}$, likely associated with the rise in VAS concentration from 1.4 g L^{-1} in P2 to 2.6 g L^{-1} in P3, resulting from enhanced biomass production under the shorter HRT.

Overall, based on the results, there is a distinct inverse relationship between the availability of biodegradable organic carbon and the biomass-specific ammonium removal rate of the biofilm. These findings collectively indicate that reducing or eliminating organic carbon minimizes the competition from heterotrophic bacteria, thereby allowing the biofilm to become highly enriched with nitrifiers and maximizing the specific nitrification capacity of the system.

An overall review of the literature consistently demonstrates that increasing organic loading or elevated COD:N ratios negatively affect the specific nitrifying activity

of attached biomass. Several studies report an inverse relationship between organic loading rate and nitrification rate, primarily driven by competition between fast-growing heterotrophic bacteria and slower-growing autotrophic nitrifiers. Under high COD conditions, heterotrophs proliferate rapidly and outcompete nitrifiers for oxygen and physical space within the biofilm, often forcing nitrifying populations into deeper layers where mass transfer resistance is greater (RITTMANN; MANEM, 1992). For example, Bassin *et al.* (2016) observed a clear decline in specific ammonium removal rates with increasing organic loading, and Lima *et al.* (2016) reported a reduction in maximum specific nitrification rates from 31 to 19 mgNH₄⁺-N gVS⁻¹ d⁻¹ as organic loading increased. Similar inverse relationships between COD:N ratio and nitrification performance were reported by Torkaman *et al.* (2015) and Carrera *et al.* (2004), both attributing the decline in nitrification to heterotrophic dominance within the biofilm under elevated organic carbon conditions. In addition, Ling and Chen (2005) investigated nitrification in industrial wastewater using three biofilters and demonstrated that increasing the influent COD:N ratio to the aerobic reactor led to an asymptotic decline in the nitrification rate.

Other studies have also highlighted the critical role of feed COD:N ratios in controlling nitrification rates. Batch activity tests conducted by Iannacone *et al.* (2019) demonstrated that lower carbon loads significantly enhanced specific nitrifying activity, while Wang *et al.* (2023) reported improved ammonia-oxidizing and nitrite-oxidizing rates as the C/N ratio decreased from 6 to 3, indicating enhanced enzymatic activity and nitrification performance under lower carbon conditions.

Despite the observed reduction in nitrification rates at higher organic loads, some studies suggest that complete ammonium removal may still be achievable under appropriate operational conditions. Carrera *et al.* (2004) demonstrated that although higher COD:N ratios caused an exponential decrease in nitrification rates, full nitrification could still be maintained in high-strength industrial wastewater systems.

Moreover, the results indicated that decreasing the HRT leads to higher specific nitrification rates, but at the same time slightly reduces the overall ammonium removal efficiency. This behavior is mainly attributed to the increased ammonium loading imposed at shorter HRTs, which stimulates nitrification activity but limits complete ammonium removal (BASSIN, DEZOTTI, 2018). This observation corroborates the work

of Welander *et al.* (1997), confirming that despite the enhanced kinetic activity at high hydraulic loads, longer retention times are requisite for achieving high-quality effluent. Based on the study by Torkaman *et al.* (2015), there is a distinct trade-off between ammonium removal efficiency and the nitrification rate when adjusting the HRT. Reducing the HRT results in a decline in ammonium removal efficiency, as the shorter contact time limits the duration available for nitrifying bacteria to oxidize the substrate. However, because the nitrification rate is proportional to the ammonium loading rate, reducing the HRT, which increases the inlet flow and thus the loading, actually promotes a higher nitrification rate. Consequently, while shorter retention times enhance the reaction rate per unit of biofilm area, they result in a lower percentage of total ammonium removed from the wastewater (NAYERI *et al.*, 2025).

Table 13 also presents the average real apparent specific removal rates measured during operational periods in which each reactor was running under the same conditions as their corresponding batch tests. The minor contribution of suspended solids to the total solids indicates that the apparent specific removal rate is primarily driven by the activity of the attached biomass, making the comparison between apparent and maximum specific removal rates appropriate. This does not imply low activity of the suspended biomass; on the contrary, its specific removal rate may be even higher than that of the biofilm, as planktonic cells are not subject to diffusion limitations of substrates (BASSIN *et al.*, 2016; LIMA *et al.*, 2016; MATHEUS *et al.*, 2020). During the initial operational phases of each reactor, the maximum biomass-specific ammonium removal rates were close to the apparent (real) removal rates. However, this discrepancy increased in the later phases, with the largest gaps observed in P5 for MBBR1 (1.6-fold), P7 for MBBR2 (2.3-fold), P7 for MBBR3 (3.0-fold), and P3 for MBBR4 (1.9-fold). This trend is consistent with expectations, as these phases exhibited enhanced nitrification performance, as summarized in Table 13. This indicates that the actual ammonium removal rates were well below the maximum achievable rates, meaning the reactors were not operating at their full capacity. In these phases, nitrification performance was high and stable, and the gap between the real and maximum rates suggests substrate limitation rather than process deterioration. This is not unfavorable; instead, it reflects that the reactors still had available treatment capacity to handle higher loads if required.

Table 13 - Ammonium removal and specific ammonium removal rate obtained in all experimental phases of MBBR1, MBBR2, MBBR3, and MBBR4.

Reactor	Phase	Ammonium removal (%)	Specific ammonium removal rate (mgNH ₄ ⁺ -N gVS ⁻¹ d ⁻¹)			VAS (g L ⁻¹)	VSS (mg L ⁻¹)
			Max ^a	Real ^b	f _{Max/Real}		
MBBR1	P1	73 ± 16	-	-	-	-	-
	P2	76 ± 1	65	68	1	2.4	96.7
	P3	86 ± 14	86	75	1.1	2.5	43.3
	P4	99 ± 1	97	58	1.7	2.5	43.3
	P5	94 ± 1	422	268	1.6	0.6	0
	P6	84 ± 14	228	181	1.3	1.5	10
MBBR2	P1	73 ± 19	-	-	-	-	-
	P2	72 ± 3	86	87	1	1.8	113.3
	P3	88 ± 15	137	129	1.1	1.4	100
	P4	99 ± 1	175	92	1.9	1.4	100
	P5	100 ± 1	346	177	1.9	0.6	0
	P6	99 ± 1	254	149	1.7	0.9	43.3
	P7	99 ± 1	242	103	2.3	1.4	56
	P8	95 ± 3	278	213	1.3	1.2	22
MBBR3	P1	79 ± 12	82	55	1.5	1.7	115
	P2	98 ± 2	106	62	1.7	2.3	130
	P3	99 ± 1	206	86	2.4	1.5	13.3
	P4	99 ± 1	214	106	2.0	1.5	6.7
	P5	97 ± 1	182	95	1.9	2.1	0
	P6	92 ± 9	211	102	2.1	2.8	26
	P7	96 ± 2	149	49	3.0	3.4	30
MBBR4	P1	61 ± 25	149	143	1	1.0	23.3
	P2	94 ± 6	240	132	1.8	1.4	0
	P3	81 ± 16	192	101	1.9	2.6	16

^aIn Max VS corresponds to VAS, since only attached biomass was present during the batch trials.

^bIn Real VS represents the sum of VAS and VSS, as this rate refers to continuous operation in which both attached and suspended biomass fractions were present.

Table 14 – pH and temperature evaluated at the beginning and end of the batch activity tests.

Reactor	Phase	pH _{initial}	pH _{final}	T _{initial} (°C)	T _{final} (°C)
MBBR1	P2	8.0	6.2	18.8	17.3
	P3	8.1	5.2	13.5	20.2
	P4	8.6	8.5	16.3	19.8
	P5	8.4	8.4	15.4	20.3
	P6	8.5	8.3	20.4	20
MBBR2	P2	7.9	6.3	18.9	17.5
	P3	7.6	8.1	16.5	20.3
	P4	8.4	8.6	16.8	20.2
	P5	8.4	8.7	17	20.8
	P6	8.3	8.5	22.3	20.1
	P7	8.0	8.5	21.4	20.3
	P8	8.5	8.7	20.5	20.2
MBBR3	P1	7.6	6.2	20.5	18.0
	P2	8.1	8.3	16.3	18.1
	P3	8.3	8.2	17.1	18.6
	P4	8.2	8.4	21.8	17.5
	P5	8.2	8.5	22.1	18.9
	P6	8.1	8.6	21	18.4
	P7	8.6	8.9	20.4	20
MBBR4	P1	8.2	8.4	22.2	16
	P2	8.1	8.3	23.6	18.3
	P3	8.4	8.7	20.6	21.1

The pH and temperature values measured at the beginning and end of the batch kinetic tests are summarized in Table 14. Throughout the tests, these values remained within or close to the optimal range for nitrification, indicating suitable conditions for reactor performance.

4.1.4 Attached and Suspended Solids Assessment

Figure 30 shows the temporal evolution of attached solids distribution and biofilm detachment behavior in the four MBBR systems throughout the different operational phases. Panels (a, c, e, g) present the concentrations of attached volatile solids (VAS) and fixed attached solids (FAS), together with the VAS/TAS ratio, reflecting changes in biofilm composition over time. Panels (b, d, f, h) illustrate the corresponding average biofilm-specific surface detachment rates.

Biofilm development involves microbial growth and accumulation, leading to gradual thickening during operation. Excessive thickness can limit nutrient and oxygen transfer, reducing microbial activity and treatment efficiency, a condition known as biofilm aging. Detachment plays a key role in restoring activity and occurs when internal structural stress exceeds the strength of the biofilm matrix, either due to mechanical forces (e.g., hydrodynamic changes) or internal weakening such as enzymatic degradation of EPS (BUTLER; BOLTZ, 2014; HUANG *et al.*, 2019). Under steady conditions, a balance between growth and detachment controls biofilm structure and functionality (NICOLELLA *et al.*, 2000). The specific biofilm detachment rates (k_d) were calculated for the reactors using Equation (12), described in Chapter 2.

Based on the results, in MBBR1, the VAS values initially increased, reaching a significant peak during P2 (19.1 g m^{-2}), which likely indicates thick biofilm formation (Figure 30a). However, this high VAS did not necessarily imply enrichment of nitrifiers. The sharp decline in VAS after P2 likely reflects biofilm detachment or heterotrophic sloughing as operational conditions changed, possibly due to the reduction of COD. This interpretation is supported by the observed rise in biofilm detachment rate from an average of $1.8 \pm 0.9 \text{ gTSS m}^{-2} \text{ d}^{-1}$ in P1 to $4.2 \text{ gTSS m}^{-2} \text{ d}^{-1}$ in P2 during which the system's carbon source was decreased (Figure 30b). From P4 to P5, the HRT in MBBR1 was progressively reduced from 6 to 4 h, significantly increasing the flow rate and operational stress within the system. As a result, VAS declined from an average of 8.5 g m^{-2} in P3 to 2.4 g m^{-2} in P5. Further reduction in HRT to 2h increased biomass sloughing events, and the detachment rate increased to an average of $1.7 \pm 1.3 \text{ gTSS m}^{-2} \text{ d}^{-1}$ in P6. However, after the initial sloughing episode, the VAS concentration increased, and the biofilm reached a VAS concentration of 6 g m^{-2} at the end of P6.

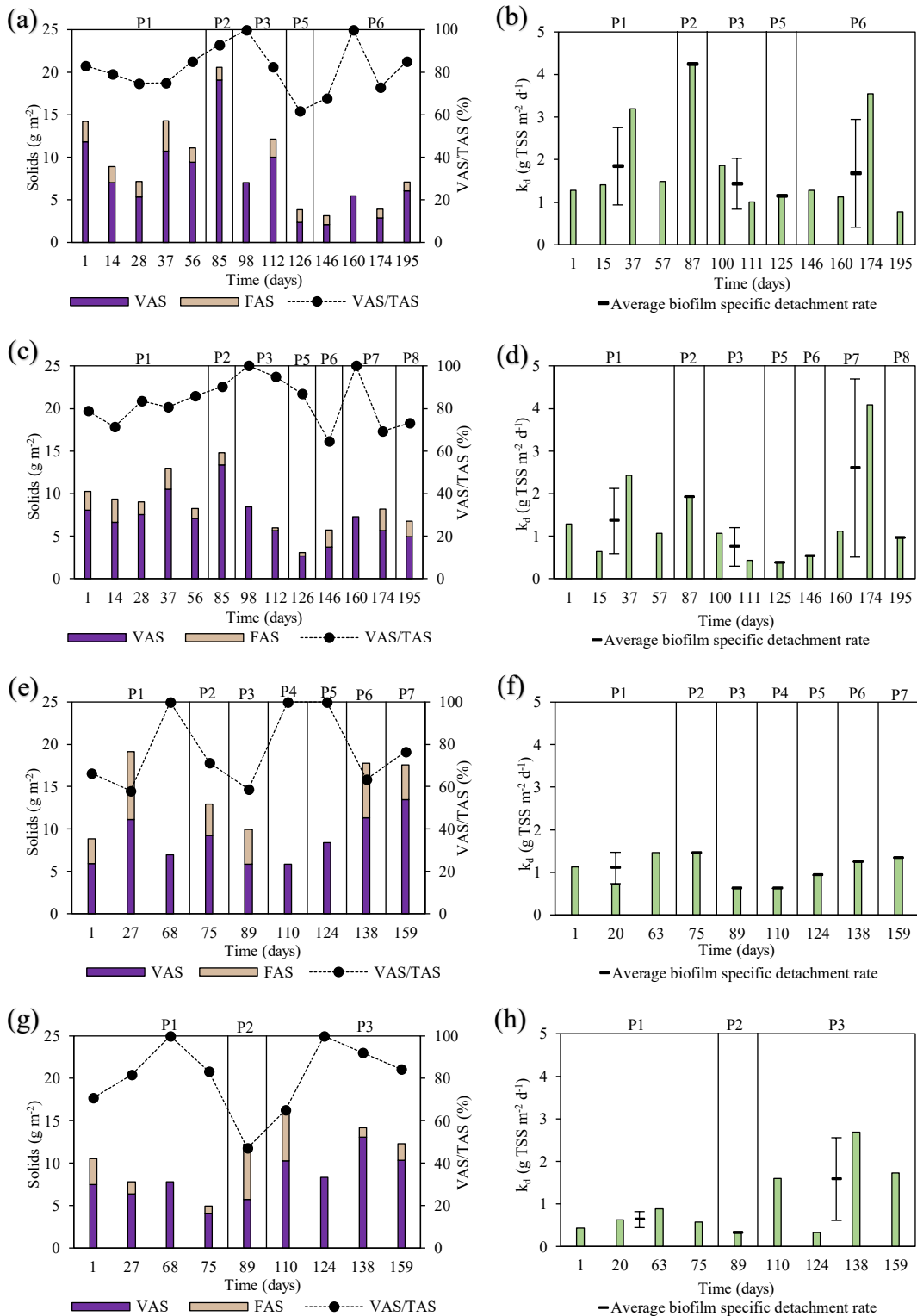


Figure 30 - Temporal variation of volatile attached solids (VAS) and fixed attached solids (FAS), and the VAS/TAS ratio and average biofilm surface-specific detachment rate (k_d) determined for experimental phases applied to each reactor: a-b) MBBR1, c-d) MBBR2, e-f) MBBR3, and g-h) MBBR4. TAS represents the sum of VAS and FAS.

Similar to MBBR1, in the early phases of MBBR2 (P1–P2), the use of synthetic wastewater with a high glucose concentration promoted the development of a relatively thick biofilm (Figure 30c), as indicated by elevated VAS levels (average of 7.9 g m⁻² in P1 and 13.4 g m⁻² in P2). When the COD was reduced in P2, the detachment rate increased slightly from an average of 1.3 ± 0.8 gTSS m⁻² d⁻¹ in P1 to 1.9 gTSS m⁻² d⁻¹ in P2 (Figure 30d). From P3 to P6, the gradual incorporation of secondary refinery wastewater introduced more complex and potentially inhibitory compounds, leading to an initial shock that resulted in a decrease in volatile attached solids from an average of 7.1 g m⁻² in P3 to 3.7 g m⁻² in P6. A similar result was observed by Zhang et al. (2025), who reported that biomass initially declined due to the toxic shock of real wastewater, but later recovered and increased as the biofilm adapted and matured. Subsequently, between P6 and P7, reducing the HRT from 6 to 4 h increased hydraulic stress, causing the detachment rate to rise from 0.5 gTSS m⁻² d⁻¹ in P6 to an average of 2.6 ± 2.1 gTSS m⁻² d⁻¹ in P7. However, a further reduction in HRT to 2 h in P8 did not intensify sloughing, and VAS remained stable at approximately 4.9 g m⁻² by the end of P8. This stability likely reflects the development of a more specialized and resilient nitrifying biofilm adapted to the increasingly challenging real wastewater conditions.

In the early phases of MBBR3 (P1–P2), there was a moderate accumulation of VAS, with an average of 8.0 g m⁻² VAS in P1 and 9.2 g m⁻² in P2 (Figure 30e). However, as influent COD was gradually reduced and then eliminated, the detachment rate increased slightly from 1.1 gTSS m⁻² d⁻¹ in P1 to 1.5 gTSS m⁻² d⁻¹ in P2, and the VAS declined to 5.8 g m⁻² in P4 (Figure 30f). During the later operational phases (P4–P6), the progressive reduction in HRT from 6 to 2 h increased the hydraulic and shear stresses imposed on the system. As a result, the detachment rate rose from 0.6 gTSS m⁻² d⁻¹ in P4 to 1.2 gTSS m⁻² d⁻¹ in P6. Despite these increased shear forces, the biofilm resisted further sloughing, and the volatile attached solids concentration exhibited a modest rise, reaching 11.3 g m⁻² by the end of P6. In the final phase (P7), the reactor maintained its performance and biofilm stability despite low ammonium availability.

In MBBR4, the variation of VAS displayed a relatively stable pattern (Figure 30g), with concentrations being lowest in P1 (average of 6.5 gVAS m⁻²), and gradually increasing toward P3 as HRT decreased to 2 h (average of 10.5 gVAS m⁻²). This gradual rise indicates a progressive biofilm development, consistent with the establishment of a slow-growing nitrifying population that promotes system stability. Similarly, the biofilm detachment rate exhibited low variation throughout the periods (Figure 30h), with only a slight increase observed in P3 (average of 1.6 ± 1 gTSS m⁻² d⁻¹), coinciding with the reduction of HRT to 2 h.

The results indicate that organic carbon availability was the main factor regulating biofilm accumulation. The presence of readily biodegradable substrates (glucose and ethanol) in MBBR1–3 promoted rapid formation of thick, high-mass biofilms largely dominated by fast-growing heterotrophic bacteria. Consistently, previous studies have reported a positive linear relationship between organic loading rate and biomass production, demonstrating that higher organic loads stimulate biofilm growth while also increasing sloughing and solids production (AYGUN *et al.*, 2008). Subsequently, the reduction or removal of organic loading acted as a major stress factor for heterotrophic organisms that rely on readily biodegradable carbon, leading to a consistent decrease in attached biomass. The decay of this heterotrophic fraction produced inert residues as well as slowly biodegradable carbonaceous and nitrogenous compounds, which required hydrolysis before being converted into readily biodegradable substrates that could subsequently be utilized by autotrophic biomass (VON SPERLING, 2007).

Consistent with the observations in this study, previous research suggests that improved formation of nitrifying biofilms can be achieved by controlling EPS production and limiting excessive heterotrophic growth (TSUNEDA *et al.*, 2001). In line with this, Bassin *et al.* (2015) reported that high influent COD increased attached biomass content (up to 2.0 gVAS L⁻¹), whereas the subsequent removal of organic carbon led to heterotrophic decay or detachment, reducing adhered biomass to approximately 1.0 gVAS L⁻¹, similar to reactors operated without organic carbon. Similarly, Tjihuis *et al.* (1994) observed that introducing acetate to a nitrifying reactor caused a low-density heterotrophic layer to overgrow the existing biofilm. However, upon switching to a nitrification medium without organic carbon, this outer heterotrophic layer was sheared off within two days, while the inner nitrifying core remained rigid and stable, allowing

nitrification activity to be rapidly restored. Together, these findings indicate that organic carbon promotes initial biofilm development but that its reduction favors the loss of outer heterotrophic layers and the formation of a thinner, more stable nitrifying biofilm.

Figure 30 also presents the VAS/TAS ratio, which indicates the organic or inorganic nature of the attached biomass. Overall, this ratio generally remains high throughout the study in all reactors (often above 70%), indicating that most of the attached solids consisted of volatile biomass, primarily composed of active microorganisms, which is a typical characteristic of pure MBBR systems operating without sludge recirculation (BASSIN, DEZOTTI, 2018). However, during specific operational phases, this ratio decreased to approximately 50–60%, indicating a substantial change in biofilm characteristics, with a high proportion of inactive cells (inert material). Despite this reduction, high nitrification efficiencies were maintained, indicating the resilience of the active biofilm fraction and the robustness of the nitrification process under varying operational conditions. These ratios are consistent with values reported in the literature (CAO *et al.*, 2016; JAHREN *et al.*, 2002).

Figure 31 illustrates the influent and effluent profiles of total, volatile, and fixed suspended solids across the different operational phases of the reactors. In the influent of the reactors treating refinery wastewater, VSS concentrations showed considerable variability, ranging from 8 to 98 mg L⁻¹. Nevertheless, these results indicate that a substantial fraction of the incoming suspended solids was of organic origin. This figure also shows the corresponding VSS/TSS ratio in the reactors effluent. Similar to the attached solids analysis, this ratio indicates that a substantial fraction of the biomass leaving the reactor was predominantly organic, remaining high (often above 60%) throughout the operational phases. This occurs because much of the suspended biomass resulted from biofilm detachment; therefore, the properties of the suspended and attached fractions are closely related. Consequently, phases with elevated suspended solids concentrations coincided with reductions in attached biomass.

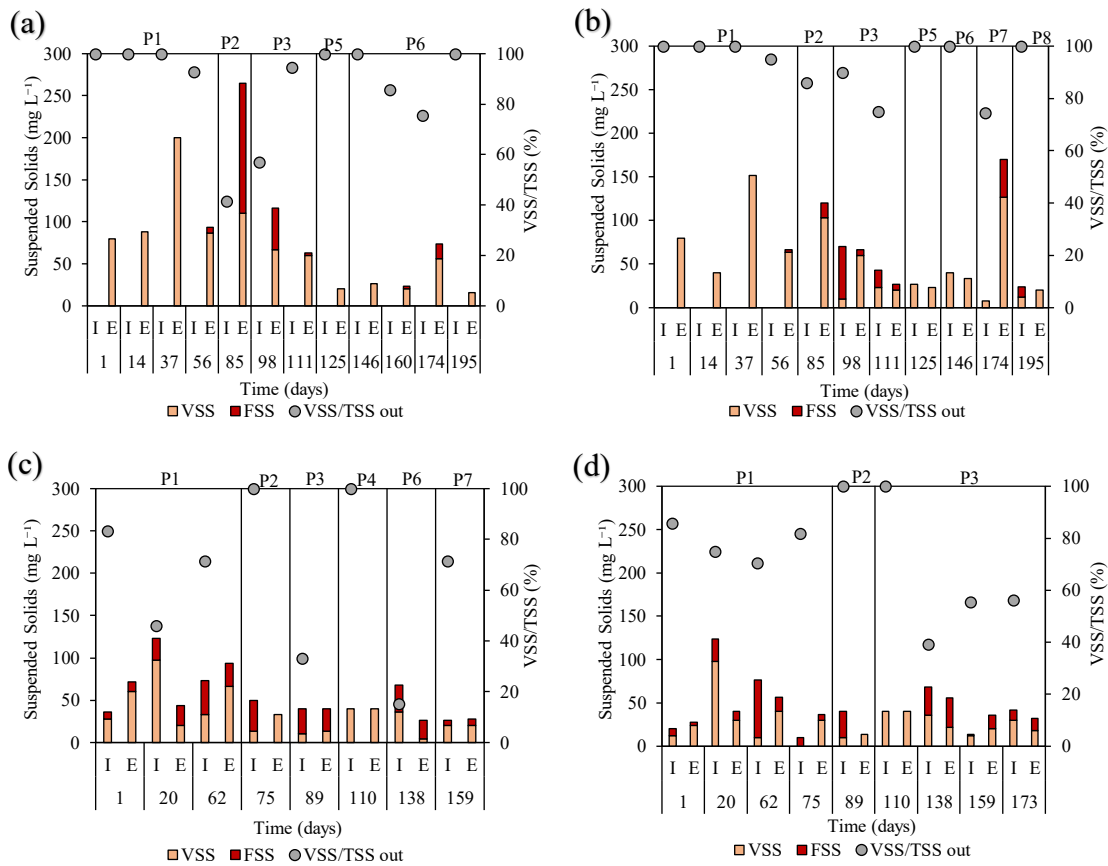


Figure 31 - Concentration of total, volatile, and fixed suspended solids in the influent (I) and effluent (E) throughout the operational phases: a) MBBR1, b) MBBR2, c) MBBR3, and d) MBBR4. (TSS = VSS + FSS).

Figure 32 displays the distribution of solids in the MBBR systems over time, broken down into attached solids, suspended solids, and the percentage of attached solids relative to total solids (TAS/TS). This parameter is important to assess the balance between biofilm-based (attached) and suspended growth within each reactor and helps interpret how favorable the environment is for nitrifying bacteria. The balance between attached and suspended growth affects process performance, with attached biomass showing higher biodegradation potential for pollutants compared to suspended biomass. This general advantage of attached biomass over suspended biomass is likely attributable to the longer residence time of microorganisms on the carriers, which may promote greater biodiversity by protecting slow-growing bacteria from washout (MAZIOTI *et al.*, 2015). Throughout the experiment, solids in all reactors were predominantly retained as attached biofilm, with TAS/TS ratios exceeding 90%, indicating excellent biomass

retention on the carriers. However, at several time points, particularly during transitional periods between operational phases, there were noticeable but temporary decreases in this ratio, suggesting episodes where suspended biomass slightly increased or the biofilm detachment occurred. Despite these fluctuations, the MBBR systems recovered quickly, and the TAS/TS ratio returned to high levels. Similar trends were reported by Forrest *et al.* (2016), who evaluated solids production in tertiary nitrifying MBBR systems and demonstrated that these reactors function predominantly as attached-growth processes. Their study showed that the total attached biofilm mass within the reactor was roughly two orders of magnitude higher than the suspended solids fraction.

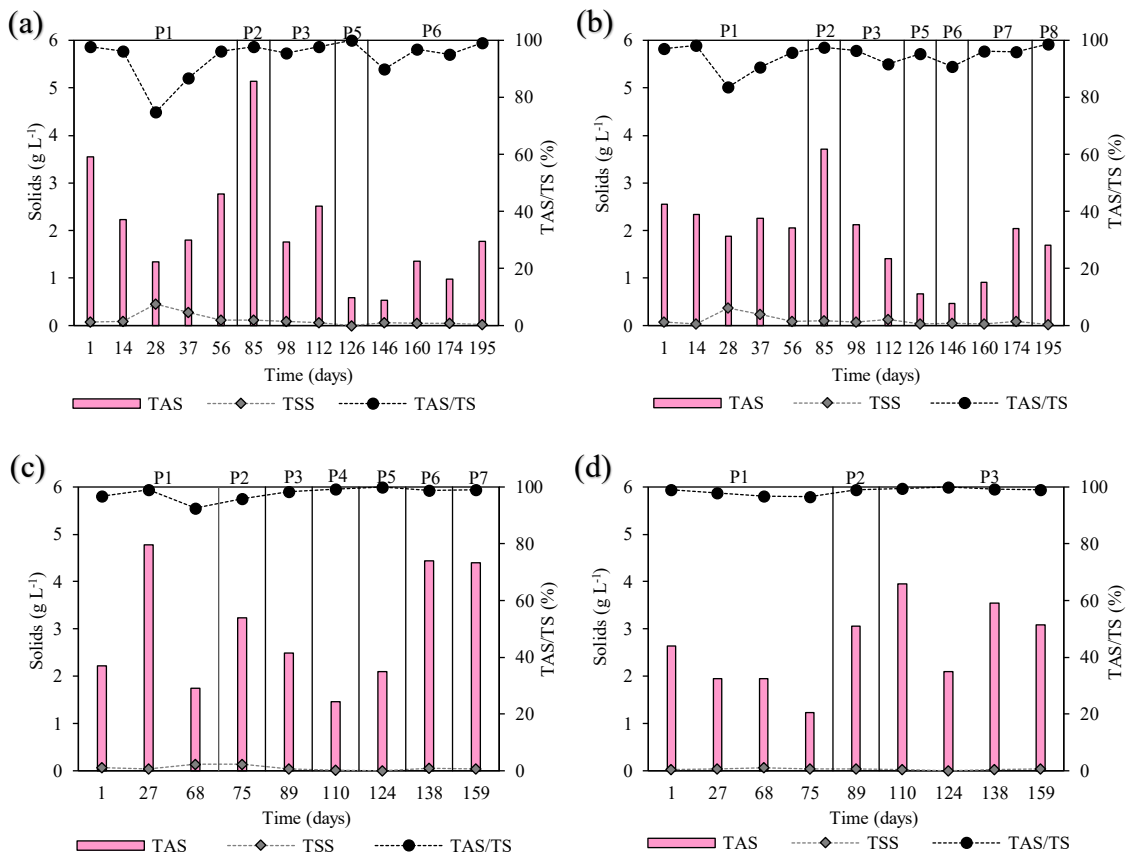


Figure 32 - Temporal distribution of total attached solids (TAS), total suspended solids (TSS), and TAS/TS ratio in reactors: a) MBBR1, b) MBBR2, c) MBBR3, and d) MBBR4. TS represents the sum of TAS and TSS.

4.1.5 Visual Observation of Attached Biomass and Biofilm Thickness

The images obtained from the K1 carriers (Figure 33b–33e) show pronounced variations in biofilm thickness across the different operational phases, reflecting the influence of changing operational conditions on biofilm development. Biofilm thickness plays a critical role in shaping microbial diversity and metabolic activity, primarily by creating mass transfer resistance that limits the diffusion and penetration of substrates into the deeper layers of the biofilm matrix (TORRESI *et al.*, 2016). As observed from the carrier images, significantly less biomass develops on the outer surfaces of the carriers compared to the inner surfaces. This is likely due to abrasion resulting from carrier–carrier collisions, which restricts biomass growth on the exterior part of the media (ØDEGAARD, 2006).

In MBBR1–3, the progressive reduction in COD loading rate significantly influenced the dynamics of attached solids. However, the adaptation pathways differed among reactors due to variations in influent composition and acclimation strategies. This structural transition is evidenced by the reduction in biofilm thickness observed in Figure 34a–34c, while nitrification performance remained stable and efficient, indicating the selective retention of active biomass well adapted to low-carbon conditions. From P1 to P4, as the influent COD decreased and eventually reached zero in MBBR1–3, biofilm thickness in MBBR1 decreased from an average of 304 μm in P1 to 161 μm in P4. Similarly, in MBBR2, biofilm thickness declined from 308 μm to 183 μm , while in MBBR3 it decreased from 130 μm to 90 μm over the same operational period. In contrast, biofilm development in MBBR4 (always fed with RW without supplementation of an external carbon source) was noticeably delayed due to the absence of biodegradable COD in the influent. With limited heterotrophic growth (mainly attributed to decaying autotrophic biomass) and the associated competitive interactions, biofilm formation relied exclusively on autotrophic microorganisms. As a result, a thin but functional nitrifying biofilm developed gradually, reaching an average thickness of 51 μm by the end of P1.

Figure 33a illustrates the relationship between influent COD concentration and biofilm thickness in MBBR1–3 during P1 to P4. Based on the results, the relationship between COD concentration and biofilm development shows a consistent negative trend in all reactors, supported by relatively high coefficients of determination (R^2). The

obtained R^2 values indicate a good fit between COD and biofilm response, confirming that variations in COD explain a significant portion of the observed changes. MBBR1, MBBR2, and MBBR3 presented strong correlations, with R^2 values of 0.84, 0.79, and 0.86, respectively, suggesting that COD reduction was a major factor governing biofilm behavior under low-carbon conditions. Similar to these observations, Ding *et al.* (2020) demonstrated that the influent C/N ratio exerted a direct influence on biofilm physical characteristics, with higher ratios leading to significantly thicker biofilms.

In MBBR1 and MBBR2, as the HRT was progressively reduced from 6 to 2 h, the biofilm retained a heterogeneous structure characterized by localized dense clusters (Figure 33b and 33c). Under these conditions, the average biofilm thickness reached 223 μm by the end of P6 in MBBR1 and 241 μm in MBBR2 by the end of P8. In contrast, MBBR3 and MBBR4 (Figure 33c and 33e) developed thinner and more uniformly distributed biofilms over the same operational changes. At an HRT of 2 h, the average biofilm thickness reached 152 μm in MBBR3 and 140 μm in MBBR4. Based on the results, the reduction in HRT seemed to stimulate biofilm growth, leading to an observable increase in average biofilm thickness across all reactors. Similarly, Dong *et al.* (2011) observed a comparable trend, concluding that a reduction in HRT (from 36 to 18 h) led to an increase in the thickness of the biofilm attached to the carriers. In addition, in a study by Kawan *et al.* (2022), the authors reported a clear relationship between HRT and biofilm thickness in MBBR, showing that decreasing the HRT from 24 to 2 h led to an increase in biofilm thickness from 102.6 to 297.1 μm .

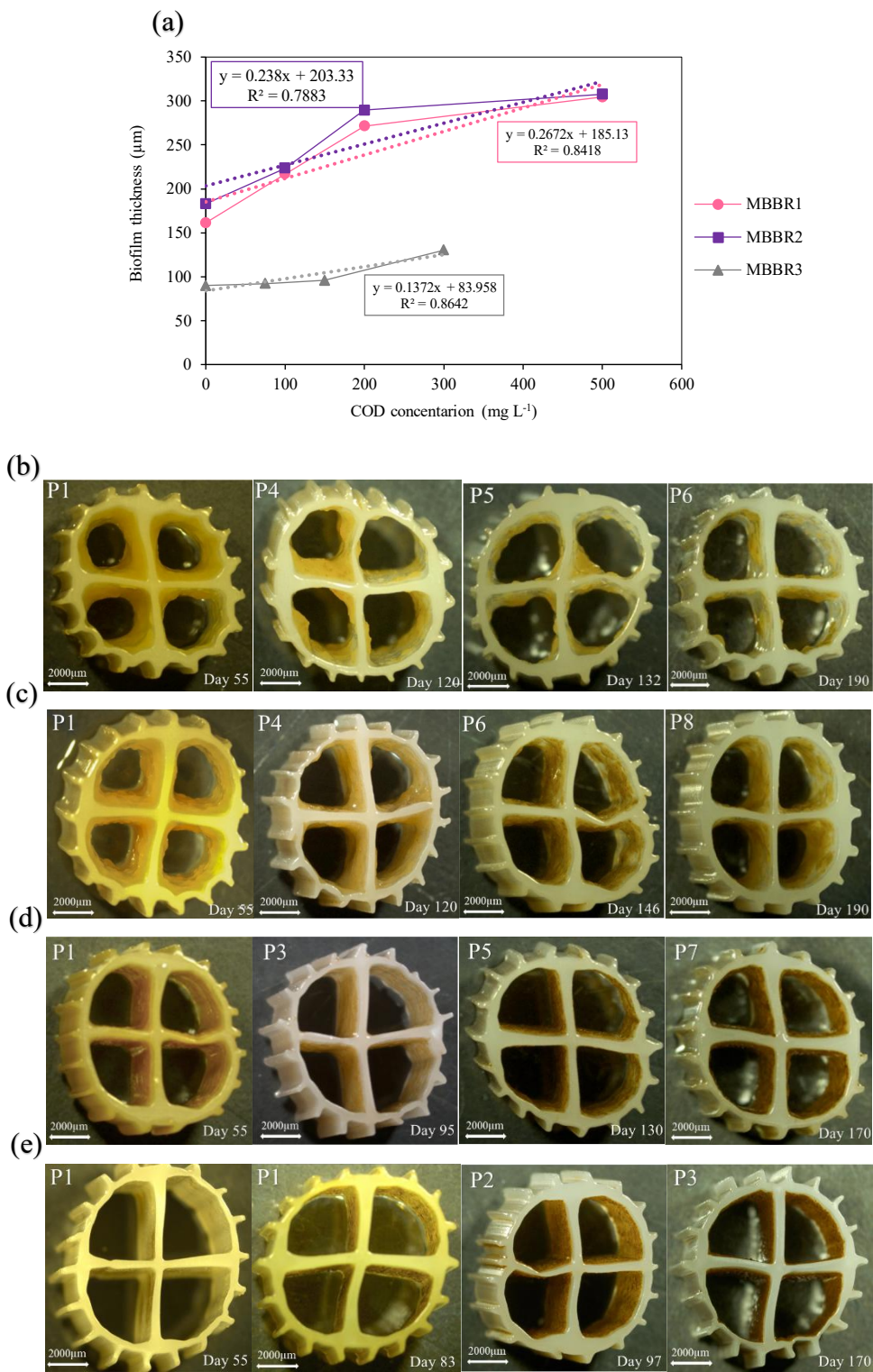


Figure 33 - (a) Biofilm thickness variation over time under different COD concentrations, and visual assessment of biofilm development on carriers in the MBBRs over the experimental phases: (b) MBBR1, (c) MBBR2, (d) MBBR3, and (e) MBBR4.

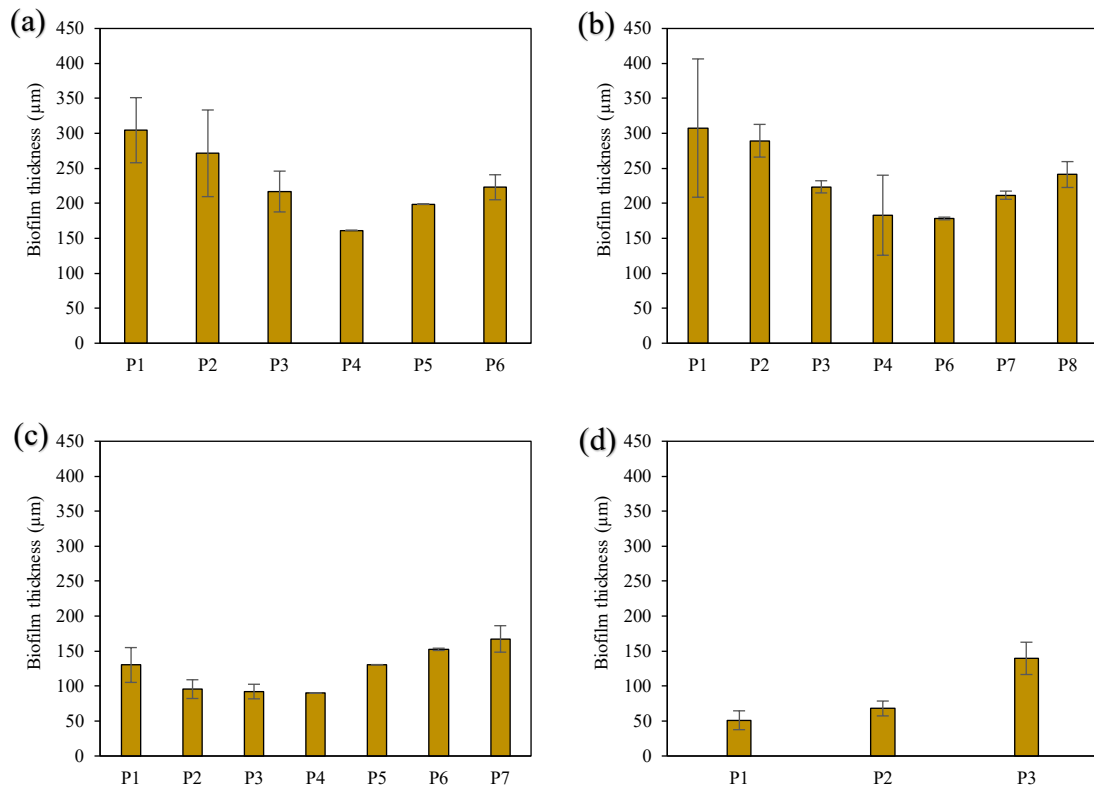


Figure 34 - Average biofilm thickness across operational phases of the reactors: (a) MBBR1, (b) MBBR2, (c) MBBR3, and (d) MBBR4.

Table 15 summarizes the biofilm thickness observed in nitrifying MBBR systems, as reported in previous studies. The results obtained for the MBBRs from this study show that the measured biofilm thickness values are consistent with the ranges previously reported in the literature.

Table 15 - Biofilm thickness in nitrifying MBBR systems.

Source	Operational Condition	Biofilm thickness (μm)	Nitrification Performance
(YOUNG <i>et al.</i> , 2016)	HRT: 2.2 hours COD: $88.8 \pm 19.9 \text{ mg L}^{-1}$ NH ₄ ⁺ -N: $440 \text{ gN m}^{-3} \text{ d}^{-1}$ NH ₄ ⁺ -N: $600 \text{ gN m}^{-3} \text{ d}^{-1}$	222 ± 17 264 ± 15	$46.1 \pm 5.7 \%$ removal $36.8 \pm 2.2 \%$ removal
(ASHKANANI <i>et al.</i> , 2019)	HRT: 5.25 hours COD: $313 \pm \text{gCOD m}^{-3} \text{ d}^{-1}$ NH ₄ ⁺ -N: $0.611 \pm 0.05 \text{ gN m}^{-2} \text{ d}^{-1}$	69.08-456.11	87.3 % removal
(TORRESI <i>et al.</i> , 2016)	HRT: 2 hours NH ₄ ⁺ -N: 50 mg L^{-1}	50-100	The reactors stabilized at an average ammonium removal rate of $2.21 \pm 0.23 \text{ gN m}^{-2} \text{ d}^{-1}$
(NOGUEIRA <i>et al.</i> , 2002)	HRT: 7 hours NH ₄ ⁺ -N: $1.26 \text{ kg m}^{-3} \text{ d}^{-1}$ COD: 0	33 ± 5	The reactors stabilized at an average ammonium removal rate of $1.20 \text{ kgN m}^{-3} \text{ d}^{-1}$.

4.1.6 Microscopic Visualization of Biofilm

The biofilm developed on the carriers in MBBR systems not only harbors bacterial communities essential for organic and inorganic matter removal but also supports a diverse microfauna, including protozoa and micrometazoans. These organisms, sensitive to changes in process conditions such as substrate concentration, oxygen levels, and the presence of toxic compounds, are often used as biological indicators of treatment efficiency. Protozoa are generally larger than bacteria and feed on them, playing a key role in the microbial food web by enabling larger organisms to indirectly utilize bacterial biomass that would otherwise be inaccessible. Through bacterial grazing, protozoa contribute to turbidity reduction, decrease particulate organic matter, and support the removal of pathogenic species (BASSIN, DEZOTTI, 2018; VON SPERLING, 2007).

Figure 35 presents the microscopic images of the biofilm from the MBBR systems across different operational phases. Microscopic analysis revealed that MBBR1, MBBR2, and MBBR3 (Figures 35a, 35b, and 35c, respectively) developed well-structured and mature biofilms, populated by abundant protozoa, rotifers, filamentous bacteria, and bacterial flocs. These communities indicate a stable trophic structure and favorable

conditions for nitrification, consistent with the reactors' high ammonium removal rates. The presence of filamentous bacteria contributes to biofilm integrity, while higher organisms suggest ecological balance and efficient biomass turnover. In contrast, MBBR4 (Figure 35d) initially exhibited poor biofilm formation, with dispersed microbial cells and low structural integrity. However, in later phases, the biofilm gradually became more compact and organized, reflecting microbial adaptation. This progression corresponded with the reactor's enhanced nitrification performance in later stages, indicating that microbial adaptation contributed to functional recovery.

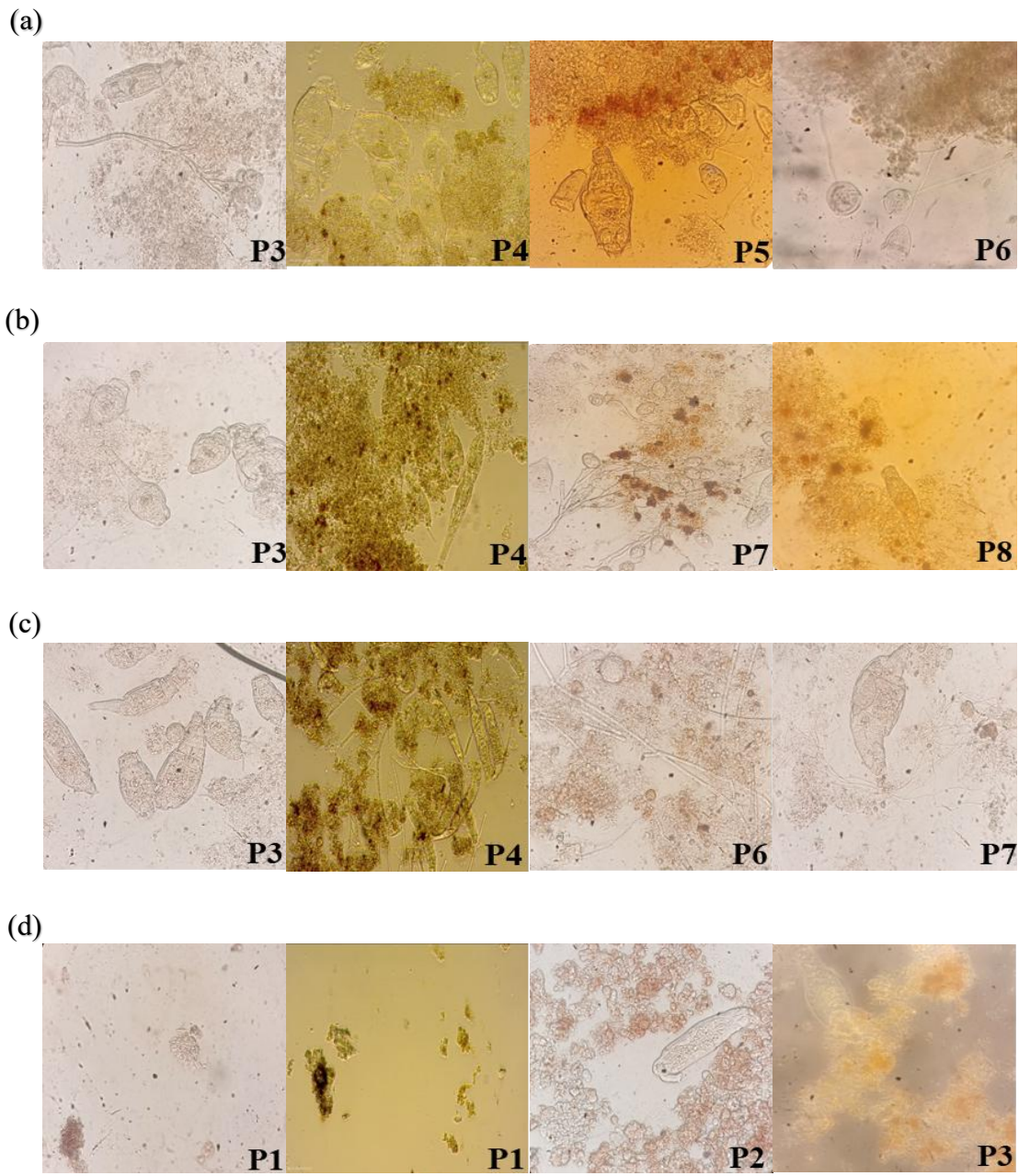


Figure 35 - Optical micrographs (400× magnification) obtained during different operational phases of the reactors: (a) MBBR1, (b) MBBR2, (c) MBBR3, and (d) MBBR4.

4.1.7 Operational Parameters: pH and Temperature

Figure 36 presents the pH variation observed during the different operational phases of the reactors. Nitrification rates are strongly dependent on pH, with optimal performance generally observed within the range of 6.5 to 8.5. Nitrification rates decrease significantly under near-neutral conditions, highlighting the importance of maintaining pH within this range to ensure stable and reliable process performance. Nitrification consumes alkalinity, leading to a decrease in pH. Therefore, pH control through the addition of alkaline compounds is often necessary to maintain stable operating conditions (RUSTEN *et al.*, 2006b).

During P1–P3, MBBR1 and MBBR2 exhibited pronounced pH fluctuations, with values ranging between 6.0 and 8.5 and an average of 7.3 ± 0.9 , including occasional decreases below pH 7.0. Such variability indicates limited buffering capacity during the initial operational period and may adversely affect nitrification stability. Following alkalinity supplementation with sodium bicarbonate, pH conditions improved markedly; from P3 onward, pH remained stable within the optimal range for nitrification. In contrast, MBBR3 and MBBR4 exhibited comparatively stable pH profiles throughout most operational phases. Both influent and effluent pH values were consistently maintained within the range of 7.0–8.5, with an average of 8.0 ± 0.3 for both reactors, a condition widely recognized as favorable for sustaining efficient and stable nitrification.

Throughout all operating conditions, the reactors were operated at an ambient temperature of 24 ± 3 °C. These values fall within the temperature range suitable for nitrification and the growth of autotrophic bacteria (4–45°C), as well as for the growth and development of aerobic microorganisms (10–40°C) (Metcalf & Eddy, 2014).

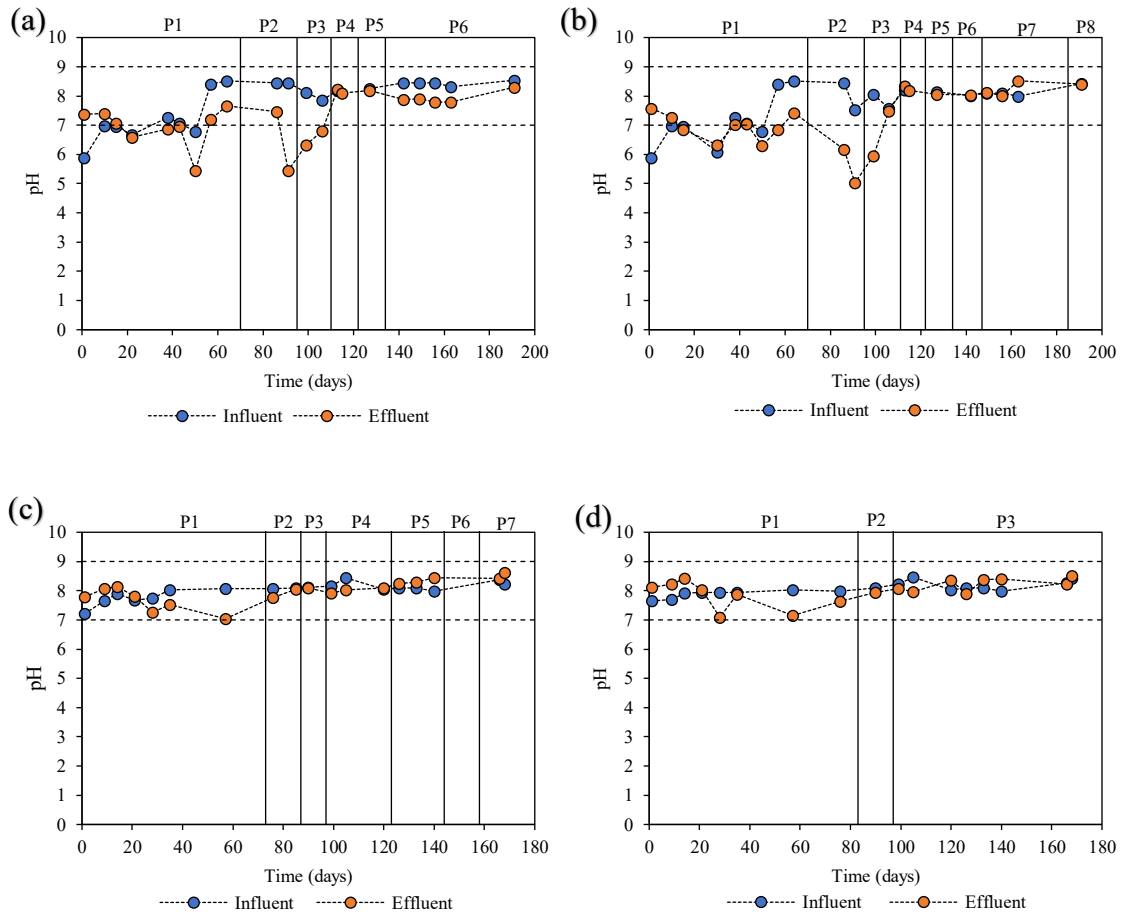


Figure 36 - pH values recorded throughout the reactors operating periods, with phase transitions indicated by vertical dashed lines. Upper and lower limits defining optimal nitrification performance are shown as dotted horizontal lines: a) MBBR1, b) MBBR2, c) MBBR3, and d) MBBR4.

4.2 Part II: Effect of Oil Concentration on Nitrification

This section presents the second part of the study, which investigates the impact of increasing oil concentrations on the established nitrifying biofilms. The methodology involved progressively exposing the reactor to higher oil loads up to 500 mg L⁻¹ to assess the system's response. The analysis focused on reactor performance and structural changes in the biofilm through visual observations, solids dynamics, oil distribution, batch activity tests, and continuous nitrification performance, along with the monitoring of key operational parameters.

4.2.1 Visual Observation

Figure 37 shows the visual changes observed in MBBR4 and its carriers during operation under normal oil concentration (10-30 mg L⁻¹) and under high oil loading conditions (300-500 mg L⁻¹). During operation without elevated oil levels, the carriers appeared relatively clean with uniform biofilm development and were freely moving within the reactor. In contrast, under high oil concentration, the carriers became noticeably darker and more coated, indicating significant oil accumulation and changes in biofilm structure and surface characteristics. The excess oil promoted the adhesion of biocarriers to each other, leading to the formation of clusters and agglomerates. As a result, the mobility of the carriers was reduced, making mixing more difficult and limiting their proper circulation inside the reactor.

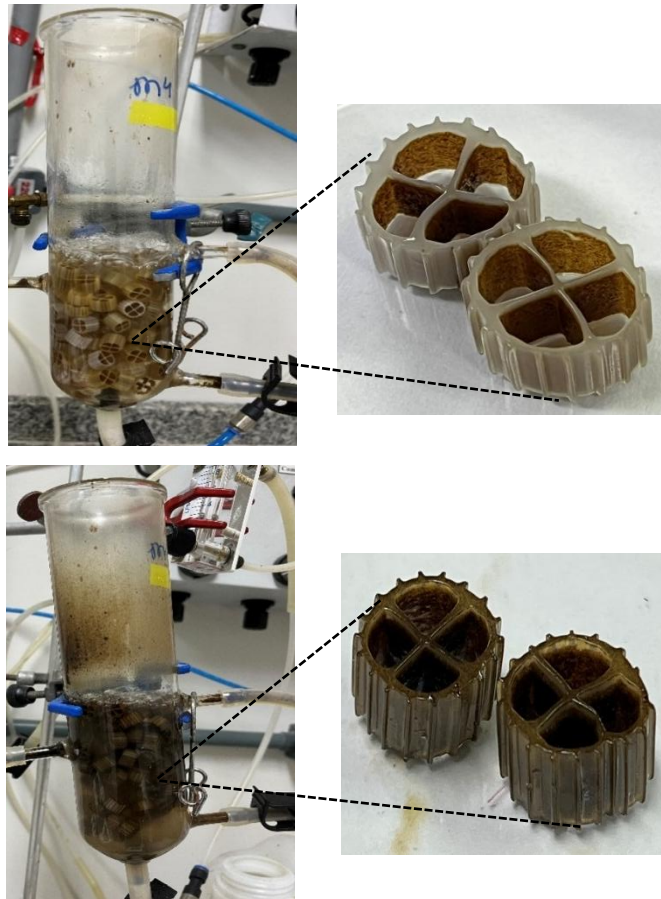


Figure 37 - Visual observation of MBBR4 before and after exposure to high oil loading (300–500 mg L⁻¹).

Moreover, a clear accumulation of solids is visible at the bottom of the reactor, forming a compact layer, while suspended particles can also be observed throughout the liquid phase (Figure 38). The visual observations suggest changes in carrier movement and overall reactor hydrodynamic behavior during this operational phase. A more detailed explanation and discussion of these observations are provided in the sections below.

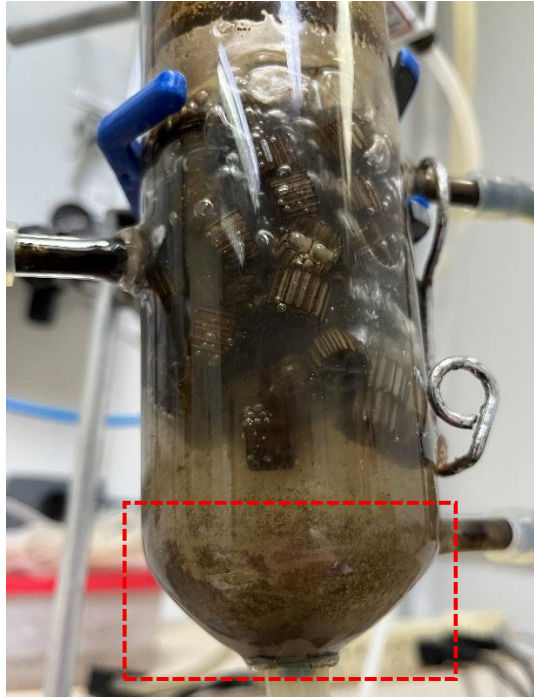


Figure 38 - Visual appearance of MBBR4 under high oil concentrations ($300\text{--}500\text{ mg L}^{-1}$), showing carrier agglomeration and accumulation of solids.

4.2.2 Biofilm Behavior and Solids Dynamics

Figure 39a depicts the evolution of total suspended solids in the influent and effluent, while Figure 39b presents the biofilm-specific detachment rates across the reactor's operational phases. Together, the changes in suspended solids and detachment rates demonstrate how progressive oil loading influenced biofilm behavior. As the influent oil concentration increased, influent TSS showed a corresponding gradual rise, reaching its highest values in P4 and P7, with averages of 233 and 219 mg L^{-1} , respectively. The elevated TSS in P4 likely resulted from solids accumulating alongside the oil in the feed container due to inadequate mixing. From P5 onward, improved agitation reduced this accumulation and ensured better dispersion of oil in the influent.

The consistently lower suspended solids concentrations in the effluent relative to the influent indicate that a fraction of the oil likely adhered to the biofilm, carriers or reactor surfaces. This interpretation is supported by the progressive accumulation of oil on the carriers, which increased from $0.11\text{ mg oil mgTAS}^{-1}$ in P5 to $0.58\text{ mg oil mgTAS}^{-1}$ in P6 and decreased to $0.51\text{ mg oil mgTAS}^{-1}$ in P7, where TAS represents the mass of

total attached solids on the carriers used for oil extraction. The higher oil concentration measured on the carrier in P6 compared to P7 can be explained by differences in sorption efficiency associated with oil concentration (BOLEYDEI *et al.*, 2018; CHOWDHURY *et al.*, 2009). In P6, the oil load likely remained within a range where individual molecules or small droplets could readily access available adsorption sites within the biofilm pores and carrier surface, promoting efficient attachment and accumulation. In contrast, the higher oil concentration applied in P7 may have favored the aggregation of oil compounds into larger clusters or micelle-like structures (BRANDÃO *et al.*, 2010). These larger aggregates have reduced ability to diffuse into biofilm pores and access internal sorption sites, limiting further accumulation on the carrier. In general, sorption sites are finite, and once they become saturated, no additional sites are available for further adsorption. Moreover, high oil concentrations can block the pores on the sorbent's external surface, preventing oil from diffusing into and accessing the internal pore structure (RAZAVI *et al.*, 2015; IBRAHIM *et al.*, 2010). As a result, despite the higher influent oil concentration in P7, the effective retention of oil on carriers decreased compared to P6.

As the operation progressed, effluent TSS also showed an increasing trend, indicating enhanced solids release and biofilm instability. As observed in Figure 39b, the biofilm detachment rate increased sharply with oil concentration, reaching its highest levels in P6 and P7, with averages of 7.1 and 9.2 gTSS m⁻² d⁻¹, respectively. This increase suggests that excessive oil loading interfered with biofilm cohesion and attachment strength and reduced the biofilm's structural integrity and stability.

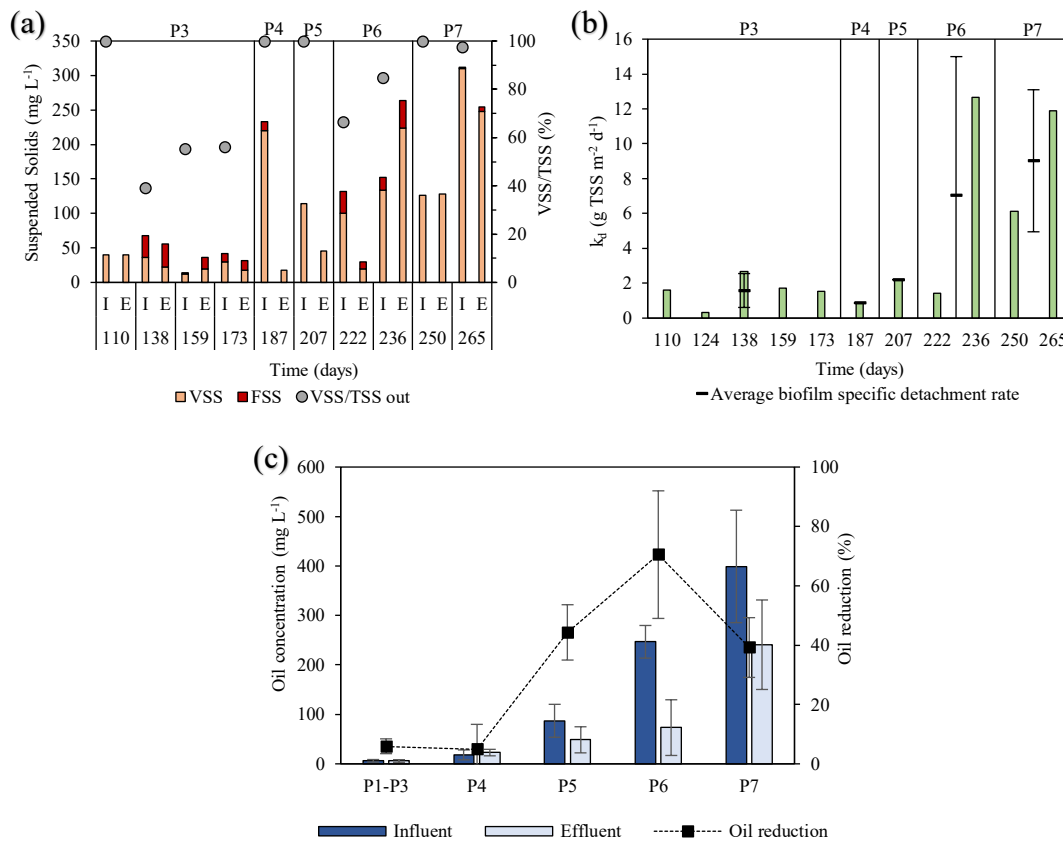


Figure 39 - Biofilm behavior and solids distribution in MBBR4 during phases P3–P7: (a) Variation of suspended solids in the influent (I) and effluent (E), (b) Biofilm specific surface detachment rate, (c) Oil concentrations in influent, effluent, and biofilm carriers, as well as oil reduction percentage.

Another important parameter illustrated in Figure 39a is the proportion of volatile suspended solids relative to total suspended solids (VSS/TSS), which provides insights into the composition of the solids discharged from the MBBR system as previously discussed. The volatile fraction primarily represents organic matter, either active biomass or organic compounds that became inert during their residence in the reactor, whereas the fixed solids correspond to inorganic, largely inert material resistant to microbial activity. In the effluent, the VSS/TSS ratio showed considerable variability, ranging from 39% to 100% and averaging around 80%. Despite this fluctuation, it is evident that a significant portion of the solids leaving the reactor was organic in nature. The fixed solids fraction tended to remain in the effluent, suggesting that the inorganic solids, unable to produce extracellular polymeric substances, did not adhere to the biofilm but persisted in suspension. Correspondingly, the biofilm also maintained a high proportion of volatile attached solids relative to total attached solids (VAS/TAS >80%), as shown in the

attached solids distribution (Figure 40a). This predominance of volatile solids suggests that the attached biomass was largely composed of metabolically active microorganisms, with a relatively low contribution from inert or inorganic material. Slight declines observed in VAS/TAS at some points may reflect short-term fluctuations in biofilm composition. Nevertheless, even during these periods, the biofilm retained its nitrification capacity, indicating that the accumulation of inert material did not compromise overall microbial functionality.

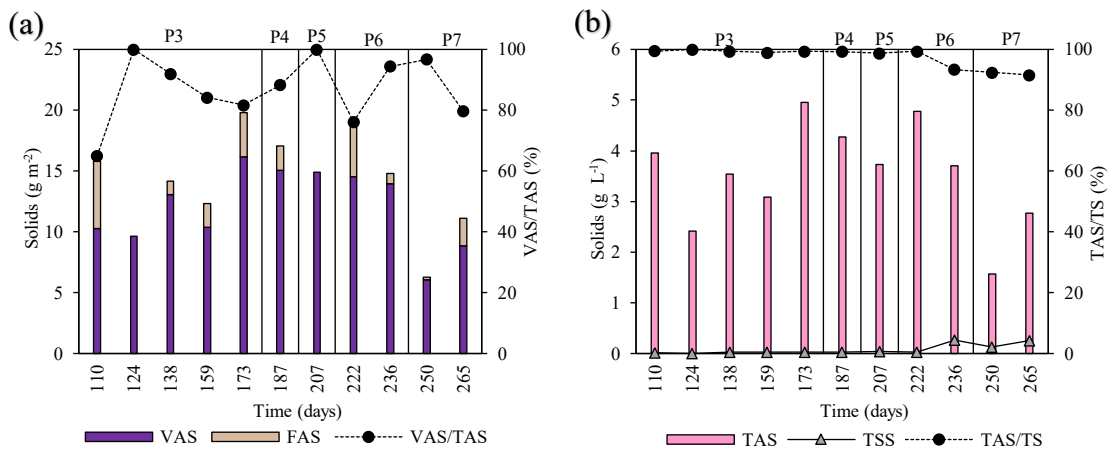


Figure 40 - Dynamics of attached and suspended biomass in MBBR4 during P3-P7: (a) Temporal variation of volatile attached solids (VAS), fixed attached solids (FAS), and the VAS/TAS ratio, (b) Temporal distribution of total attached solids (TAS), total suspended solids (TSS), and TAS/TS ratio in the reactor. TS represents the sum of TAS and TSS.

From P3 to P4 (Figure 40a), the introduction of a low oil concentration (≤ 50 mg L⁻¹) promoted biomass accumulation, with VAS increasing from an average of 11.92 g m⁻² in P3 to 15.1 g m⁻² in P4. As the oil concentration increased from P4 to P6, VAS values remained relatively stable, averaging 14.9 g m⁻² in P5 and 14.25 g m⁻² in P6. However, in P7, when the oil concentration reached 399 ± 114 mg L⁻¹, a significant reduction in VAS occurred, decreasing to an average of 7.45 g m⁻². This decline indicates that excessive oil loading negatively affected biofilm development and led to alterations in its structural integrity. The reduction in VAS concentration during P7 is consistent with the increased biomass detachment observed in this phase.

Figure 40b presents the temporal distribution of solids in the MBBR systems, TAS, TSS, and the percentage of attached solids relative to the total solids (TS), where TS is defined as the sum of TAS and TSS. During P3-P5, the majority of the solids throughout the experiment were retained as attached biofilm, indicating excellent biomass retention on the carriers. However, during P6-P7 this ratio decreased to an average of 92%, suggesting that suspended biomass slightly increased or the biofilm detachment occurred.

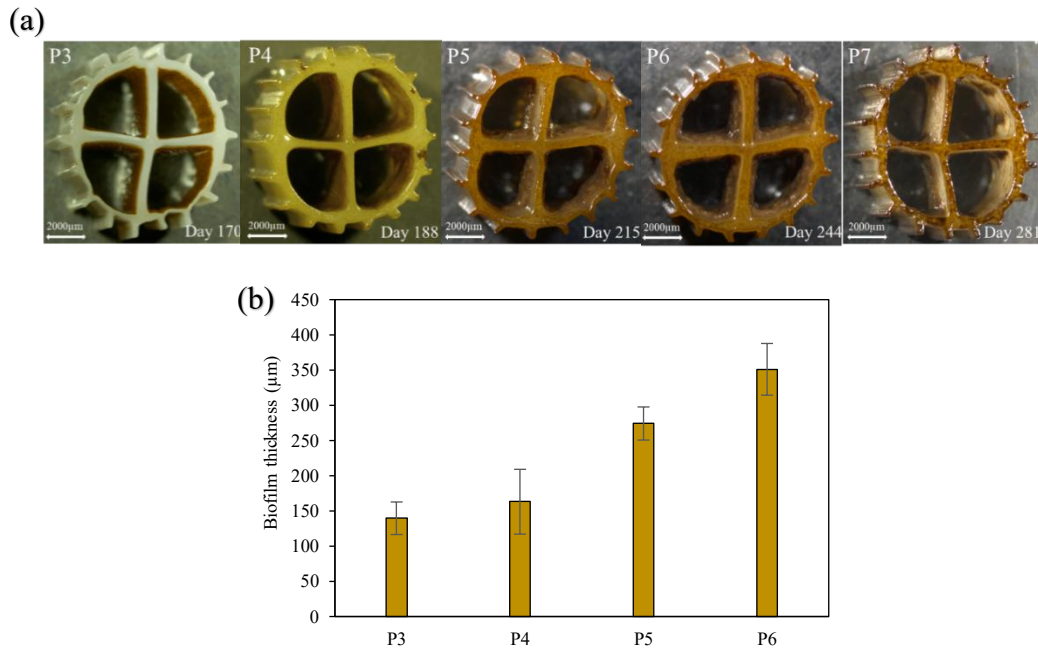


Figure 41 - (a) Visual characterization of biofilm development on Kaldnes K1 carriers in MBBR4 during P3–P7 and (b) average biofilm thickness across operational phases.

Overall, the biofilm formed on the carrier surface exhibited a visibly developed thickness, as evidenced by the stereomicroscopic images presented in Figure 41a. These images clearly demonstrate the gradual transformation in biofilm morphology and color as the oil concentration increased. During P3 and P4, the biofilm formed on the carriers appeared thin, uniform, and brownish, with average thicknesses of $139 \pm 23 \mu\text{m}$ and $163 \pm 46 \mu\text{m}$, respectively.

As the oil concentration increased from P5 to P6, the biofilm became thicker and darker, reaching average thicknesses of $274 \pm 26 \mu\text{m}$ in P5 and $351 \pm 37 \mu\text{m}$ in P6. However, this increased thickness likely introduced mass transfer limitations. In P7, as the oil concentration increased further, the biofilm surface became irregular and patchy,

showing clear signs of detachment and reduced coverage across the carrier surface. Due to this pronounced nonuniformity, biofilm thickness could not be reliably measured during this phase.

Overall, the results demonstrate that excessive oil loading adversely affected biofilm integrity, promoting a transition from a stable and well-attached structure to a partially unstable state characterized by increased sloughing, biomass washout, and reduced biofilm thickness. This behavior indicates that elevated oil concentrations disrupted the dynamic equilibrium between biofilm growth and detachment, thereby decreasing attachment strength and structural cohesion. Although mature biofilms are generally resistant to external disturbances, the fundamental stages of biofilm development, including transient attachment, irreversible adhesion, and the formation of adhesive structures, are governed by tightly regulated cellular mechanisms that are sensitive to environmental stress (SZCZEPANSKI; LIPSKI, 2013). Disruption of these processes under high oil loading conditions likely impaired the development and maintenance of stable attached microbial communities, ultimately resulting in biofilm instability.

This observation can be interpreted in light of mechanisms reported in the literature. Oil adsorption onto biomass occurs through interactions between hydrophobic hydrocarbon compounds and functional groups present on biological surfaces, together with the porous and hydrophobic characteristics of the biomass that favor rapid attachment and accumulation (BOLEYDEI *et al.*, 2018). Biofilms consist of microbial cells attached to a substratum and embedded within a matrix of EPS of biological origin. This matrix, primarily composed of proteins and polysaccharides with smaller fractions of lipids and nucleic acids, may account for up to 50–90% of the total organic carbon of the biofilm and plays a central role in maintaining mechanical stability (FLEMMING *et al.*, 2016; RAS *et al.*, 2013). Owing to its heterogeneous composition and layered structure, EPS contains both hydrophilic and hydrophobic domains, which enable interactions with a wide range of compounds (POMPILIO *et al.*, 2008).

Given the low solubility and predominantly non-polar, hydrophobic nature of most oil constituents (PARTOVINIA *et al.*, 2021), the EPS matrix provides numerous adsorption sites that facilitate oil retention within the biofilm structure. Consequently, the accumulation of oil within the biofilm structure led to an increase in biofilm thickness, as

shown in Figure 41, and this excessive growth may have surpassed the effective oxygen penetration depth in the biofilm matrix. According to the literature, oxygen diffusion declines progressively as biofilm thickness increases, typically limiting aerobic activity to the outer layers while favoring the formation of anoxic zones in the inner regions (HIBIYA *et al.*, 2004). Consequently, this restricted oxygen diffusion and the resulting anoxic conditions in the deeper layers could weaken the structural integrity of the matrix, ultimately leading to the destabilization of the biofilm. Consistent with this interpretation, Mallick and Chakraborty (2021) reported pronounced fluctuations in solids concentration in an aerobic reactor following abrupt increases in influent crude oil loading from 300 mg L⁻¹ to 600 mg L⁻¹ and subsequently to 900 mg L⁻¹. During the oil shock event, attached biomass decreased to 16.05 ± 0.02 g L⁻¹, while suspended biomass increased to 3.03 ± 0.01 g L⁻¹, indicating enhanced biofilm sloughing.

Figure 42 presents optical microscopy images of the biofilm in MBBR4 across the different operational phases under increasing oil loading conditions. Throughout the study period, microscopic observations indicated the development of a well-structured and mature biofilm, characterized by the presence of protozoa, rotifers, and bacterial flocs. As discussed previously, these organisms are sensitive to variations in operational conditions and are commonly used as biological indicators of treatment performance. Their sustained abundance indicates that the progressive increase in oil concentration during reactor operation did not exert a toxic effect on the sludge microfauna (metazoans and protozoans). Consistently, the reactor maintained stable and efficient nitrification performance throughout the operational period, confirming the robustness and functional resilience of the biofilm under harsh conditions. These observations strongly correlate with established literature on biological adaptation to oily wastewater (ALKHATIB; THIEM, 1988; HYDROSCIENCE, INC., 1971).

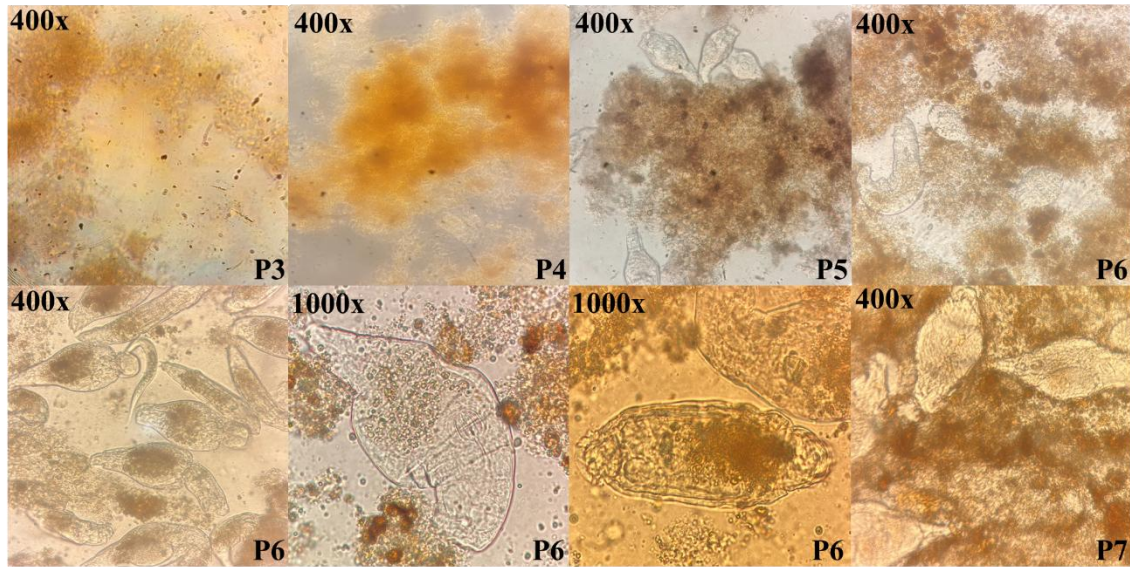


Figure 42 - Optical micrographs (400× and 1000× magnification) obtained during P3-P7 from MBBR4.

4.2.3 Nitrification Performance

Ammonium removal and the profiles of nitrogen species throughout all operational phases are presented in Figure 43, while Figure 44 illustrates the average concentrations of these oxidized nitrogen species in each phase. Overall, MBBR4 consistently maintained robust nitrification, quickly recovering and sustaining high ammonium removal even under increasing oil loads. The high nitrite and nitrate concentrations detected during certain phases in the influent of MBBR4, which was fed with real wastewater from the secondary treatment stage of the petroleum refinery, were attributed to the intrinsic characteristics of this wastewater.

During P3, the reactor exhibited pronounced variability, with ammonium removal efficiencies fluctuating between 50% and 80%. Over time, performance steadily improved, ultimately reaching 97% after 64 days. At this stage, effluent ammonium concentrations dropped to below $1 \text{ mgNH}_4^+-\text{N L}^{-1}$, demonstrating that the biofilm had fully acclimated and was functioning under stable and favorable operating conditions. When the oil concentration was increased to $30\text{--}50 \text{ mg L}^{-1}$ in P4, a temporary decline in nitrification efficiency was observed, dropping to $95 \pm 2\%$ at the beginning of the phase and reaching a minimum removal of 83% with effluent ammonium increasing to 5.5

$\text{mgNH}_4^+-\text{N L}^{-1}$. Nonetheless, the system quickly recovered, restoring stable nitrification at approximately 94% removal, demonstrating strong biofilm resilience and adaptive capacity. During P5, with oil concentration gradually increased to 50–100 mg L^{-1} , the system maintained excellent stability, sustaining an average ammonium removal of $95 \pm 1\%$. After around 15 days of operation, the reactor reached near-complete nitrification, with effluent ammonium consistently remaining below 1 $\text{mgNH}_4^+-\text{N L}^{-1}$. This performance indicates that the biofilm had matured, enabling efficient and sustained oxidation of ammonium to nitrate. Even in P6, when oil concentrations rose further to 200–300 mg L^{-1} , MBBR4 maintained high nitrification efficiency close to 100%, indicating that the biofilm provided effective protection against potential inhibitory effects of oil.

In the final phase (P7), under high oil concentrations (300–500 mg L^{-1}), a slight reduction in performance occurred, with average ammonium removal declining to $95 \pm 1\%$. Similar to P4, high oil load temporarily reduced efficiency to 82% with effluent ammonium increasing to 6.4 $\text{mgNH}_4^+-\text{N L}^{-1}$. However, the MBBR system once again recovered, achieving stable and efficient nitrification by the end of the phase with an average of $95 \pm 1\%$ removal rate.

Overall, the results show that MBBR4 maintained high functional stability under oil stress, supported by a mature and resilient biofilm capable of withstanding and recovering from short-term inhibitory effects. Across P3–P7 (Figure 43b), the reactor consistently sustained effective nitrification, with complete ammonium oxidation and only minor nitrite accumulation ($< 2 \text{ mgNO}_2^--\text{N L}^{-1}$), despite fluctuations in influent oil loading.

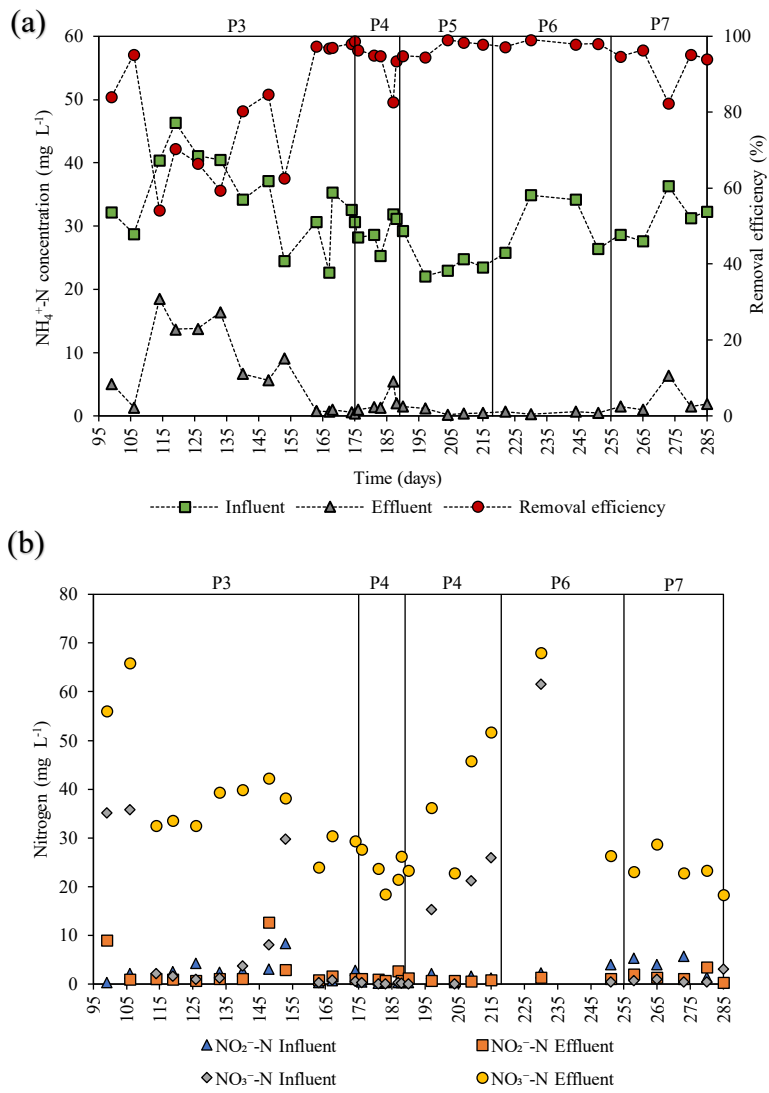


Figure 43 - (a) Evolution of ammonium removal efficiency and (b) corresponding influent and effluent oxidized nitrogen species during the operational phases of MBBR4.

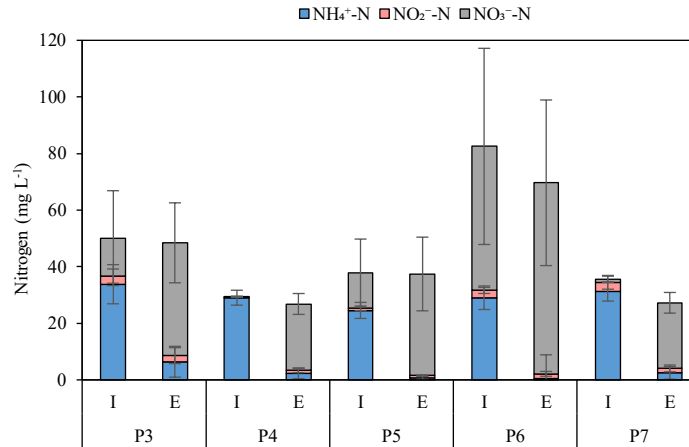


Figure 44 - Average Influent (I) and Effluent (E) nitrogen species profiles in MBBR4 across operational phases.

The nitrification performance of the reactor is further corroborated by the patterns in ammonium SLR and SRR, as shown in Figure 45a. In P3, ammonium SLR and SRR averaged 1.7 ± 0.3 and 1.3 ± 0.2 $\text{gNH}_4^+-\text{N m}^{-2} \text{d}^{-1}$, respectively. In P4, despite increasing the oil concentration to 30–50 mg L^{-1} , the reactor maintained a stable SLR and SRR of approximately 1.4 ± 0.2 $\text{gNH}_4^+-\text{N m}^{-2} \text{d}^{-1}$ and 1.3 ± 0.1 $\text{gNH}_4^+-\text{N m}^{-2} \text{d}^{-1}$, respectively. From P5 through P6, SLR and SRR remained closely matched, even as oil concentrations rose to 200–300 mg L^{-1} . In P7, under the highest oil range (300–500 mg L^{-1}), the reactor continued to perform reliably, removing 1.4 ± 0.1 $\text{g NH}_4^+-\text{N m}^{-2} \text{d}^{-1}$ against an applied load of 1.5 ± 0.2 $\text{gNH}_4^+-\text{N m}^{-2} \text{d}^{-1}$. These trends reflect a mature, robust autotrophic biofilm capable of maintaining efficient nitrification under elevated oil stress.

Figure 45b shows a strong linear relationship between the ammonium SLR and SRR ($R^2 = 0.97$), indicating stable and efficient nitrification during the increase in oil load. Most data points lie close to the 100% removal line, demonstrating that the reactor was able to oxidize nearly all the influent ammonium nitrogen. The slope slightly below unity (0.86) suggests minor limitations at higher loads. Still, overall, the results confirm that increasing oil load did not impair nitrification performance and that the reactor maintained a high nitrification capacity under these conditions.

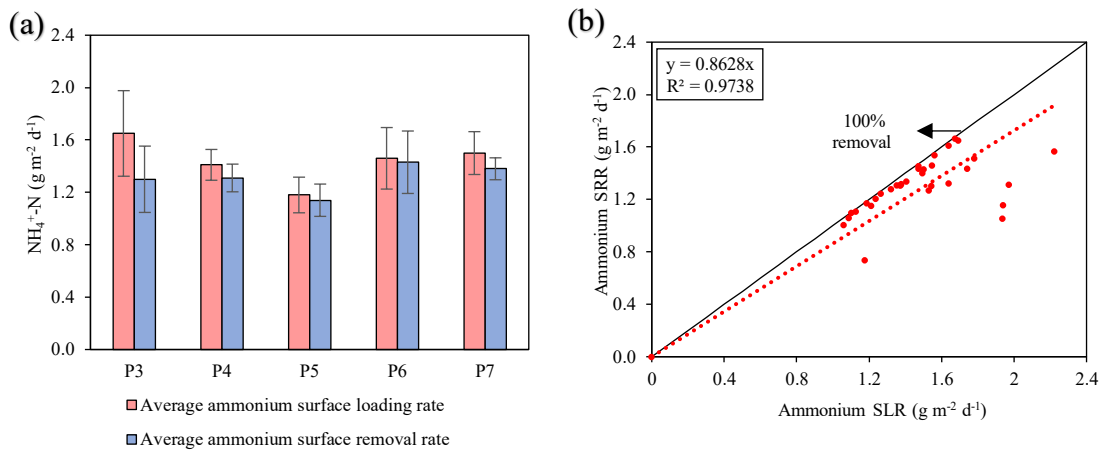


Figure 45 - (a) Average ammonium surface loading rate (SLR) and ammonium removal rate (SRR), and (b) relationship between ammonium SLR and SRR in MBBR4 during P3–P7.

Overall, when considered together with the solids observations, the results suggest that although the biofilm experienced substantial structural disruption, the remaining attached biomass exhibited clear resilience, allowing nitrification performance to remain relatively stable. This behavior may reflect the adaptive capacity of oil-tolerant microbial populations within the biofilm. Furthermore, while nitrifying bacteria generally possess hydrophobic cell surfaces, many of these hydrophobic regions are not directly exposed to the bulk liquid. Instead, they are embedded within the biofilm matrix and partially protected by hydrophilic components such as EPS. As a result, the outer biofilm surface is typically less hydrophobic than individual microbial cells, thereby limiting direct interactions between hydrophobic compounds and nitrifying microorganisms unless the biofilm structure becomes destabilized (POMPILIO *et al.*, 2008).

The present observations indicate that elevated biofilm detachment did not necessarily translate into immediate deterioration of reactor performance. This behavior is consistent with findings reported by Elenter *et al.* (2007), who observed that substantial biofilm sloughing, removing nearly half of the biofilm thickness, did not significantly affect ammonia removal rates. Their results highlighted that system performance was primarily governed by effective diffusion depth and the presence of an active surface layer rather than by total biomass (ELENER *et al.*, 2007).

The inhibition pattern observed in this study appears to be predominantly physical in nature. Instability in biological systems treating oily wastewater has been mainly

associated with physical interactions, such as rapid adsorption of oil onto biological solids, alterations in particle density, and subsequent biomass washout, without clear evidence of direct microbial toxicity (HYDROSCIENCE, INC., 1971). In addition, Ali and Aziz (2024) demonstrated that a combined DAF–MBBR system was able to maintain effective nitrification even under elevated oil and grease concentrations ($1500 \pm 150 \text{ mg L}^{-1}$) in synthetic wastewater. The MBBR exhibited stable nitrification performance, achieving average ammonia removal efficiencies of up to 86% in the presence of oil.

4.2.4 Batch Trials

Figure 46 shows the temporal profiles of nitrogen species concentrations obtained from batch tests conducted at the end of each operational phase of MBBR4 under increasing oil concentrations. During phases P3 and P5, ammonium was progressively oxidized to nitrite and subsequently to nitrate. In contrast, during phases P6 and P7, this conversion occurred more rapidly, resulting in less pronounced nitrite accumulation.

Maximum ammonium nitrogen removal was reached at different times across the operational phases. During P3 to P6, complete $\text{NH}_4^+\text{-N}$ removal was achieved within approximately 60 min, while in P7 it occurred after about 120 min. Overall, the increasing oil load did not affect the time required to reach maximum $\text{NH}_4^+\text{-N}$ removal. Moreover, ammonium removal consistently occurred within or below the applied hydraulic retention time of 2 h, indicating stable nitrification performance under elevated oil concentrations.

Data obtained from biofilm quantification and batch trials performed at the end of each phase were used to calculate the maximum specific ammonium removal rate (Table 16). The reactor reached its highest maximum specific ammonium removal rate of $192 \text{ mgNH}_4^+\text{-N gVAS}^{-1} \text{ d}^{-1}$ during P3 when the oil concentration was very low ($< 10 \text{ mg L}^{-1}$). During P3–P6, this rate gradually decreased and reached $132 \text{ mgNH}_4^+\text{-N gVAS}^{-1} \text{ d}^{-1}$ in P6, likely associated with the concurrent rise in VAS concentration from 3.0 g L^{-1} in P3 to 3.6 g L^{-1} in P6. The trend observed during P3–P6 aligns with a previous study, which reported that increasing the oil load from 600 mg L^{-1} to 900 mg L^{-1} led to a decrease in the specific ammonium removal rate from 19.49 ± 0.02 to $18.32 \pm 0.02 \text{ mgNH}_4^+\text{-N gVS}^{-1} \text{ d}^{-1}$ (MALLICK; CHAKRABORTY, 2021). However, with increasing oil concentration

in P7 and subsequent reduction in VAS concentration to 1.9 mg L⁻¹, the maximum specific ammonium removal rate rose again to 170 mgNH₄⁺-N gVAS⁻¹ d⁻¹.

Table 16 also summarizes the average real apparent specific ammonium removal rates measured during the operation under conditions matching each batch test. Throughout P3–P6, the maximum specific removal rates were higher than the real apparent values, with the largest difference observed in P3, when the maximum rate was approximately two times higher. In P7, the real apparent rate nearly matched the maximum value, indicating that the reactor was operating close to its nitrification capacity.

Table 16 - Ammonium removal and specific ammonium removal rate obtained during P3-P7 of MBBR4

Phase	Ammonium removal (%)	Specific ammonium removal rate (mg NH ₄ ⁺ - N g VS ⁻¹ d ⁻¹)			VAS (g L ⁻¹)	VSS (mg L ⁻¹)
		Max ^a	Real ^b	f _{Max/Real}		
P3	81 ± 16	192	132	1.5	3.0	19
P5	97 ± 2	144	76	2.0	3.7	46
P6	98 ± 1	132	90	1.5	3.6	85
P7	93 ± 6	170	185	0.9	1.9	111

^aIn Max VS corresponds to VAS, since only attached biomass was present during the batch trials.

^bIn Real VS represents the sum of VAS and VSS, as this rate refers to continuous operation in which both attached and suspended biomass fractions were present.

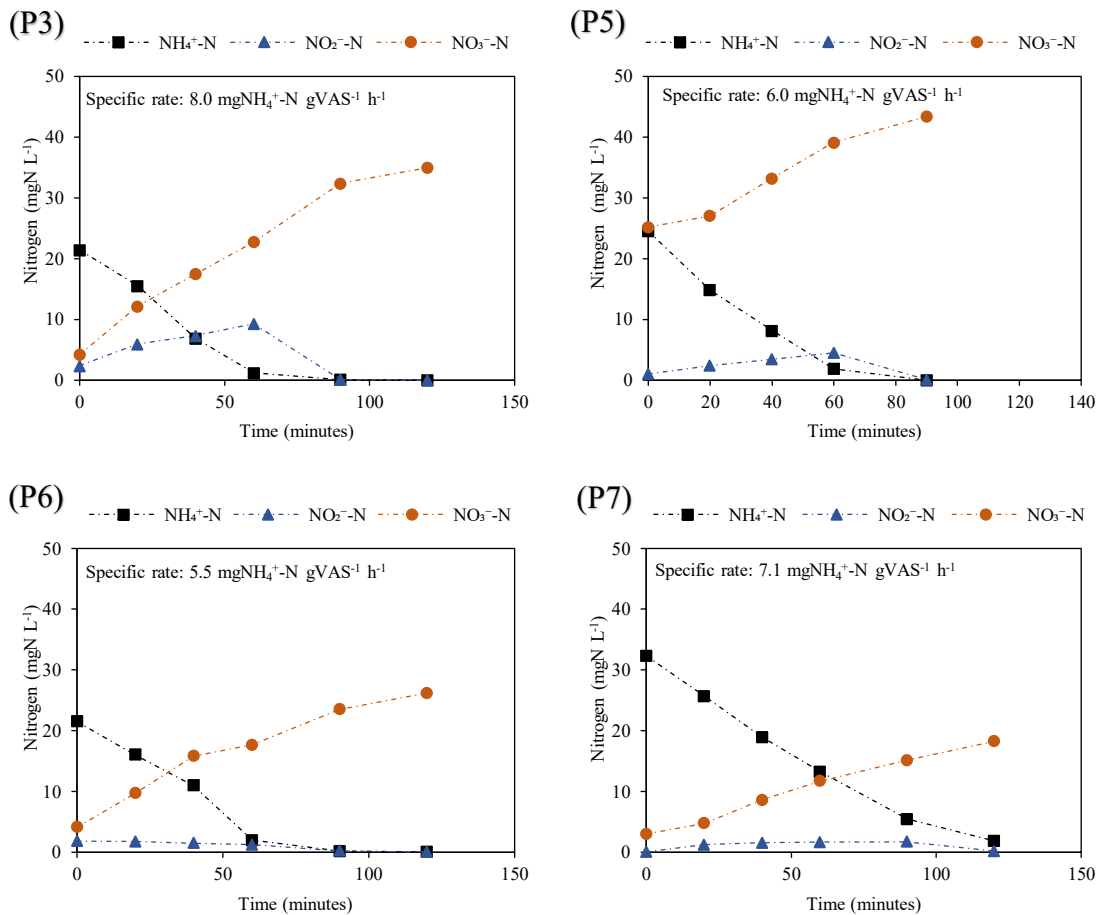


Figure 46 - Temporal profiles of nitrogen species in MBBR4 obtained during batch tests corresponding to phases P3, P5, P6, and P7.

4.2.5 Operational Parameters: pH and Temperature

Figure 47 shows the pH profile across the operational phases of MBBR4, and Table 17 reports the pH and temperature values at the start and end of the batch activity assays. MBBR4 exhibited stable pH profiles throughout all operational phases with oil addition. Both influent and effluent pH values were consistently maintained within the range of 7.0–8.5, with an average of 8.1 ± 0.4 , which is widely recognized as favorable for sustaining efficient and stable nitrification. Similarly, during the batch activity tests, pH values remained within or close to this optimal range, indicating suitable conditions for nitrification.

Table 17 - Parameters evaluated at the beginning and end of the activity batch tests.

Reactor	Phase ^a	pH _{initial}	pH _{final}	T _{initial} (°C)	T _{final} (°C)
MBBR4	P3	8.4	8.7	20.6	21.1
	P5	8.3	8.8	22.1	18.9
	P6	8.3	8.5	22.2	18
	P7	8.3	8.4	21.9	17

^aDuring P4, activity batch test was not conducted because of the short duration of this phase.

Under all operating conditions, including both continuous operation and batch tests, MBBR4 was maintained at ambient temperature (24 ± 3 °C), which is within the range reported as adequate for nitrifying activity.

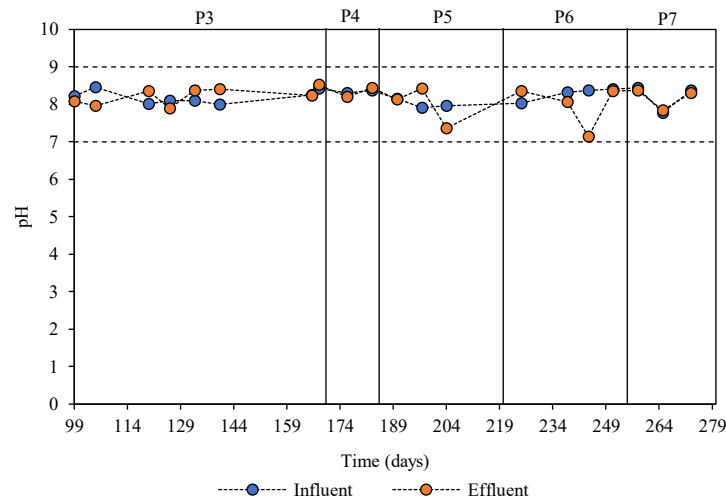


Figure 47 - pH values recorded throughout the MBBR4 operational period with oil addition. Upper and lower discharge limits defining optimal nitrification performance are shown as dotted horizontal lines.

CHAPTER 5

CONCLUSIONS

5.1 Conclusions of Part I

The results from Part I demonstrated that stable tertiary nitrification of real oil refinery wastewater from the secondary treatment stage can be successfully achieved and maintained in MBBR systems operating under variable operational conditions, allowing biofilm to progressively adapt to real wastewater and maintain high and stable nitrification performance.

The acclimation strategy employed significantly dictates the initial stability and resilience of the MBBR systems. Direct exposure to real wastewater resulted in prolonged instability and delayed nitrification due to potential inhibitory compounds. In contrast, reactors supported with external organic carbon or gradual acclimation from synthetic to real wastewater achieved faster biofilm establishment, higher and more stable removal efficiencies, and greater resistance to operational changes. Overall, strategies promoting the addition of easily biodegradable organic carbon during initial stages accelerated biofilm formation by promoting the growth of heterotrophic bacteria, which produce extracellular polymeric substances that act as a fixation matrix, thereby facilitating the subsequent colonization of nitrifiers and reducing startup time compared to systems relying solely on slow autotrophic colonization. Furthermore, the findings indicate that there is a distinct inverse relationship between the availability of biodegradable organic carbon and the specific ammonium removal rate of the biofilm. High organic loads favor fast-growing heterotrophs that compete with nitrifiers for oxygen and space. Consequently, the reduction or elimination of external organic carbon was essential for minimizing heterotrophic competition, allowing the biofilm to become enriched with autotrophic nitrifiers and maximizing the specific nitrification capacity of the system.

The results also showed that reducing the HRT to 2 h acted as a major hydraulic stress that exposed kinetic limitations within the biofilm, particularly affecting the stability of nitrite-oxidizing bacteria. While the immediate disruption to overall ammonium removal varied with the specific operational setup, all conditions consistently highlighted the sensitivity of NOB, resulting in a distinct, temporary accumulation of

nitrite. Ultimately, all reactors demonstrated strong recovery capacity, overcoming this initial bottleneck as the systems adapted. The dynamics of solids were also found to be strongly influenced by the availability of biodegradable organic carbon and operational stress factors. The presence of readily biodegradable substrates promoted the rapid development of thick biofilms with high volatile attached solids concentrations during the initial phases. This accumulation was attributed to the proliferation of fast-growing heterotrophic bacteria. However, as the external carbon source was progressively reduced and eliminated to favor nitrification, a distinct decline in attached biomass was observed across these reactors. Conversely, the reactor that operated without carbon supplementation exhibited a much slower initial biofilm development with relatively lower biomass mass, confirming that organic carbon is a primary driver of biofilm accumulation.

Regarding the composition of the solids, the biomass within the reactors remained predominantly organic and active. The ratio of volatile to total attached solids (VAS/TAS) generally exceeded 70% throughout the study, indicating that the biofilm was composed mainly of active microorganisms rather than inorganic inert material. The study also confirmed that the MBBRs functioned as true attached-growth systems, with the ratio of attached solids to total solids (TAS/TS) consistently remaining above 90%.

Finally, visual observations and thickness measurements revealed a strong correlation between influent COD and biofilm structure. In reactors supplemented with carbon, declining COD concentrations corresponded to reduced biofilm thickness, showing a clear negative trend. In contrast, the reactor without external carbon supplementation developed a thin, uniform biofilm from the start, reflecting the absence of heterotrophic overgrowth.

5.2 Conclusions of Part II

MBBR demonstrated remarkable resilience and functional stability when subjected to increasing oil concentrations. Although influent oil concentrations increased from relatively low levels of 10–30 mg L⁻¹ to as high as 300–500 mg L⁻¹, the system consistently maintained high nitrification efficiency. While increases in oil concentration caused temporary declines in performance, the system exhibited a rapid recovery capacity, restoring stable nitrification within a short period. This indicates that the established nitrifying biofilm possesses a robust adaptive capacity capable of withstanding the inhibitory pressures typical of oil refinery wastewater fluctuations.

While biological activity remained high, elevated oil concentrations exerted significant physical impacts on the biofilm and carrier media. High oil loading led to the accumulation of oil on the biocarriers, causing them to darken, agglomerate, and suffer from reduced mobility within the reactor. The biofilm thickness initially increased with oil concentration, reaching up to 351 µm, likely due to the adsorption of oil compounds into the extracellular polymeric substance matrix. However, at the highest oil concentrations (300–500 mg L⁻¹), the biofilm became irregular and patchy, and detachment rates increased sharply, leading to a significant loss of attached volatile solids. This suggests that excessive oil disrupts the adhesive forces within the biofilm, compromising its structural integrity.

Despite the visible accumulation of oil and structural instability, the specific nitrifying activity of the biomass remained robust. Microscopic analysis confirmed the persistence of a mature and diverse microbial community, including protozoa and rotifers, throughout the operation, indicating that the oil did not exert a lethal toxic effect on the microfauna.

Overall, the study confirmed that well-acclimated nitrifying biofilms exhibit strong resistance to the inhibitory effects of oil while maintaining high ammonium removal efficiencies. Despite increased biofilm restructuring and solids detachment under high oil load conditions, the reactors demonstrated sustained biological functionality and adaptive capacity. These findings support the feasibility of applying MBBR technology to refinery wastewater treatment and provide important insights into biofilm resilience and process stability under real industrial scenarios, where operational problems in oil–water separation units may lead to rapid increases in oil and other contaminants due to

accidental releases, process upsets, or fluctuations in production. Such events can suddenly alter the influent composition and introduce high oil concentrations into biological treatment systems, challenging their stability and potentially inhibiting sensitive processes such as nitrification.

5.3 Suggestions for Future Works

As future perspectives and potential developments arising from this work, several experimental approaches and research directions may be further investigated, as outlined below:

- 1) While the current study utilized optical microscopy and stereomicroscopy to observe biofilm morphology and identify microfauna, these methods cannot identify specific bacterial species. Future work should employ advanced molecular techniques to better understand the ecological shifts between AOB, NOB, and heterotrophic populations during acclimation, oil exposure, and hydraulic stress. Furthermore, it would be valuable to track how the microbial community structure shifts in response to the specific acclimation strategies and increasing oil loads, identifying if oil-degrading bacteria are being enriched within the biofilm matrix.
- 2) The discussion hypothesized that the physical adsorption of oil onto the biofilm is mediated by hydrophobic interactions with the EPS matrix. Future research should move beyond quantitatively analyzing the chemical composition of the EPS (e.g., protein-to-polysaccharide ratio). Understanding how oil exposure alters EPS production would provide deeper insight into the mechanism of biofilm thickening and detachment observed in Part II.
- 3) The current study exclusively utilized Kaldnes K1 carriers, which have a protected specific surface area of $500 \text{ m}^2 \text{ m}^{-3}$. Future research should evaluate carriers with different geometries and higher specific surface areas. Testing carriers with smaller pore sizes or different protective grid structures could reveal designs that better shield the biofilm from the shear forces caused by oil-induced agglomeration while maintaining sufficient void space to prevent clogging during high-oil loading phases.
- 4) A critical avenue for future research would be to conduct a "stress test" by progressively increasing the oil load until the system reaches failure. Since the current study only observed physical stress indicators without a collapse in metabolic activity,

extending the oil concentration beyond 500 mg L⁻¹ is necessary to identify the operational breaking point. This investigation aims to pinpoint the specific threshold where the physical barrier created by oil adsorption transitions from a manageable diffusion limitation to a complete inhibition of oxygen and substrate transfer, or where the biofilm detachment becomes so severe that it exceeds the specific growth rate of nitrifiers, leading to washout. Defining this failure limit would establish the true safety margins for MBBR technology in handling high oil loads from oil refinery upsets.

CHAPTER 6

REFERENCES

AKTAN, Ç., DINLER, V., MESUM, B., *et al.* "A new approach for treating ammonia-rich wastewater deficient in organic matter: A tandem process for nitrification/nitritation in MBBR followed by sulfur-based denitrifying column reactor". *Chemical Engineering Journal*, v. 513, p. 163061, 2025.

AL-ATTABI, A. W. N. *Treatment of petroleum refinery wastewater in an innovative sequencing batch reactor*. Tese (Doutorado) – Department of Civil Engineering, Liverpool John Moores University, Liverpool, 2018.

ALI, S., AZIZ, S. Q. "Biofilm formation monitoring using SEM in synthetic wastewater pollutant removal by combination of DAF and modified MBBR". *Ain Shams Engineering Journal*, v. 15, pp. 1-8, 2024.

ALJUBOURY, D., PALANIANDY, P., AZIZ, H., *et al.* "Treatment of petroleum wastewater by conventional and new technologies A review", *Global Nest Journal*, Set. 2017.

ALKHATIB, E. A., THIEM, L. T. "In-situ Adaptation of Activated Sludge by Shock Loading to Enhance Treatment of High Ammonia Content Petrochemical Wastewater". *Water Science and Technology*, v. 20, n. 10, pp. 31-44, 1988.

APHA (AMERICAN PUBLIC HEALTH ASSOCIATION), Standard Methods for the Examination of Water and Wastewater, 14^a ed., American Water Works Association, Water Environment Federation, Washington, D.C., 1976.

APHA (AMERICAN PUBLIC HEALTH ASSOCIATION), Standard Methods for the Examination of Water and Wastewater, 18^a ed., American Water Works Association, Water Environment Federation, Washington, D.C., 1992.

APHA (AMERICAN PUBLIC HEALTH ASSOCIATION). Standard Methods for the Examination of Water and Wastewater, 21a. ed., American Water Works Association, Water Environment Federation, Washington, D.C., 2005.

APHA, AWWA, WEF. Standard Methods for the Examination of Water and Wastewater (23rd edition). 23rd. ed. USA, American Public Health Association; American Water Works Association; Water Environment Federation, 2017.

AQEEL, H., WEISSBRODT, D., CERRUTI, M., *et al.* "Drivers of bioaggregation from flocs to biofilms and granular sludge". *Environmental Science: Water Research & Technology*, v. 5, 2019.

ASHKANANI, A., ALMOMANI, F., KHRAISHEH, M., *et al.* "Bio-carrier and operating temperature effect on ammonia removal from secondary wastewater effluents using moving bed biofilm reactor (MBBR)", *Science of The Total Environment*, v. 693, p. 133425, Nov. 2019.

AYGUN, A., NAS, B., BERKTAY, A. "Influence of High Organic Loading Rates on COD Removal and Sludge Production in Moving Bed Biofilm Reactor". *Environmental Engineering Science*, v. 25, pp. 1311-1316, 2008.

BAHADORI, A. Waste Management in the Chemical and Petroleum Industries, 2. ed., Hoboken, John Wiley & Sons, Inc., 2020.

BASSIN, J., KLEEREBEZEM, R., ROSADO, A., *et al.* "Effect of Different Operational Conditions on Biofilm Development, Nitrification, and Nitrifying Microbial Population in Moving-Bed Biofilm Reactors", *Environmental science & technology*, v. 46, pp. 1546-1555, Fev. 2012.

BASSIN, J. P., DEZOTTI, M. "Moving Bed Biofilm Reactor (MBBR)". In: *Advanced Biological Processes for Wastewater Treatment: Emerging, Consolidated Technologies and Introduction to Molecular Techniques*, Cham, Springer International Publishing, pp. 37-74, 2018.

BASSIN, J. P., ABBAS, B., VILELA, C. L., *et al.* "Tracking the dynamics of heterotrophs and nitrifiers in moving-bed biofilm reactors operated at different COD/N ratios". *Bioresource Technology*, v. 192, pp. 131-141, 2015.

- BASSIN, J. P., BASSIN, I. D., CAO, S., *et al.* "Effect of increasing organic loading rates on the performance of moving-bed biofilm reactors filled with different support media: Assessing the activity of suspended and attached biomass fractions". *Process Safety and Environmental Protection*, v. 100, 2016.
- BASSIN, J. P., DEZOTTI, M., SANT'ANNA, G. L. "Nitrification of industrial and domestic saline wastewaters in moving bed biofilm reactor and sequencing batch reactor", *Journal of Hazardous Materials*, v. 185, n. 1, pp. 242-248, 2011.
- BHANDARI, V. M., RANADE, V. V. "Advanced Physico-chemical Methods of Treatment for Industrial Wastewaters". In: RANADE, V. V., BHANDARI, V. M. (eds.), *Industrial Wastewater Treatment, Recycling and Reuse*, Butterworth-Heinemann, pp. 81-140, 2014.
- BHAT, M. R., ROOPALI, HIREMATH, S., *et al.* "Correlation between BOD, COD and TOC". *Journal of Industrial Pollution Control*, v. 20, n. 1, pp. 187-191, 2004.
- BOLEYDEI, H., MIRGHAFARI, N., FARHADIAN, O. "Comparative study on adsorption of crude oil and spent engine oil from seawater and freshwater using algal biomass". *Environmental Science and Pollution Research*, v. 25, 2018.
- BOOPATHY, R., KARTHIKEYAN, S., MANDAL, A. B., *et al.* "Adsorption of ammonium ion by coconut shell-activated carbon from aqueous solution: kinetic, isotherm, and thermodynamic studies". *Environmental Science and Pollution Research*, v. 20, n. 1, pp. 533-542, 2013.
- BRANDÃO, P., SOUZA, T., FERREIRA, C., *et al.* "Removal of petroleum hydrocarbons from aqueous solution using sugarcane bagasse as adsorbent". *Journal of Hazardous Materials*, v. 175, pp. 1106-1112, 2009.
- BUTLER, C. S., BOLTZ, J. "Biofilm Processes and Control in Water and Wastewater Treatment". In: *Comprehensive Water Quality and Purification*, v. 3, Amsterdam, Netherlands, Elsevier, pp. 90-107, 2014.
- CANFIELD, D., GLAZER, A., FALKOWSKI, P. "The Evolution and Future of Earth's Nitrogen Cycle". *Science*, v. 330, pp. 192-196, 2010.

CAO, S., FONTOURA, G., DEZOTTI, M., et al. "Combined organic matter and nitrogen removal from a chemical industry wastewater in a two-stage MBBR system", *Environmental technology*, v. 37, pp. 1-39, Jun. 2015.

CAPONE, D., POPA, R., FLOOD, B., et al. "Geochemistry. Follow the nitrogen". *Science*, v. 312, pp. 708-709, 2006.

CARRERA, J., VICENT, T., LAFUENTE, F. "Effect of influent COD/N ratio on biological nitrogen removal (BNR) from high-strength ammonium industrial wastewater". *Process Biochemistry*, v. 39, pp. 2035-2041, 2004.

CHAN-PACHECO, C. R., VALENZUELA, E. I., CERVANTES, F. J., et al. "Novel biotechnologies for nitrogen removal and their coupling with gas emissions abatement in wastewater treatment facilities". *Science of The Total Environment*, v. 797, pp. 149228, 2021.

CHEN, J., ZHANG, X., ZHOU, L., et al. "Metagenomics Insights into High-Rate Nitrogen Removal from Municipal Wastewater by Integrated Nitrification, Partial Denitrification and Anammox at an Extremely Short Hydraulic Retention Time". *SSRN Electronic Journal*, 2023.

CHOWDHURY, A., SARKAR, A., BANDYOPADHYAY, A. "Rice Husk Ash as a Low Cost Adsorbent for the Removal of Methylene Blue and Congo Red in Aqueous Phases". *CLEAN – Soil, Air, Water*, v. 37, pp. 581-591, 2009.

COELHO, A., CASTRO, A., DEZOTTI, M., et al. "Treatment of petroleum refinery sourwater by advanced oxidation processes", *Journal of hazardous materials*, v. 137, pp. 178-184, Oct. 2006.

COLLOS, Y., HARRISON, P. J. "Acclimation and toxicity of high ammonium concentrations to unicellular algae". *Marine Pollution Bulletin*, v. 80, n. 1–2, pp. 8-23, 2014.

D'LAMARE, A., JUNIOR, C., AMORIM, J., et al. "Oily Wastewater Treatment: Methods, Challenges, and Trends". *Processes*, v. 10, 2022.

DEENA, S. R., KUMAR, G., VICKRAM, A. S., *et al.* "Efficiency of various biofilm carriers and microbial interactions with substrate in moving bed-biofilm reactor for environmental wastewater treatment". *Bioresource Technology*, v. 359, 2022.

DELASHOUB, A., BORGHEI, S. M. "Optimization of multistage biological nutrient removal reactors for removal of nitrogen and phosphorus from saline refinery wastewater". *International Journal of Environmental Science and Technology*, v. 17, 2020.

DEZOTTI M., *Processos e Técnicas para o Controle Ambiental de Efluentes Líquidos*. Rio de Janeiro: E-papers, 2008.

DI BIASE, A., KOWALSKI, M., DEVLIN, T., *et al.* "Moving bed biofilm reactor technology in municipal wastewater treatment: A review". *Journal of Environmental Management*, v. 247, pp. 849-866, 2019.

DING, F., LIANG, D., WU, Y., *et al.* "Effect of C/N on partial nitrification in an MBBR at low temperature". *Environmental Science: Water Research & Technology*, v. 6, 2020.

DONG, Z., LU, M., HUANG, W., *et al.* "Treatment of oilfield wastewater in moving bed biofilm reactors using a novel suspended ceramic biocarrier". *Journal of Hazardous Materials*, v. 196, pp. 123-130, 2011.

ELENER, D., MILFERSTEDT, K., ZHANG, W., *et al.* "Influence of detachment on substrate removal and microbial ecology in a heterotrophic/autotrophic biofilm". *Water Research*, v. 41, pp. 4657-4671, 2007.

ELMOBARAK, W. F., HAMEED, B. H., ALMOMANI, F., *et al.* "A Review on the Treatment of Petroleum Refinery Wastewater Using Advanced Oxidation Processes", *Catalysts*, v. 11, n. 7, p. 782, 2021.

EMERSON, K., RUSSO, R. C., LUND, R. E., *et al.* "Aqueous Ammonia Equilibrium Calculations: Effect of pH and Temperature". *Journal of the Fisheries Research Board of Canada*, v. 32, n. 12, pp. 2379-2383, 1975.

ENGLANDE, A. J., KRENKEL, P., SHAMAS, J. "Wastewater Treatment & Water Reclamation". In: *Reference Module in Earth Systems and Environmental Sciences*, Elsevier, 2015.

EPA - Environmental Protection Agency – USA, Nitrogen Control, EPA/625/R-93/010, 1993.

Fang, F., Ni, B.J., Li, X.Y. *et al.* Kinetic analysis on the two-step processes of AOB and NOB in aerobic nitrifying granules. *Appl Microbiol Biotechnol* **83**, 1159–1169, 2009.

FANG, H. Y., CHOU, M. S., HUANG, C. W. "Nitrification of ammonia-nitrogen in refinery wastewater", *Water Research*, v. 27, n. 12, pp. 1761-1765, 1993.

FIGUEROLA, E. L., ERIJMAN, L. "Diversity of nitrifying bacteria in a full-scale petroleum refinery wastewater treatment plant experiencing unstable nitrification", *Journal of Hazardous Materials*, v. 181, n. 1-3, pp. 281-288, Set. 2010.

FLEMMING, H. C., WINGENDER, J., SZEWZYK, U., *et al.* "Biofilms: An emergent form of bacterial life", *Nature Reviews Microbiology*, v. 14, pp. 563-575, Ago. 2016.

FORREST, D., DELATOLLA, R., KENNEDY, K. "Carrier Effects on Tertiary Nitrifying Moving Bed Biofilm Reactor: An Examination of Performance, Biofilm and Biologically Produced Solids". *Environmental Technology*, v. 37, pp. 1-28, 2016.

FRANCIS, C., BEMAN, M., KUYPERS, M. "New processes and players in the nitrogen cycle: The microbial ecology of anaerobic and archaeal ammonia oxidation". *The ISME Journal*, v. 1, pp. 19-27, 2007.

GALI, V., KUMAR, P., MEHROTRA, I. "Treatment of Phenol and Cresols in Upflow Anaerobic Sludge Blanket (UASB) Process: A Review", *Water Research*, v. 39, pp. 154-170, Fev. 2005.

GHALEHKHONDABI, V., FAZLALI, A., FALLAH, B. "Performance analysis of four-stage rotating biological contactor in nitrification and COD removal from petroleum refinery wastewater". *Chemical Engineering and Processing*, 2021.

GUPTA, B., GUPTA, A., GHOSAL, P., *et al.* "Recent advances in application of moving bed biofilm reactor for wastewater treatment: Insights into critical operational parameters,

modifications, field-scale performance, and sustainable aspects". *Journal of Environmental Chemical Engineering*, v. 10, p. 107742, 2022.

GÜVEN, H., ERSAHIN, M., OZGUN, H., *et al.* "Energy and material refineries of future: Wastewater treatment plants", *Journal of Environmental Management*, v. 329, p. 117130, Mar. 2023.

GZAR, H., AL-REKABI, W., KHALID, Z. "Applicaion of Moving Bed Biofilm Reactor (MBBR) for Treatment of Industrial Wastewater: A mini Review". *Journal of Physics: Conference Series*, v. 1973, p. 012024, 2021.

HAN, B., BUTTERLY, C., ZHANG, W., *et al.* "Adsorbent materials for ammonium and ammonia removal: A review". *Journal of Cleaner Production*, v. 283, pp. 124611, 2021.

HIBIYA, K., NAGAI, J., TSUNEDA, S., *et al.* "Simple prediction of oxygen penetration depth in biofilms for wastewater treatment". *Biochemical Engineering Journal*, v. 19, pp. 61-68, 2004.

HOLMES, D. E., DANG, Y., SMITH, J. A. "Chapter Four - Nitrogen cycling during wastewater treatment". In: GADD, G. M., SARIASLANI, S. (eds.), *Advances in Applied Microbiology*, v. 106, Academic Press, pp. 113-192, 2019.

HOUDA, N., CHATTI, A., RAJEB, A., *et al.* "Tertiary Nitrification Using Moving-Bed Biofilm Reactor: A Case Study in Tunisia", *Current Microbiology*, v. 70, Jan. 2015.

HUANG, H., PENG, C., PENG, P., *et al.* "Towards the biofilm characterization and regulation in biological wastewater treatment". *Applied Microbiology and Biotechnology*, v. 103, 2019.

HUANG, J., KANKANAMGE, N. R., CHOW, C., *et al.* "Removing ammonium from water and wastewater using cost-effective adsorbents: A review". *Journal of Environmental Sciences*, v. 63, pp. 174-197, 2018.

HYDROSCIENCE, INC. "*The impact of oily materials on activated sludge systems*". Washington, D.C.: Environmental Protection Agency, Water Quality Office, 1971. (Water Pollution Control Research Series, 12050 DSH 03/71).

IANNACONE, F., DI CAPUA, F., GRANATA, F., *et al.* "Effect of carbon-to-nitrogen ratio on simultaneous nitrification denitrification and phosphorus removal in a microaerobic moving bed biofilm reactor". *Journal of Environmental Management*, v. 250, 2019.

IBRAHIM, S., WANG, S., ANG, H. "Removal of Emulsified Oil from Oily Wastewater Using Agricultural Waste Barley Straw". *Biochemical Engineering Journal*, v. 49, pp. 78-83, 2010.

JAFARINEJAD, S. "Simulation for the Performance and Economic Evaluation of Conventional Activated Sludge Process Replacing by Sequencing Batch Reactor Technology in a Petroleum Refinery Wastewater Treatment Plant", *ChemEngineering*, v. 3, p. 45, Mai. 2019.

JAHREN, S., RINTALA, J., ØDEGAARD, H. "Aerobic moving bed biofilm reactor treating thermomechanical pulping whitewater under thermophilic conditions". *Water Research*, v. 36, pp. 1067-1075, 2002.

KAWAN, J., ABU HASAN, H., SUJA, F., *et al.* "A review on sewage treatment and polishing using moving bed bioreactor (Mbbr)". *Journal of Engineering and Applied Sciences*, v. 11, pp. 1098-1120, 2016.

KAWAN, J., SUJA, F., PRAMANIK, S. K., *et al.* "Effect of Hydraulic Retention Time on the Performance of a Compact Moving Bed Biofilm Reactor for Effluent Polishing of Treated Sewage". *Water*, v. 14, p. 81, 2022.

KAYSER, Rolf. Activated Sludge Process. In: JÖRDENING, Hans-Joachim; WINTER, Josef (Ed.). *Environmental Biotechnology: Concepts and Applications*. Weinheim: Wiley-VCH, 2004. p. 79-119.

KERR, C. J., OSBORN, K. S., RICKARD, A. H., *et al.* "Biofilms in water distribution systems". In: Mara, D., Horan, N. (eds), *Handbook of Water and Wastewater Microbiology*, Amsterdam, Netherlands, Academic Press, pp. 757-775, 2003.

KINDICHI, T.; KAWANO, Y.; ITO, T.; SATOH, H.; OKABE, S. Population dynamics and in situ kinetics of nitrifying bacteria in autotrophic nitrifying biofilms as determined by real-time quantitative PCR. *Biotechnology and Bioengineering*, Hoboken, v. 94, n. 6, p. 1111–1121, 20 ago. 2006. DOI: 10.1002/bit.20926.

KUMAR, K., SHARMA, R., GOYAL, S. K. "Performance of different biocarriers in MBBR and SBBR systems for wastewater treatment: A review", *Water Science and Engineering*, v. 19, n. 1, pp. 97-109, 2026.

KUMAR, L., CHUGH, M., KUMAR, S., et al. "Remediation of petrorefinery wastewater contaminants: A review on physicochemical and bioremediation strategies", *Process Safety and Environmental Protection*, v. 159, 2022.

LAZAROVA, V., MANEM, J. "Biofilm characterization and activity analysis in water and wastewater treatment". *Water Research*, v. 29, n. 10, pp. 2227-2245, 1995.

LI, T., LIU, J. "Factors affecting performance and functional stratification of membrane-aerated biofilms with a counter-diffusion configuration". *RSC Advances*, v. 9, pp. 29337-29346, 2019. #

LIMA, P., DEZOTTI, M., BASSIN, J. "Interpreting the effect of increasing COD loading rates on the performance of a pre-anoxic MBBR system: implications on the attached and suspended biomass dynamics and nitrification-denitrification activity". *Bioprocess and Biosystems Engineering*, v. 39, 2016.

LING, J., CHEN, S. "Impact of organic carbon on nitrification performance of different biofilters". *Aquacultural Engineering*, v. 33, n. 2, pp. 150-162, 2005.

LU, M., GU, L.-P., XU, W.-H. "Treatment of petroleum refinery wastewater using a sequential anaerobic-aerobic moving-bed biofilm reactor system based on suspended ceramsite". *Water Science and Technology*, v. 67, pp. 1976-1983, 2013.

MAHMOUDKHANI, R., AZAR, A. M., DEHGHANI, A. M., et al. "Treatment of Contaminated Waters with Petroleum by Moving Bed Biofilm Reactor (MBBR)". 2012.

- MAHTO, K. U., DAS, S. "Bacterial biofilm and extracellular polymeric substances in the Moving Bed Biofilm Reactor for wastewater treatment: A review". *Bioresource Technology*, v. 345, p. 126476, 2021.
- MALLICK, S. K., CHAKRABORTY, S. "Treatment of synthetic refinery wastewater in anoxic-aerobic sequential moving bed reactors and sulphur recovery". *Journal of Environmental Science and Health, Part A*, v. 52, n. 13, pp. 1257-1268, 2017.
- MALLICK, S. K., CHAKRABORTY, S. "Effect of crude oil shock load on anoxic-aerobic sequential moving bed reactors during petroleum refinery wastewater treatment", *Journal of Cleaner Production*, v. 329, p. 129795, Nov. 2021.
- MATHEUS, M. C., LOURENÇO, G. R., SOLANO, B. A., *et al.* "Assessing the impact of hydraulic conditions and absence of pretreatment on the treatability of pesticide formulation plant wastewater in a moving bed biofilm reactor". *Journal of Water Process Engineering*, v. 36, p. 101243, 2020.
- MATHEUS, Maurício Carvalho. Assessing the performance, biosolids dynamics and microbial profiles of moving bed biofilm reactors treating wastewaters from pesticide and pulp & paper industries. Tese (Doutorado em Engenharia Química) – Instituto Alberto Luiz Coimbra de Pós-Graduação e Pesquisa de Engenharia (COPPE), Universidade Federal do Rio de Janeiro, Rio de Janeiro, 2020.
- MAURYA, A., KUMAR, R., RAJ, A. "Biofilm-based technology for industrial wastewater treatment: current technology, applications and future perspectives". *World Journal of Microbiology and Biotechnology*, v. 39, 2023.
- MAURYA, A., RAJ, A. "Recent advances in the application of biofilm in bioremediation of industrial wastewater and organic pollutants". In: SINGH, P., KUMAR, A., BORTHAKUR, A. (eds.), *Abatement of Environmental Pollutants: Trends and Strategies*, Elsevier, pp. 81-118, 2020.
- MAZIOTI, A. A., STASINAKIS, A. S., PANTAZI, Y., *et al.* "Biodegradation of benzotriazoles and hydroxy-benzothiazole in wastewater by activated sludge and moving bed biofilm reactor systems". *Bioresource Technology*, v. 192, pp. 627-635, 2015.

- MCQUARRIE, J., BOLTZ, J. "Moving Bed Biofilm Reactor Technology: Process Applications, Design, and Performance". *Water Environment Research*, v. 83, pp. 560-575, 2011.
- MEENA, M., DIVYANSHU, K., KUMAR, S., *et al.* "Regulation of L-proline biosynthesis, signal transduction, transport, accumulation and its vital role in plants during variable environmental conditions", *Heliyon*, v. 5, Dez. 2019.
- METCALF & EDDY, TCHOBANOGLOUS, G., BURTON, F. L., *et al.* *Wastewater Engineering: Treatment and Reuse*. 4 ed., McGraw-Hill, 2003.
- METCALF & EDDY, TCHOBANOGLOUS, G., STENSEL, H. D., *et al.* *Wastewater Engineering: Treatment and Resource Recovery*. 5 ed. USA, McGraw-Hill, 2014.
- MISITI, T., TANDUKAR, M., TEZEL, U., *et al.* "Inhibition and biotransformation potential of naphthenic acids under different electron accepting conditions". *Water Research*, v. 47, n. 1, pp. 406-418, 2013.
- MURSHID, S., ANTONYSAMY, A., DHAKSHINAMOORTHY, G., *et al.* "A review on biofilm-based reactors for wastewater treatment: Recent advancements in biofilm carriers, kinetics, reactors, economics, and future perspectives". *Science of The Total Environment*, v. 892, pp. 164796, 2023.
- NAGDA, A., MEENA, M., SHAH, M. "Bioremediation of industrial effluents: A synergistic approach", *Journal of Basic Microbiology*, v. 62, Set. 2021.
- NAYERI, D., KHAMUTIAN, S., SHOKOOHIZADEH, M. J. "A review on the effect of biofilm thickness in moving bed bioreactor for the nitrogen compounds removal". *Desalination and Water Treatment*, v. 323, pp. 101385, 2025.
- NICOLELLA, C., LOOSDRECHT, M., HEIJNEN, S. "Wastewater Treatment with Particulate Biofilm Reactors". *Journal of Biotechnology*, v. 80, pp. 1-33, 2000.
- NOGUEIRA, R., MELO, L., PULRKHOLD, U., *et al.* "Nitrifying and heterotrophic population dynamics in biofilm reactors: effects of hydraulic retention time and the presence of organic carbon". *Water Research*, v. 37, 2003.

ØDEGAARD, H., GISVOLD, B., STRICKLAND, J. "The influence of carrier size and shape in the moving bed biofilm process", *Water Science and Technology*, v. 41, pp. 383-391, Feb. 2000.

ØDEGAARD, H. "Innovations in wastewater treatment: The moving bed biofilm process", *Water science and technology: a journal of the International Association on Water Pollution Research*, v. 53, pp. 17-33, Jun. 2006.

OKABE, S., KINDAICHI, T., ITO, T., *et al.* "Analysis of Size Distribution and Areal Cell Density of Ammonia-Oxidizing Bacterial Microcolonies in Relation to Substrate Microprofiles in Biofilms". *Biotechnology and Bioengineering*, v. 85, pp. 86-95, 2004.

OMAR, A., ALMOMANI, F., QIBLAWEY, H., *et al.* "Advances in Nitrogen-Rich Wastewater Treatment: A Comprehensive Review of Modern Technologies". *Sustainability*, v. 16, n. 5, pp. 2112, 2024.

OTITOJU, T., AHMAD, A. L., SENG, O. "Polyvinylidene fluoride (PVDF) membrane for oil rejection from oily wastewater: A performance review", *Journal of Water Process Engineering*, Nov. 2016.

PARTOVINIA, A., SOORKI, A. A., KOOSHA, M. "Synergistic adsorption and biodegradation of heavy crude oil by a novel hybrid matrix containing immobilized *Bacillus licheniformis*: Aqueous phase and soil bioremediation". *Ecotoxicology and Environmental Safety*, v. 222, 2021.

PICULELL, M., WELANDER, P., JONSSON, K., *et al.* "Evaluating the Effect of Biofilm Thickness on Nitrification in Moving Bed Biofilm Reactors". *Environmental Technology*, v. 37, pp. 1-28, 2016.

POMPILIO, A., PICCOLOMINI, R., PICCIANI, C., *et al.* "Factors associated with adherence to and biofilm formation on polystyrene by *Stenotrophomonas maltophilia*: the role of cell surface hydrophobicity and motility". *FEMS Microbiology Letters*, v. 287, n. 1, pp. 41-47, 2008.

POURROSTAMI NIAVOL, K., ANDALURI, G., ACHARY, M., *et al.* "How does carbon to nitrogen ratio and carrier type affect moving bed biofilm reactor (MBBR):

Performance evaluation and the fate of antibiotic resistance genes", *Journal of environmental management*, v. 377, p. 124619, Fev. 2025.#

PROSSER, J. I. "Autotrophic Nitrification in Bacteria". In: ROSE, A. H., TEMPEST, D. W. (eds), *Advances in Microbial Physiology*, London, UK, Academic Press, v. 30, pp. 125-181, 1990.

QUINN, P. K., ASHER, W. E., CHARLSON, R. J. "Equilibria of the marine multiphase ammonia system". *Journal of Atmospheric Chemistry*, v. 14, n. 1, pp. 11-30, 1992.

RAJITHA, K., YARLAGADDA, V. N., VENUGOPALAN, V. "Acid soluble extracellular matrix confers structural stability to marine *Bacillus haynesii* pellicle biofilms". *Colloids and Surfaces B: Biointerfaces*, v. 194, pp. 111160, 2020.

RAS, M., LEFEBVRE, D., DERLON, N., *et al.* "Distribution and hydrophobic properties of Extracellular Polymeric Substances in biofilms in relation towards cohesion". *Journal of Biotechnology*, v. 165, pp. 85-92, 2013.

RAZAVI, Z., MIRGHAFARI, N., REZAEI, B. "Adsorption of crude and engine oils from water using raw rice husk". *Water Science and Technology*, v. 69, pp. 947-952, 2015.

RITTMANN, B. E., MANEM, J. A. "Development and experimental evaluation of a steady-state, multispecies biofilm model". *Biotechnology and Bioengineering*, v. 39, n. 9, pp. 914-922, 1992.

RITTMANN, B. E., MCCARTY, P. L. ***Environmental Biotechnology: Principles and Applications***. New Delhi, India, Tata McGraw Hill Education Private Limited, 2012.

RUSTEN, B., EIKEBROKK, B., ULGENES, Y., *et al.* "Design and operation of the Kaldness moving bed biofilm process", *Aquacultural Engineering*, v. 34, pp. 322-331, Mai. 2006.

RUSTEN, B., KOLKINN, O., ODEGAARD, H. "Moving bed biofilm reactors and chemical precipitation for high efficiency treatment of wastewater from small communities". *Water Science and Technology*, v. 35, n. 6, pp. 71-79, 1997.

RUSTEN, B., MCCOY, M. A., PROCTOR, R., *et al.* "The innovative moving bed biofilm reactor/solids contact reaeration process for secondary treatment of municipal wastewater". *Water Environment Research*, v. 70, 1998.

SALVETTI, R., AZZELLINO, A., CANZIANI, R., *et al.* "Effects of temperature on tertiary nitrification in moving-bed biofilm reactors", *Water Research*, v. 40, pp. 2981-2993, Set. 2006.

SANTO, C., VILAR, V., BHATNAGAR, A., *et al.* "Biological treatment by activated sludge of petroleum refinery wastewaters", *Desalination and Water Treatment*, v. 51, Fev. 2013.

SATAPATHY, Monalisa; JAYAPAL, Anandkumar. Biodegradation of Phenol and Ammonia from Refinery Wastewater in Hybrid MBBR System by Native Mixed Bacterial Culture. *Journal of Environmental Engineering*, v. 149, n. 1, jan. 2023.

SCHNEIDER, E., CERQUEIRA, A., DEZOTTI, M. "MBBR evaluation for oil refinery wastewater treatment, with post-ozonation and BAC, for wastewater reuse". *Water Science and Technology*, v. 63, pp. 143-148, 2011.

SHETTIMA LAWAN, M., KUMAR, R., RASHID, J., *et al.* "Recent Advancements in the Treatment of Petroleum Refinery Wastewater", *Water*, v. 15, p. 3676, Out. 2023.

SHORE, J., M'COY, W., GUNSCH, C., *et al.* "Application of a moving bed biofilm reactor for tertiary ammonia treatment in high temperature industrial wastewater", *Bioresource technology*, v. 112, pp. 51-60, Fev. 2012.

SHI, Y., WEI, N., WU, G. "Tertiary denitrification of the secondary effluent in biofilters packed with composite carriers under different carbon to nitrogen ratios". *Environmental Engineering Research*, v. 21, pp. 311-317, 2016.

SINGH, M. P., SINGH, P., LI, H. B., *et al.* "Microbial biofilms: Development, structure, and their social assemblage for beneficial applications". In: Yadav, M. K., Singh, B. P. (eds), *New and Future Developments in Microbial Biotechnology and Bioengineering: Microbial Biofilms*, 1 ed., chapter 10, Amsterdam, Netherlands, Elsevier, pp. 125-138, 2020.

SINGH, S., SHIKHA. "Treatment and Recycling of Wastewater from Oil Refinery/Petroleum Industry". In: Singh, R. L., Singh, R. P. (eds), *Advances in Biological Treatment of Industrial Waste Water and their Recycling for a Sustainable Future*, Singapore, Springer Singapore, pp. 303-332, 2019.

SONWANI, R., SWAIN, G., GIRI, B., *et al.* "A novel comparative study of modified carriers in moving bed biofilm reactor for the treatment of wastewater: Process optimization and kinetic study", *Bioresource Technology*, v. 281, pp. 335-342, Feb. 2019.

SZCZEPANSKI, S., LIPSKI, A. "Essential oils show specific inhibiting effects on bacterial biofilm formation". *Food Control*, v. 36, pp. 224-229, 2013.

TANSEL, B., REGULA, J., SHALEWITZ, R. "*Treatment of fuel oil and crude oil contaminated waters by ultrafiltration membranes*", *Desalination*, v. 102, pp. 301-311, 1995.

THORAT, B., SONWANI, R. "Current technologies and future perspectives for the treatment of complex petroleum refinery wastewater: A review", *Bioresource Technology*, v. 355, p. 127263, Mai. 2022.

TIJHUIS, L.; VAN LOOSDRECHT, M. C. M.; HEIJNEN, J. J. Dynamics of population and biofilm structure in the biofilm airlift suspension reactor for carbon and nitrogen removal. *Water Science and Technology*, v. 29, n. 10-11, p. 377-384, 1994.

TORKAMAN, M., BORGHEI, S. M., TAHMASEBIAN, S., *et al.* "Nitrogen removal from high organic loading wastewater in modified Ludzack-Ettinger configuration MBBR system", *Water Science and Technology*, v. 72, pp. 1274-1282, Out. 2015.

TORRESI, E., FOWLER, J., POLESEL, F., *et al.* "Biofilm Thickness Influences Biodiversity in Nitrifying MBBRs-Implications on Micropollutant Removal". *Environmental Science & Technology*, v. 50, 2016.

TSUNEDA, S., PARK, S., HAYASHI, H., *et al.* "Enhancement of nitrifying biofilm formation using selected EPS produced by heterotrophic bacteria". *Water Science and Technology*, v. 43, pp. 197-204, 2001.

UAN, D. K. "Potential application of membrane bioreactor (MBR) technology for treatment of oily and petrochemical wastewater in Viet Nam - an overview", *Petrovietnam Journal*, v. 6, pp. 64-71, 2013.

URAKAWA, H., GARCIA, J. C., BARRETO, P. D., *et al.* "A sensitive crude oil bioassay indicates that oil spills potentially induce a change of major nitrifying prokaryotes from the archaea to the bacteria". *Environmental Pollution*, v. 164, pp. 42-45, 2012.

URAKAWA, H., RAJAN, S., FEENEY, M. E., *et al.* "Ecological response of nitrification to oil spills and its impact on the nitrogen cycle". *Environmental Microbiology*, v. 21, n. 1, pp. 18-33, 2019.

UNAL TURHAN, E., ERGINKAYA, Z., KORUKLUOGLU, M., *et al.* "Beneficial Biofilm Applications in Food and Agricultural Industry". In: Malik, A., Erginkaya, Z., Erten, H. (eds), *Health and Safety Aspects of Food Processing Technologies*, 1 ed., chapter 15, Cham, Switzerland, Springer, pp. 445-469, 2019.

VAN HAANDEL, A., VAN DER LUBBE, J. ***Handbook of Biological Wastewater Treatment***. London, UK, IWA Publishing, 2012.

VERHAGEN, F. J. M., LAANBROEK, H., J., 1991, "Competition for Ammonium between Nitrifying and Heterotrophic Bacteria in Dual Energy-Limited Chemostats", *Applied and Environmental Microbiology*, V. 57, pp. 3255-3263.

VISHNIAC, W., SANTER, M. "The Thiobacilli", *Bacteriological Reviews*, v. 21, n. 3, pp. 195-213, 1957.

VON SPERLING, M. *Basic Principles of Wastewater Treatment*. London, UK, IWA Publishing, 2007.

WANG, Q., WU, S., CHU, G., *et al.* "Metagenomic analysis and microbial activity shifts reveal the effect of the carbon/nitrogen ratio on the nitrogen removal performance of a moving bed biofilm reactor treating mariculture wastewater", *Journal of Water Process Engineering*, v. 51, p. 103363, Feb. 2023.

WELANDER, U., HENRYSSON, T., WELANDER, T. "Nitrification of landfill leachate using suspended-carrier biofilm technology". *Water Research*, v. 31, n. 9, pp. 2351-2355, 1997.

WONG, C., BARTON, G., BARFOR, J. "The nitrogen cycle and its application in wastewater treatment". In: MARA, D., HORAN, N. (eds), *Handbook of Water and Wastewater Microbiology*, Amsterdam, Netherlands, Academic Press, pp. 427-439, 2003.

WU, H., YANG, T., ZHANG, M., et al. "Effect of HRT on nitrogen removal from low carbon source wastewater enhanced by slurry and its mechanism", *Chemical Engineering Journal*, v. 477, p. 147159, Nov. 2023.

YOUNG, B., DELATOLLA, R., REN, B., et al. "Pilot Scale Tertiary MBBR Nitrification at 1°C: Characterization of Ammonia Removal Rate, Solids Settleability and Biofilm Characteristics", *Environmental technology*, v. 37, pp. 1-28, Jan. 2016.

YOUNIS, S. A., ALI MAITLO, H., LEE, J., et al. "Nanotechnology-based sorption and membrane technologies for the treatment of petroleum-based pollutants in natural ecosystems and wastewater streams", *Advances in Colloid and Interface Science*, v. 275, p. 102071, 2020.

ZABERMAWI, N. M., BESTAWY, E. E. "Effective treatment of petroleum oil-contaminated wastewater using activated sludge modified with magnetite/silicon nanocomposite", *Environmental Science and Pollution Research*, v. 31, pp. 17634-17650, Mar. 2024.

ZAGKLIS, D., BAMPOS, G. "Tertiary Wastewater Treatment Technologies: A Review of Technical, Economic, and Life Cycle Aspects", *Processes*, v. 10, p. 2304, Nov. 2022.

ZHANG, Q., LIANG, S., TAN, S., et al. "MBBR start-up with HN-AD bacteria inoculation: Comparative analysis in simulated and real wastewater for performance, microbial characteristics, and nitrogen removal mechanism", *Journal of Water Process Engineering*, v. 58, p. 104786, Feb. 2024.

ZHANG, R. X., LIU, Y., HUANG, D. N., et al. "Influence of Influent Load on Nitrification/Denitrification with MBBR for Oil Shale Retorting Wastewater Treatment: Performance and Microbial Community Structure", *Water, Air, & Soil Pollution*, v. 236, Nov. 2024.